

FACULTY OF SCIENCE - UNIVERSITY OF ZURICH
DEPARTMENT OF GEOGRAPHY
PHYSICAL GEOGRAPHY – HYDROLOGY AND CLIMATE H₂K

MASTER THESIS - GEO511

Performance Assessment of Three Weather
Datasets in Hydrological Simulations and
Future Impacts of Climate Change on
Water Resources in the Watershed of the
Hydropower Reservoir Gigerwaldsee

August 8th 2014

Author

Simon Etter

simon.etter@outlook.com

09-706-375

Supervisor

Dr. David Finger

Water Resources Expert

fingerd@gmx.net

Icelandic Meteorological Office

Bústaðavegi 9

150 Reykjavík

Faculty Member

Prof. Dr. Jan Seibert

Abstract

The global climate is changing. The changing temperatures and precipitation patterns will force glaciers to shrink and diminish snow cover in mountain environments. The runoff of Alpine Catchments will be affected by these changes. The catchment of the Gigerwald lake, a water resource for hydro power production in the Swiss Alps, will also be affected by those changes. The Gigerwald catchment is a subcatchment of the Rhine river. The Commission for the Hydrology of the Rhine Basin (CHR) tries to quantify the melt waters entering the Rhine river. To drive those hydrological simulations an adequate weather dataset is needed. Therefore the gridded dataset from MeteoSwiss (GRID) is compared to the HYRAS dataset from the German Weather Service and to a simple interpolated dataset of station data (IDW) of the SwissMetNet using inverse distance weighting. The comparison is done using the semi-distributed hydrological model HBV. Over a calibration period of 1999 to 2002 and a validation period of 2003 to 2006 the simulations using the three datasets were compared to observed discharge and snowcover from MODIS snowcover images in their performance regarding the four objective functions Nash Sutcliffe Efficiency, logarithmic Nash-Sutcliffe Efficiency, Volume Error and Snowcover RMSE. The calibration with multiple objective functions was done by selecting the Pareto Optimal parameter sets out of 150'000 runs of a Monte Carlo simulation. From the resulting 157 sets, those that were above some user-defined thresholds were selected. The Results show that the best model reproduction of the discharge is generally achieved using the HYRAS dataset, even though the differences are only marginal and might not be transferable to other catchments.

In the second part the future climate scenarios from global circulation models were used to drive the HBV-light model to simulate future weather scenarios. The used version has a new feature, which dynamically adapts the glaciers during the simulation, according to its losses from melt water. Seven different model combinations of Global Circulation Models (GCM) with Regional Climate Models (RCM) were corrected using quantile mapping (QM). The correction for the regional peculiarities of the weather inside the catchment was based on observations from the GRID dataset. The calibration procedure was slightly changed in this part. Again, from 150'000 runs of a Monte Carlo simulation the Pareto optimal sets were selected. But then the 10 best out of these 159 according to an overall score were used to drive the HBV. The resulting scenarios cover a mid-term scenario from 2036 - 2065 and a long-term scenario from 2069 - 2098. In the mid-term period three possible glacier extent and thickness scenarios were used to simulate the glaciers in the near future. Interpolated measurements were used to parametrize the glaciers in the reference period from 1992 - 2021. The changes relative to the reference period predict an increase of discharge during winter and spring due to higher temperatures and increased precipitation during that time and a decrease of

discharge in the summer months due to reduced snow cover that outlasts into the late summer months. These trends are manifested stronger in the long-term period than in the mid-term period. Even though the changes are not statistically significant due to the large variation in the data, the trend is clearly visible and also in line with results from other works. Using an analysis of variance the relative contribution of the climate scenarios and the different model parameters was assessed. The climate scenarios make up the largest fraction of roughly 80% of the variance in the future discharge scenarios. The parameter mostly make up less than 10% throughout the year and the contribution of the glaciers is negligible, the remaining fraction of the variance emerges from interactions between the contributors. According to the findings the glaciers in the Calfeisental are not a key player in the discharge production in the catchment, because of their small size. The total annual discharge into the Gigerwaldsee is projected to decrease by 3.5% in the mid-term and by 6% in the long-term. Snow melt water will have a decreasing and rain water an increasing influence on the discharge.

Contents

1. Introduction	1
1.1. Alpine Hydrological Changes	3
1.2. Hydropower	3
1.3. Rhine Basin	4
1.4. Structure of this Thesis	4
1.5. Research Questions	5
2. Study Site	6
3. Data	10
3.1. Interpolated Station Data (IDW)	10
3.2. MeteoSwiss Grid Data (GRID)	11
3.3. HYRAS Grid Data (HYRAS)	13
3.4. Evaporation data	14
3.5. Discharge Data	14
3.6. MODIS Snowcover Data	15
3.7. Glacier Data	16
3.8. Climate Scenarios	16
4. Methods	24
4.1. Statistical Comparison of the Weather Datasets	24
4.2. The HBV Model	24
4.2.1. Model Structures	25
4.2.2. Catchment Characterisation	25
4.2.3. Performance Measures	26
4.3. Comparison of Different Model Runs using Multivariable Calibration	28
4.4. Performance Assessment of the Weather Datasets	30
4.4.1. Model Calibration 1999 - 2002 and Validation 2003 - 2006	30
4.5. Discharge Scenarios	31
4.5.1. HBV Simulations	31
4.5.2. HBV Calibration for Climate Scenarios	33
4.5.3. Analysis of Uncertainties	38
5. Results	40
5.1. Comparison of Weather Datasets	40
5.1.1. Results of Multivariable Calibration for the Weather Datasets	43

Contents

5.1.2.	Results of Weather Dataset Evaluation	43
5.2.	Discharge Scenarios	48
5.2.1.	Multivariable Calibration	48
5.2.2.	Model Performance during Calibration and Validation Period . . .	50
5.2.3.	Climate Change Effects on Discharge	52
5.2.4.	Analysis of Uncertainties	56
6.	Discussion	57
6.1.	Differences in Weather datasets	57
6.1.1.	Correction of Altitude Bias	57
6.1.2.	Assessment of Differences in GRID, HYRAS and IDW	59
6.1.3.	Calibration and Validation using GRID, HYRAS and IDW	60
6.2.	Multi-variable Calibration	61
6.3.	Climate Scenarios	63
6.3.1.	Performance of the HBV when using Climate Scenarios during Cal- ibration Period	64
6.3.2.	Changes in Runoff due to Climate Change	65
6.3.3.	Uncertainties	66
7.	Conclusion	68
7.1.	Comparison of weather datasets	68
7.2.	Climate Scenarios	68
A.	Appendix	85
A.1.	Figures of the Calibration and Validation Period of the 3 Datasets	85
A.1.1.	Dotty Plots	85
A.1.2.	Discharge Plots	87
A.1.3.	Errors	88

1. Introduction

Global View

The Earth's Climate is changing. According to the Intergovernmental Panel on Climate Change (IPCC) Assessment Report 5 (AR5) the global average air and ocean temperatures have been observed to rise, as well as the global average sea level. Furthermore a widespread melting of snow and ice has been reported. In the last century almost the entire globe experienced surface warming and, including latest measurements, the global average temperature difference over land and oceans combined between 1880 and 2012 is 0.85 °C. This corresponds to an average warming of 0.12 °C per decade from 1951 - 2012. The precipitation increased over mid latitude areas in the Northern Hemisphere since 1951. On a global scale the number of cold days and nights has decreased whereas the number of warm days and nights has increased. Extreme events are likely to have occurred more often. Heat waves occurred more often over Europe, Asia and Australia in the latest decades. Precipitation has increased over more land masses than it has decreased. Namely it has increased in eastern and north-western North America, parts of Europe and Russia, southern South America and Australia, and has declined in the Sahel and other locations. Also the frequency and intensity of heavy precipitation has increased in North America and Europe, elsewhere this is not certain (Hartmann et al., 2013). The upper 75 m of the oceans warmed on average by 0.11 °C per decade from 1971 - 2010. During that time 60% of the net energy decrease was stored in the upper oceans (0-700m) and 30% in greater depths. Regions of evaporation become more saline and regions of precipitation fresher since 1970 (Rhein et al., 2013).

A trend of increasing average ice losses from 226 to 275 Gty⁻¹ from glaciers that are not connected to ice caps has been observed in the years 1993 - 2009 compared to 1971 - 2009. In Greenland the average ice loss increased from 34 to 215 Gty⁻¹ from the period 2002 - 2011 compared to 1992 - 2001. Further the mean annual Arctic sea ice extent decreased between 3.5 and 4.1% per decade during the years 1979 - 2012. Further also the sea ice thickness decreased between 1980 and 2008 by 1.3 to 2.3 m. In contrast the Antarctic sea ice increased by 1.2 - 1.8% per decade over the years 1979 to 2012 but with strong regional differences of gains and losses. The snow cover extent in the Northern Hemisphere declined significantly, with average losses in June of 53% over the period 1967 - 2012. Over a longer time period, 1922 - 2012, where data was only available for March and April it shows a decline of 7%. Permafrost shows higher temperatures in most regions since 1980 but with strongly varying rates (Vaughan et al., 2013).

An effect of all the above can be seen in the sea level rise. From 1901 - 2010 the sea level rose by 0.19 m. The rate of rise was getting higher during that period. Over the

1. Introduction

whole period it is 1.7 mmy^{-1} , from 1971 - 2010 it was 2 mmy^{-1} and from 1993 - 2010 it was 3.2 mmy^{-1} (Rhein et al., 2013). The glacier mass loss and the thermal expansion contribute to about 75% of the rise (IPCC, 2013).

The observed trends are believed to persist in the coming decades. The simulations of global circulation models (GCM) predict a temperature rise of $0.3 - 0.7^\circ\text{C}$ for the period 2016 - 2035 compared to 1988 - 2005, although only with medium confidence. For the period 2081 - 2100 these are 0.3 to 4.8°C depending on the greenhouse gas concentration. However it seem to be clear, that the Arctic regions will warm up faster than others. With a very high probability the trend towards more frequent hot and fewer cold temperature extremes will persist. Therefore heat waves will occur more often, whereas on the other hand single cold extremes will most probably still occur from time to time. Furthermore the trend to more extreme and intense precipitation events will also persist (IPCC, 2013). Some correlations in historical records (i.e. cold summers/warm winters being rather wet and hot summers/cold winters being rather dry) are believed to persist in the future (Beniston, 2009; Vidale et al., 2007). In addition to that Beniston (2009) state that warm/dry & warm/wet events will increase further as they already have in the recent past.

Alpine View

The ecological effects of climate change on Alpine areas are manifold. During the last century from 1946 - 1999 the mean winter precipitation increased across northern Europe (IPCC, 2008; Klein Tank et al., 2002). In the eastern Mediterranean area the yearly precipitation decreased over the same timespan, especially during the rainy seasons from October to March (Narrant and Douguédroit, 2006). The trend for enhanced winter precipitation is believed to persist in the future, especially in Alpine areas. At the same time summer precipitation is projected to decrease (Zierl and Bugmann, 2005). Furthermore the mean precipitation per wet day shows an increasing magnitude in areas that are getting wetter as well as in areas that are getting drier (Klein Tank et al., 2002). According to these findings Europe became and will be drier in the south and wetter in the north. If a precipitation event occurs, there is a higher chance of it being an extreme event, rising the risk of flash floods in both areas.

Trends of a decreasing snow cover, as well as a trend for a decreasing number of days with snowfall since the 1980s until 1999 have been observed. However these effects are mainly visible in mid and low altitudes, whereas high altitudes show only small changes (Laternser and Schneebeli, 2003). The reason for the shorter snow cover persistence at lower latitudes is believed to be rather the earlier snow melt in spring than a later onset of snowfalls (Martin and Etchevers, 2005). On the other hand simulations of Zierl and Bugmann (2005) showed that snow cover might even increase at elevations above 2700 m due to increased precipitation in winter. However this was only found for the first decades of the the 21st century, afterwards the enhanced precipitation is outweighed by the rising temperatures.

1.1. Alpine Hydrological Changes

The snow cover and glaciers acting as natural water reservoirs are projected to decline further in the 21st century. Even though the total annual runoff is believed to stay at about the same level with only a small tendency towards a decrease, the seasonal distribution will change substantially (Zierl and Bugmann, 2005). Annual runoff regimes are believed to change towards increasing runoff in winter months and decreasing runoff in the low flow season with high confidence (IPCC, 2008). Zierl and Bugmann (2005) found that the summer runoff will decrease substantially in high alpine catchments, while today the highest fraction of runoff occurs at this time. During the first decades the predicted summer losses are believed to be compensated by the increased winter gains. This is in line with the findings of (Finger et al., 2012) who state that the melt season starts earlier but later on during the melt season the runoff will be strongly reduced because of glacier retreat and heavy snow melt in the spring months. However, in the short term, the enhanced glacier melt is believed to increase the summer runoff of the alpine rivers, but as glaciers shrink the runoff is believed to decrease (Hock et al., 2005) by up to 50% (Zierl and Bugmann, 2005). This of course depends on the size of the remaining glaciers.

1.2. Hydropower

The future climatic changes and their consequences on the runoff are potentially strongly influencing the hydropower production (IPCC, 2008). Lehner et al. (2005) modelled the consequences of the changing water availability for all of Europe for the years 2020 and 2070. Depending on the method and the regional climate model (RCM) they found a loss of 14.0 or 14.4% of gross hydropower potential. For the change in already developed hydropower potential their results predict, depending on the RCM, a change of -4.2 (ECHAM4) or +0.2% (HadCM3) for the year 2020 and -5.2% or 15.5% for the year 2070. The future alterations in discharge regimes could lead to "unstable regional trends" (Lehner et al., 2005). On the one hand predictions for increases in water availability are made, and therefore up to 15% (Lehner et al., 2005) or even 30% (IPCC, 2008) increased potential for hydropower, for northern Scandinavia and Russia as well as north eastern Europe and on the other hand decreases of 20 to 50% in hydropower potential are predicted for large parts of eastern and south-eastern Europe due to drier climate and increased human water need. In western and central Europe the hydropower potential is not believed to change drastically (Lehner et al., 2005). This is in line with the findings of Zierl and Bugmann (2005) who predict only a slight trend towards decreasing total annual runoffs from Alpine catchments.

In western Europe and Scandinavia the current potential is virtually exploited. This includes also Switzerland, where around 58% of the electricity production is covered by hydropower. Nevertheless, the potential for new sites is rather small. Difficulties arise from environmental and social concerns from various groups (World Commission on Dams, 2000). To not waste any of the existing potential it is important that the existing structures perform at their optimum. Therefore possible changes need to be

1. Introduction

found even if the effects seem to be small compared to northern and southern Europe. Adaptive measures have to be taken, probably for every site itself. Finger et al. (2012) showed that current hydropower infrastructures in the Vispa Valley are not suitable for future climatic conditions. Accordingly hydropower companies need to deal with the changes in the coming decades before the end of the 21st century. The company in the Vispa Valley will have to adapt their infrastructures towards to increased runoff in fall due to extreme events and have to deal with a drastically reduced amount of water due to less ice melt in summer (Finger et al., 2012).

1.3. Rhine Basin

As can be seen from the above discussion the Alpine areas contain a lot of water in various forms. The Alps as water towers for Europe play a big role in many areas affecting every day life from drinking water and food production to health, from industrial development to environmental concerns and energy production (Mountain Agenda, 1998). Some major European rivers emerge from Alpine catchments. Namely these are the Po in the South, the Rhone in south-western direction, the Danube in eastern direction and the Rhine leaving the Alps in northern direction. The latter is of big interest to the International Commission for the Hydrology of the Rhine Basin (CHR)¹. The CHR is interested in flood management, impacts of climate change, sediment transport and deposition and the assessment of contributions of snow and glacial melt waters to runoff tributaries.

In this work such a catchment is investigated. For hydrological simulations for e.g. assessing the impacts of climate change the CHR project needs a consistent weather dataset for the entire catchment of the Rhine river. The HYRAS dataset (Rauthe et al., 2013) of the German Weather Service (*German: Deutscher Wetterdienst*) (DWD)² fulfils this criteria. However its performance in hydrological modelling in Alpine catchments has not yet been tested and compared to weather datasets created specifically for Alpine areas. One such dataset is built of the gridded temperature (Frei, 2014) and precipitation (Isotta et al., 2013) datasets from MeteoSwiss³. A third dataset for comparison is created directly from station data around the catchment. All three datasets are built upon SwissMetNet (Roulet et al., 2010) station data. The result of this study should build the base for a decision whether the HYRAS dataset is suitable for hydrological simulations in Alpine Catchments.

1.4. Structure of this Thesis

In the first part of the work I will compare the three weather datasets and assess the contributions to the water flowing into the Gigerwaldsee. This will be done using an updated version of the Hydrologiska Byråns Vattenavdelning (HBV)-light model (Seibert and Vis, 2012). In the recent times the HBV model has been equipped with new

¹<http://www.chr-khr.org/en/projects> (accessed: 17.07.2014)

²<http://www.dwd.de> (accessed: 17.07.2014)

³<http://www.meteoschweiz.admin.ch> (accessed: 17.07.2014)

routines and possibilities to use more datasets. It is now able to split the runoff into the contribution of snow melt, glacier melt and rain water to the total discharge and can be calibrated to these datasets of snowcover and glacier mass balances Finger et al. (submitted). For the first part of this work a version of the model was used that includes the possibility to calibrate for the fraction of snow covered area derived from Moderate Resolution Imaging Spectrometer (MODIS) snow cover products, but not yet for glacier mass balances.

In the second part of this thesis I will look at the same Alpine catchment again. This time the future impacts of climatic changes are elaborated. The goal is to simulate the expected changes until the end of the 21st century by using an updated HBV version compared to the first part. It includes dynamic simulation of present glaciers based on glacier thicknesses and extents. The simulations are driven by downscaled climate scenarios from global circulation model (GCM) which all are derived from the A1B scenario (IPCC, 2008). I will try to quantify the relative shares of rain, glacial and snow melt water contributing to the hydrograph. The scenarios should then offer new insights on the changing dynamics in the catchment and in the best case become a base for decision of how to adapt to climatic changes for the company running the hydro power system.

1.5. Research Questions

By comparing the weather datasets in the first part and assessing the future changes in the catchment in the second part the following research questions shall be answered:

Research Question I: Which of the weather datasets GRID, HYRAS and IDW performs best in hydrological simulations using the HBV model?

Research Question II: What is the improvement of using multiple datasets to calibrate the HBV model?.

Research Question III: How will changing temperatures and precipitation patterns affect the amount and distribution of water flowing into the Gigerwaldsee?

Research Question IV: How big are the contributions of snow melt, glacial melt and rain water now and how will their relative and absolute shares change throughout the 21st century?

Research Question V: What is the contribution of the model parameters and the seven climate scenarios on the variance of the resulting future discharge scenarios?

2. Study Site

For a better readability and easier localization on Swiss maps the Swiss names of several locations are used:

Gigerwaldsee:	the dammed lake of Gigerwald
Mapraggsee:	the dammed lake of Mapragg
Calfeisental:	the valley called Calfeisental
Weisstannental:	the valley called Weisstannental
Sardonagletscher:	the Sardona glacier
Chline Gletscher:	the Chline glacier

The catchment of the Gigerwaldsee lies in the community of Pfäfers in the South of the canton of St. Gallen in eastern Switzerland. The Gigerwaldsee is fed naturally by a small mountainous catchment of about 52 km² which extends from the upper part of the Calfeisental, where the Sardonagletscher (0.45 km²) and the Chline Gletscher (0.21 km²) are located until the end of the dam. Furthermore the lake is also fed by partial catchments of the Weisstannental (total of 45km²), which are located north of the Calfeisental (see Table 2.1 and Figure 2.1). There the water is collected at seven intakes (1-7) and guided into the Gigerwaldsee in subsurface conduits (see Figure 2.2) and also outside the two catchments in the Tersolbach (8) and guided into the Gigerwaldsee (9). The exact location of the eight intakes and of the Gigerwaldsee can be seen in Table 2.1. The coordinates are provided in Swiss Grid Coordinates (CH1903). The size of the catchments feeding the conduits is rather small, however summed up, they have approximately the same size as the natural catchment of the Gigerwaldsee.

Table 2.1.: Details of the water intakes

Number on Map	Water intake	Location	Catchment Size [km ²]	Height [m a.s.l.]
1	Siezbach	739530 / 204225	7.98	1389
2	Mattbach	739035 / 203295	1.86	1386
3	Seez	739260 / 203100	10.87	1374
4	Seitenbach Seez	739365 / 203110	0.63	1373
5	Scheusbach	742180 / 204150	6.64	1413
6	Lavtinabach	745680 / 203225	11.01	1003
7	Gafarrabach	746960 / 205960	5.34	1382
8	Tersolbach	749580 / 198310	7.83	1382
9	Gigerwaldsee	748729 / 197589	52	1335
10	Power plant Mapragg	755480 / 201724	-	835
11	Power plant Sarelli	759758 / 205045	-	515
12	Sardonagletscher	738400 / 197704	-	2700
13	Chline Gletscher	738520 / 198579	-	2570

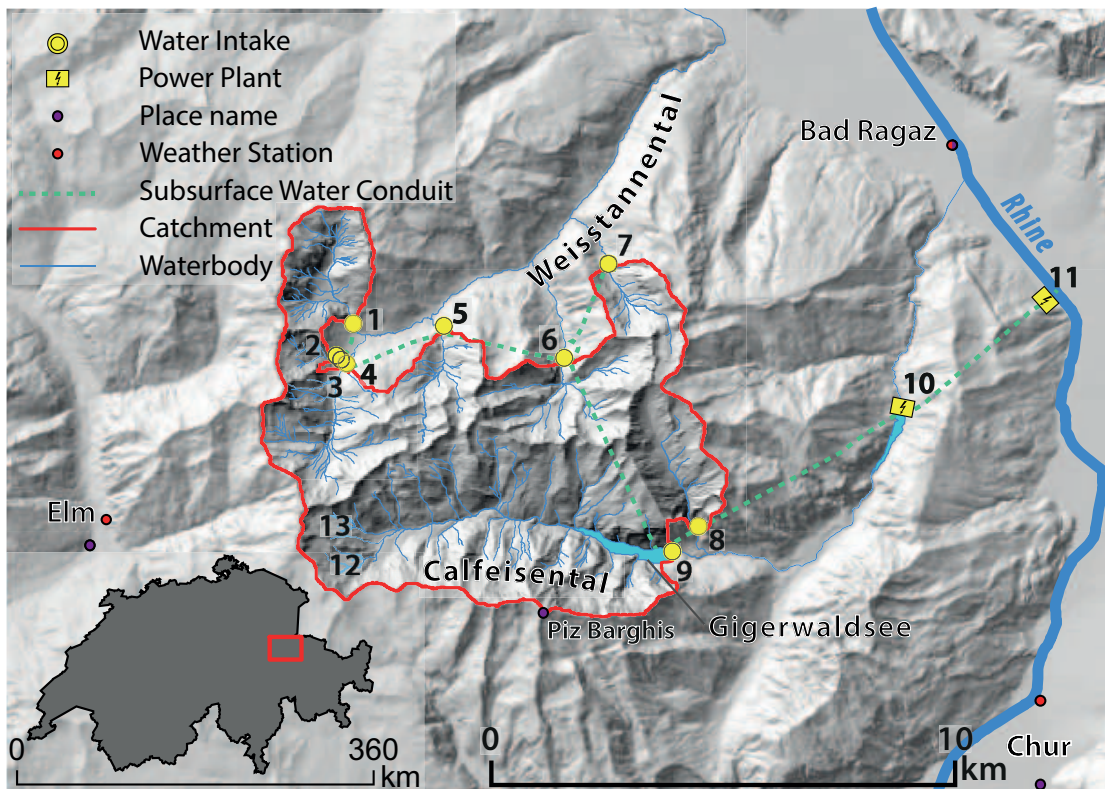


Figure 2.1.: Scheme of the Catchment

2. Study Site

The system consists of two power plants, one is located at the Mapraggsee (10) and the second is at the valley bottom in Sarelli (11). The whole catchment including the Taminatal encompasses an area of 160 km² with its highest elevation at the Piz Barghis at 3247 m. The Gigerwaldsee has a maximal volume of usable water of 33.4 M m³. The lower Mapraggsee has volume of only 2.7 Mm³, it collects the waters of the intermediate catchment of the Taminatal, serves as a compensating reservoir for the lower stage to the power plant Sarelli and at the same time as the lower basin for pumping water (back) up into the Gigerwaldsee. During the years 2000 to 2009 the mean annual energy production at the Mapragg power plant consisted of 117 M kWh in winter and of 201 M kWh in summer. Thereof 36 M kWh in winter and 132 M kWh in summer are produced from natural inflow. This sums up to an average energy production of 168 M kWh per year from natural inflow into the Gigerwaldsee during the period from 2000 - 2009. Including the power plant Sarelli the produced energy was 166 and 323 M kWh in winter and summer respectively. This means that 34% of the electricity is produced in winter and 66% in summer. However in winter 97 M kWh and in summer 114 M kWh are used for pumping water back up into the Gigerwaldsee¹. The mean annual potential energy of the inflow into the Gigerwaldsee, computed from the provided discharge data and the following Formula:

$$E_{pot} = V * \rho * g * \delta h \quad (2.1)$$

is roughly 311 M kWh per year over the period 2000 - 2009. Therefore the efficiency of the power plant Mapragg derived from this value and the mean annual production over the same period provided by the company is around 54%. A similar value of 56% was calculated for the Kárahnjúkar hydropower plant, the biggest dammed lake in Iceland (Finger, 2014). According to the Kraftwerke Sarganserland AG the remaining 46% are lost due to changes in the lake level of the Gigerwaldsee. When the lake is not filled completely, the pressure on the water falling on the turbine changes. Further this can also be influenced by the pump storage operation of on the whole site (Walter Uehli, Kraftwerke Sarganserland AG, 2014, personal communication). In addition it might be necessary to open up the dam during extreme events in order to prevent damage on the construction, that way also some of the potential can be lost.

¹These values were provided by the Kraftwerke Sarganserland AG.



Figure 2.2.: Gigerwaldsee, on the right side of the lake (northern side) the waters collected in the Weisstannental are guided into the lake (Picture taken by Corin Meier, 30.03.2014).

3. Data

One objective of the present thesis was to evaluate the performance of the three weather datasets. These are the gridded dataset from MeteoSwiss with its precipitation dataset (Isotta et al., 2013) and temperature dataset (Frei, 2014), the HYRAS dataset (Rauthe et al., 2013) of the German Weather Service DWD (*German: Deutscher Wetterdienst*) and a self-made dataset from measurements of SwissMetNet weather stations (Roulet et al., 2010). In the following sections the properties of these datasets are described to compare the datasets themselves and how their performance in the hydrological modelling study is assessed.

3.1. Interpolated Station Data (IDW)

Besides the gridded datasets Meteoswiss provides long time measurement series of a vast number of climate variables from 210 measurement stations (Roulet et al., 2010). From the three stations Elm, Bad Ragaz and Chur (see figure 2.1 and table 3.1) the variables mean daily temperatures 2 m above ground and daily precipitations sums were downloaded from the IDAWEB-Portal¹. Since the three stations surround the catchments in the Calfeisental and the Weisstannental, a simple inverse distance weighting-interpolation as described in Lu and Wong (2008) was applied:

$$z_G = \frac{\sum_{i=1}^n \frac{z_i}{(d_{i-G})^x}}{\sum_{i=1}^n \frac{1}{(d_{i-G})^x}} \quad (3.1)$$

where z_G is the temperature or precipitation value at the position G (Gigerwaldsee), as a result of the sum of the values at positions i , each divided by its distance (d_{i-G}) to the Gigerwaldsee and this in turn divided by the sum of the inverse distances. The distances remained in the first power ($x = 1$).

With the above formula only the distance between the stations is considered but not the difference in altitude. For correcting the temperature with respect to altitude a simple transformation was applied. Therefore the data of the three stations was scaled a reference altitude of 500 m, then Formula 3.1 was applied and the result was scaled to the average catchment elevation (2135 m). The scaling for altitude was done again using the lapse rate of 0.6 °C/100 m (Dodson and Marks, 1997). This results in -9.81 °C compared to the temperatures at 500 m.

¹<http://www.meteosuisse.admin.ch/web/de/services/datenportal/idaweb.html> (accessed: 17.07.2014)

Table 3.1.: Weather stations around the Gigerwaldsee which were used for the precipitation and temperature Interpolation using Inverse Distance Weighting

Weather Station	Location [CH1903 LV03]	Height [m a.s.l.]	Distance to Gigerwaldsee [km]
Elm	732265 / 198425	958	16.6
Bad Ragaz	756907 / 209340	496	14.3
Chur	759471 / 193157	556	11.6
Catchment (IDW)	748736 / 197602	2135	0

For the precipitation the correction would not have been as easily applicable, since there also dry days, which would then disappear by such an operation. Within this work it was only possible to correct the temperature dataset because correcting a precipitation dataset would have gone beyond the scope of this work. Therefore and since the HBV model is able to correct for such systematic errors by specifying the height where the measurements were made (Seibert and Vis, 2012), the precipitation values were not corrected.

3.2. MeteoSwiss Grid Data (GRID)

The dataset obtained from MeteoSwiss is a gridded dataset, interpolated between weather stations. The analysis method is quite new and considers the local precipitation-topography relationships at the climatological time-scale using a distance and angular weighting interpolation technique. The datasets for daily mean temperature (*TabsD_ch02.lonlat*) and daily precipitation (*RhiresD_ch02.lonlat*) have a resolution of 5 km, however the spacing between the measurement stations is bigger. It varies with the density of measurement stations throughout the whole dataset. In densely covered areas the spacing between the stations is between 10 and 15 km and elsewhere up to 25 km (Isotta et al., 2013).

The calculation of the gridded dataset for temperature from the point measurements across Switzerland is a very complex process and also allows dynamic adjustments to the weather situations present at a certain day. The temperature calculation is split up into a background and a residual field. The background field is designed to represent large-scale weather phenomena at the basin scale. It includes a representation of a vertical temperature profile allowing to account e.g. for inversion layers with varying properties and other non-linear states of the atmosphere. These background profiles vary horizontally. Therefore the whole area is divided into sub-regions (northern, alpine and southern part) which are given a certain weighting factor that attributes a location to a field. Using this weighting factor and a topographic parameter the background field is then calculated for every location, i.e. grid cell of the final product. For these background fields, manually identified outliers, e.g. stations in cold pools are removed, since such anomalies are accounted for in the residual field calculation (Frei, 2014).

The residual fields account for effects that are determined as the difference between

3. Data

station measurements and values of the background fields, but can not be captured in their entire manifestation. Their interpolation in space relies on non-Euclidean distances. Having an adaptable, so-called "layering-factor" for a certain situation, it allows to favour propagation of anomalies along certain altitudes. So e.g. residuals from a mountain ridge are more likely to be connected to other mountain tops than to the closer (in 2-dimensional Euclidean distance) valley bottom. These generalized distances are calculated in advance for a range of possible weather phenomena. Then, the residual fields are calculated for the grid points using simple inverse distance weighting (see Formula 3.1 with a factor $x = 2$, but only over the four closest stations. The final value is then the result of the combination of the background and the residual fields (Frei, 2014).

The calculation of precipitation also depends on the approach of calculating a background fields depending on a long term mean monthly value from 1971 - 1990, which are called reference conditions in Isotta et al. (2013). The reference conditions were calculated using a linear regression of elevation and precipitation, called PRISM (Precipitation-elevation Regressions on Independent Slopes Model). Thereby stronger weights are assigned to stations having more similar, digital elevation model (DEM)-derived attributes such as exposition and aspect to the observed grid cell (Daly et al., 1994; Isotta et al., 2013). Schwarb (2000) used an adapted version PRISM for the Alpine area and produced a grid with mean monthly precipitation with 2 km resolution. Isotta et al. (2013) scaled this product to a 5 km grid, which was then used as the reference field.

The anomalies are calculated using an adapted version of the SYMAP algorithm by Shepard (1984). This is performed using a weighting scheme including inverse distance weighting amongst others (Shepard, 1984), so that measurements closer to the grid point get a higher weight (Isotta et al., 2013). Further the weight is also adapted to its directional isolation (Isotta et al., 2013). This directional isolation is calculated with respect to the stations within the search neighbourhood (Frei and Schär, 1998). This neighbourhood consists of all cells, or stations respectively inside a minimal radius of 15 km. This radius is increased in steps of 5 km (due to the grid spacing) until at least three stations are found, with a maximum size of 60 km. If there are not three stations within 60 km the cell value is returned as 'missing'. This procedure is said to take account of the variable station density throughout the area, especially in boundary regions between high-density and low-density station regions (Frei and Schär, 1998). However small scale information can be displayed only where the station network is dense (Isotta et al., 2013).

The data from MeteoSwiss comes stored in multidimensional NetCDF files. The DEM used for calculation was the GTOPO30² by the United States Geological Survey (USGS), which has a resolution of 30" (arc seconds) in East-West direction and 60" in the North-South direction. This corresponds to approximately 1.6 and 2.3 km, respectively.

The average temperature and precipitation over the catchment was extracted from the data and merged into an average time series using R (R-Team, 2005).

Since the resolution of the DEM is so coarse, it consists of smoothed maximum and minimum elevation values, which means that mountain peaks are too low and valley bottoms too high. Therefore such a dataset can not account for all the variability on

²<http://www.eorc.jaxa.jp/JERS-1/en/GFMP/AM-3/docs/html/gtopo30.htm> (accessed: 17.07.2014)

small scales of the strongly varying terrain (Daly, 2006) inside narrow alpine valleys with big height gradients, like in this study. Not covered extreme events can not be corrected easily, therefore only the systematic part of the error in the temperature dataset is corrected in this work. The average catchment height derived from the GTOPO30 was 2087 m, whereas the one from the DHM25 (by Swisstopo³, considered as "ground truth", was slightly higher with 2135 m a.s.l. Using a lapse rate of 0.6 °C/100 m the underestimation correction factor of -0.288 °C was calculated and finally added to the measurements.

3.3. HYRAS Grid Data (HYRAS)

The data for the HYRAS Dataset mainly comes from German weather stations, but also from stations located in Switzerland, Austria, France and the Czech Republic. It was created for the purpose to cover Germany and the catchments of the rivers Rhine, Donau and the Elbe. In this dataset there are also stations from MeteoSwiss covering the catchment of the Rhine included. So to some extent the same data as in the two other datasets was used for HYRAS as well. However the calculation of the gridded product differs.

The underlying DEM is again the USGS GTOPO30. A grid covering the desired area was created and the elevation values were interpolated to the nearest grid point center locations using ordinary Kriging.

For the precipitation the REGNIE (*German*: REGionalisierung der NIEderschlagshöhen, *English*: Regionalization of Precipitation Sums) method was used. Therefore again background fields were calculated. Here, they are created using multiple linear regression with location dependent determining factors such as latitude, longitude, height and exposition. These factors and the monthly average value (of the period 1961 to 1990) are known for each station. Using the least squares method, the regression-coefficients are calculated. The residuals of the regression are then interpolated between the stations, where all stations within 20 km to the target cell are considered. Then the regression value is added to the residual, which results in the background field value. The measured precipitation value of a single day (in the dataset used here) is then divided by the value of the background field of the corresponding grid cell. This dimensionless values are then interpolated using inverse distance weighting, but with $x = 2$ (see Formula 3.1). Now, as the final precipitation value, for every raster cell this quotient is multiplied with the background field value (Steiner, 2009).

For the temperature this is slightly different. The measurements at the stations are divided into a background value and an anomaly value. The background value is calculated using multiple linear regression of the station data, the latitude and longitude and the height. The anomaly value is then the remaining value, that can not be explained by the regression, and can therefore be compared spatially. The interpolation weights are determined by a similarity measure, so that the closer a station and the more similar its

³<http://www.swisstopo.admin.ch/internet/swisstopo/en/home/products/height/dhm25.html>
(accessed: 17.07.2014)

3. Data

values are to a certain grid cell the more weight it gets in the calculation of the anomaly value of a certain cell. This value is then added to the background value and results in the final temperature at a certain grid position (Steiner, 2009).

Since the HYRAS was created as well using the GTOPO30 DEM, the same shift as described in Section 3.2 of $-0.288\text{ }^{\circ}\text{C}$ was used to correct for the mean altitude underestimation in the catchment.

3.4. Evaporation data

Furthermore the HBV model needs an evaporation time series for its calibration. This data can be either daily values or monthly averages (Seibert and Vis, 2012). The evaporation series were calculated with Formula 3.2 from McGuinness and Bordne (1972) described in Oudin et al. (2005):

$$PE = \frac{R_e(j, lat)}{\lambda \rho} * \frac{T_a + K_2}{K_1} \quad \text{if } T_a + K_2 > 0^{\circ}\text{C} \quad (3.2)$$
$$PE = 0 \quad \text{otherwise}$$

where R_e is the extraterrestrial radiation computed according to Allen et al. (1998), which needs the day of year (j) and the latitude (lat) of the desired location as inputs. λ is the latent heat flux [2.26 MJ kg^{-1}] and ρ is the density of water [1000 kgm^{-3}]. The only kind of data that needs to be sampled is therefore the mean daily air temperature T_a [$^{\circ}\text{C}$]. The factors K_1 ($=81*1000$) and K_2 ($=5^{\circ}\text{C}$) are empirical scaling factors. Oudin et al. (2005) showed that simple equations like the one by McGuinness and Bordne (1972) are equally suitable for hydrological applications as the more physically correct and more complex equation by Penman (1948).

For the performance assessment of the weather datasets monthly averages were regarded as sufficient, since the observed period was rather short with eight years. For the climate scenarios which had a simulation time of 30 years, daily values were chosen in order to adapt to changes during the simulation.

3.5. Discharge Data

The discharge data was provided by the "Kraftwerke Sarganserland AG". It was computed from lake level observation using a volume-level relation of the Gigerwaldsee. Since the HBV model uses discharge in Millimetres, it had to be divided by the catchment area of roughly 96 km^2 . The mean discharge per month is shown in Figure 3.1.

The discharge is biggest during months May and June. In addition to that the Pardé Coefficients (Pardé, 1933) were calculated. This coefficient is calculated monthly and is defined as the quotient of the mean monthly discharge and the mean annual discharge of a station. Thereby it is possible to determine different types of discharge regimes

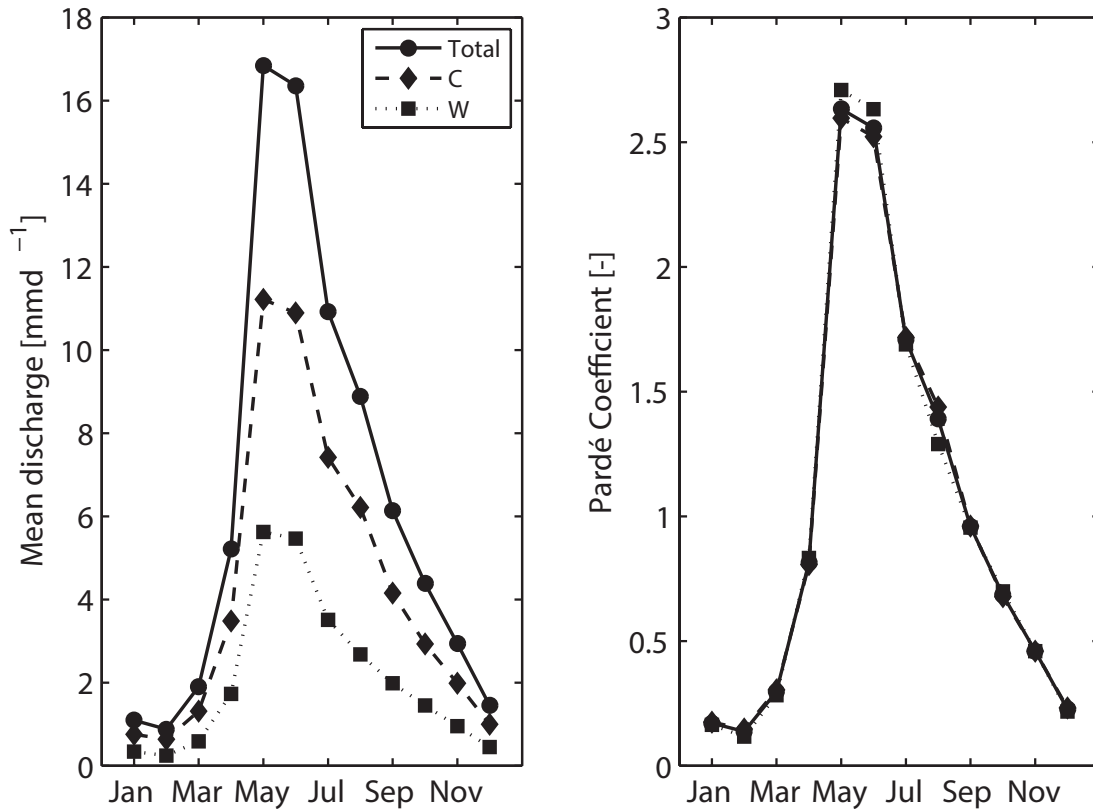


Figure 3.1.: left: Monthly average discharge into the Gigerwaldsee from 01.08.1997 to 31.12.2011. The total discharge is the sum of the discharge from Calfeisental (C) and Weisstannental (W). right: Pardé Coefficients of the three discharges on the left.

(Leibundgut et al., 1984). The Gigerwald catchment shows the characteristics of a "nival-alpin" discharge regime after Aschwanden and Weingartner (1985). This is characterised by high discharges during late spring and summer, with a peak in May and June and relatively low discharges in the winter months due to frozen conditions. Even though there are small glaciers in the catchment it does rather not fit into the "nivo-glaciare" category, since there a single peak in June would have to be present.

3.6. MODIS Snowcover Data

Satellite derived snowcover images were obtained from the MOD10A1 version 5 product of the MODIS sensor on the *Terra* satellite⁴. It uses the reflectance in bands 4 (0.545 - 0.565 μm) and 6 (1.628 - 1.652 μm). The product is provided with a resolution of 500 m at a daily time scale and is composited to prevent gaps due to cloud cover (Hall et al.,

⁴<http://nsidc.org/data/mod10a1> (accessed: 17.07.2014)

3. Data

2002). The data was available from 2001 to 2008. Using Formula 3.3 the Normalized Difference Snow Index (NDSI) after Hall et al. (1995) is calculated:

$$NDSI = \frac{band_4 - band_6}{band_4 + band_6} \quad (3.3)$$

A pixel is then mapped as snow when the NDSI is ≥ 0.4 and if the reflectance in MODIS band 2 (0.841 - 0.876 μm) is $> 11\%$. But if the reflectance in band 4 is $< 10\%$, then it is not classified as snow. Further information on the products are provided in Hall et al. (2002). The data was prepared the same way as in Finger et al. (submitted) and also provided by them.

3.7. Glacier Data

For the second part of this thesis where glaciers were included into the hydrological simulation of the HBV, several informations about the glaciers present in the catchment where needed. In order to characterize the catchment prior to the simulation runs, the relative glacierized area per elevation zone needs to be known. These were extracted from shapefiles that showed the extent of the glaciers present in the catchment. Those glacier extents were calculated using the Glacier Evolution Runoff Model (GERM) of Huss et al. (2010). The model was initialized with the glacier extents from 1973 obtained from a glacier inventory Müller et al. (1976). Only the extent of 2010 was obtained from the newer Swiss Glacier Inventory (SGI) (Fischer et al., submitted). The ice thickness distribution from the glaciers in the catchment was determined according to Huss and Farinotti (2012) by inverting the glaciers surface topography using DEMs of Shuttle Radar Topography Mission (SRTM) and Advanced Space-borne Thermal Emission and Reflection Radiometer (ASTER) satellite images and glacier outlines from the Randolph Glacier Inventory (RGI). This dataset was in turn necessary to set up the GERM to calculate the extents for 1990, 2000 and 2010.

The glacier mass balances were calculated from long-term measurements from 1985 - 2008 (Fischer and Huss, in prep.). All the available measured mass balances of the Swiss Glaciers during those 23 years were interpolated also unmeasured glaciers using the methodology of Huss (2012). Since the data was based on observational ice volume changes from the years 1985 - 2008, the values for the years 2010 and 2011 could not be calculated the same way. They were estimated from yearly mass balance measurements conducted at the Pizol glacier since 2006, which lies inside the Gigerwald catchment (Huss (2014), personal communication). All the above glacier data was provided by Matthias Huss.

3.8. Climate Scenarios

For assessing the impact of the change in future climate on the discharge regime of the catchment of the Gigerwaldsee climate scenarios are used. There exist multiple

climate scenarios that seem possible under certain circumstances concerning economic growth and social changes. There are the categories *A1*, *A2*, *B1* and *B2*. *A* stands for a world with more emphasis on the economic growth, whereas *B* stands for a rather environmental emphasis. *1* stands for a global integration of all countries and players and *2* stands for a more regional emphasis. In the *A1* scenario a market oriented world is assumed with strong economic growth. The population is assumed to peak in 2050 at 8.7 billions. Further there are three subgroups concerning the energy-technologies: The *A1F* which stands for a scenario where intense use is made of fossil energy sources, the *A1T* where non-fossil energy sources are used and finally the *A1B* where a balanced use of all kinds of energy sources is assumed (IPCC, 2008). The *A1B* scenario, which was used here, assumes an increase in carbon dioxide from 360 to 600 ppm and a global warming of 2.3°C. The other models assume an increase of 1.3 to 5°C. The *A1B* is therefore considered as a medium to slightly optimistic future scenario (Lehner et al., 2005). According to (Prein et al., 2011) the choice of the emission scenario has no big effect, only in the second half of the century the impacts become stronger, where the *A1B* lies between the *B1* and *A2* scenario (Finger et al., 2012).

Based on this scenario different institutes have generated GCMs to simulate a global climate, whereas other institutes have developed regional climate models (RCMs) to downscale the global circulation simulations to a regional scale. In the ENSEMBLES⁵ project combinations of 7 GCMs and 15 RCMs are available (van der Linden and Mitchell, 2009). From these the GCM-RCM combinations shown in Table 3.2 were downloaded from the RT2B experiments⁶. These are simulations of past and future climate ranging from 1951 up to approximately 2100 which all depend on the *A1B* scenario.

As can be seen in Table 3.2, were four different GCMs were chosen. These are the same as in Finger et al. (2012) as they were judged to be adequate for mountainous areas.

⁵<http://www.ensembles-eu.org/> (accessed: 17.07.2014)

⁶<http://ensemblesrt3.dmi.dk/> (accessed: 17.07.2014)

3. Data

Table 3.2.: Comparison of the seven climate models compared to observed and height-bias corrected climate in the period 1980 - 2009. The values are quantile-mapped and the temperatures are also height-bias corrected.

Nr	GCM	Institute	RCM ¹	MD _T ² (°C)	R _T ² (-)	MD _P (mmd ⁻¹)	R _P (-)
1	ARPEGE	CNRM	ALADIN5.1	0.001	1.000	0.015	1.009
2	ARPEGE	DMI	HIRHAM5	0.001	1.000	-0.001	1.004
3	HadCM3Q0	ETHZ	CLM	-0.013	1.002	-0.004	1.004
4	HadCM3Q0	HC	HadRM3Q0	-0.006	1.001	0.013	1.009
5	ECHAM5- r3	KNMI	RACMO2	0.000	1.000	0.023	1.016
6	ECHAM5- r3	MPI	REMO	-0.000	1.000	0.005	1.002
7	BCM	SMHI	RCA	-0.001	1.000	0.006	1.003

¹ The RCMs are available from the ENSEMBLES project (<http://ensembles-eu.org/>).

² MD represents the mean differences between each day of the scenario and the measurements. R is the ratio of the standard deviation of the datasets 1-7 and the observed data from the GRID dataset. The indices *P* and *T* are for precipitation and temperature respectively.

The GCMs normally produce results in a resolution of around 3° or 4° latitude and 4° to 10° in longitude (Prudhomme et al., 2002). Such resolutions correspond to about 330 to 440 km in latitude and to about 300 to 760 km in longitude. At such a scale a lot of the regional patterns and weather signals are lost (Prudhomme et al., 2002). A strong locality of weather phenomena can be observed in Alpine areas due to large topographic variability over short spatial distances (Daly, 2006). Therefore it comes clear that such data has a much too coarse resolution for driving hydrological models at daily resolutions such as in this study. The next step was therefore to scale the models from a global to a more regional scale, using a RCM. These RCMs are driven by GCM data as a starting and spatial boundary conditions (Akhtar et al., 2009). The resolution of these products is typically in a range of around 10 to 50 km, which is closer to the scale of the modelled processes.

Déqué et al. (2012) showed that the choice of the GCM and the RCM play a crucial role in the outcome. Therefore depending on only one model for a hydrological impact study would be too simplistic and lead to erroneous results. To account for this uncertainty seven RCMs depending on four different GCMs are chosen. These RCMs are the same as in Finger et al. (2012), who conducted a similar study for the Vispa valley in the Swiss Alps. The choice of the same GCM-RCM combinations should allow a better comparability between the two studies. Model simulations which were regarded as unrealistic such as HadCM3Q3 and HadCM3Q16 (van der Linden and Mitchell, 2009) were excluded from the study as it was done in Finger et al. (2012). To give an even weight to the used GCM, simulations with the same driving GCM were sorted out, only the BCM was available just once (see Table 3.2). The intention of the selection was to not reduce the global uncertainty of the initial 15 simulations, in order to prevent an underestimation of uncertainty (Andreas Gobiet, 2014, personal communication).

Teutschbein and Seibert (2013) point out several problems of using RCM simulations. First they are affected by random and systematic model errors. These are e.g. incorrect seasonal variations of precipitation (Christensen et al., 2008; Terink et al., 2009; Teutschbein and Seibert, 2010a) or too many simulated drizzle days (Ines and Hansen, 2006) so that in the end they do not agree with observed time series. Further they pointed out that they therefore are not suitable for hydrological impact studies. One possible solution therefore are the aforementioned ensembles of RCM simulations (Déqué et al., 2007), since the median of the ensembles may fit the observations better (Teutschbein and Seibert, 2013) and choosing multiple combinations of GCMs and RCMs has the advantage that more possible scenarios are covered and the uncertainty can be quantified better (van der Linden and Mitchell, 2009). The former is said to be especially true for temperature simulations (Teutschbein and Seibert, 2013), whereas the precipitation ensemble median often still deviates from the observed one.

Sharma et al. (2010) found that further downscaled RCMs produce better hydrological simulations than the raw RCM data. Especially for small- to meso-scale catchments like the one of the Gigerwaldsee, the RCM data is still too coarsely resolved (Teutschbein and Seibert, 2013). This bias can be corrected with empirical-statistical post processing methods (Suklitsch et al., 2010). Teutschbein and Seibert (2013) evaluated seven different bias-correction methods for five Swedish catchments and their performance compared to raw RCM outputs. They found that more complex bias-correction methods such as "distribution-mapping" performed better than for example the more simple "delta-change" method.

These methods have been evaluated for ERA40⁷ data, therefore it is not necessarily given that the findings of Teutschbein and Seibert (2013) are simply transferable to GCM-RCM datasets. It is rather believed that GCM-driven RCM-simulations contain even more uncertainties introduced by the GCM simulations (Akhtar et al., 2009; Teutschbein and Seibert, 2013). However Teutschbein and Seibert (2012) state that RCM models introduce biases by themselves due to systematic model errors (Jacob et al., 2007) because these biases occur also in models that were driven even with data at almost perfect boundary conditions (i.e. ERA40 data) Jaeger et al. (2008); Kotlarski et al. (2005); Teutschbein and Seibert (2010b).

However the transformation algorithm that was used in this work is "Distribution-Mapping" recommended by (Teutschbein and Seibert, 2013), or called "Empirical Quantiles" according to (Gudmundsson et al., 2012). In this thesis this method will be called Quantile Mapping (QM) according to several other sources in the literature (Boé and Terray, 2007; Sun et al., 2011; Wood et al., 2004). QM is based on the cumulative distribution functions (CDFs) after the empirical transformation of Panofsky and Brier (1968) (Boé and Terray, 2007). The method uses observational data and the RCM-outputs of the climate modelling chain. The reference period is observational data of the 30 years from

⁷The ERA40 is a dataset of meteorological variables. These stem from a re-analysis of meteorological observations from September 1957 until August 2002. The data was assimilated from various sources of observational methods by the European Centre for Medium-Range Weather Forecasts (ECMWF) (Uppala et al., 2005).

3. Data

1980 to 2009 from MeteoSwiss GRID Dataset, which was also used to calibrate the HBV model (see Section 3.2). The CDF of both the observed and the simulated data are created. Then, for every day, and every one of hundred percentiles the value of the simulation is replaced by the observed value from the same percentile at the day. This results in a function which is then applied to the whole RCM output (Sun et al., 2011). This is done for temperature and precipitation time series. An example result is provided in Figure 3.2.

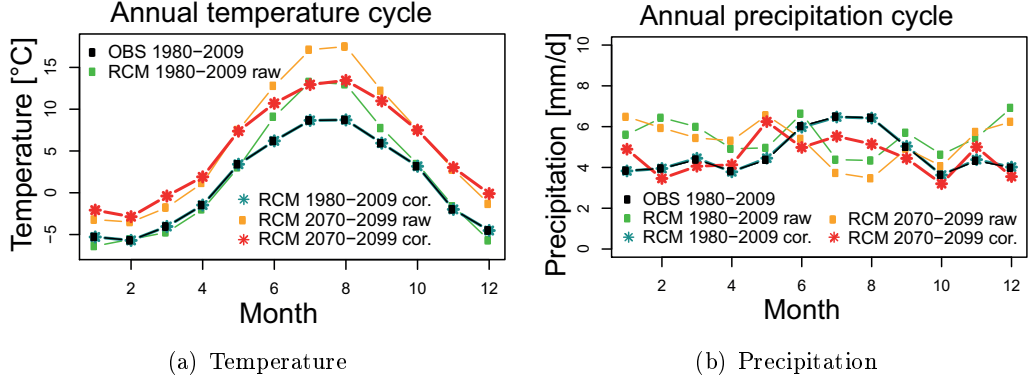


Figure 3.2.: Bias correction using QM of the simulated (a) temperature and (b) precipitation during the calibration period 1980-2009 and an example simulated scenario from 2070-2099. The underlying model is number (3) from Table 3.2. Figures have been adapted from N. Addor (2014)

The underlying assumptions of bias corrections like QM are that the model error does not change over time (Teutschbein and Seibert, 2013). Further the bias correction is done for the precipitation and temperature separately, which adds some uncertainty to the end result, so that a single day can turn out differently, however the characteristics of a specific day are surely preserved. Further their statistical variability is not the same as for observed weather for periods shorter than a month (Nans Addor, 2014, personal communication).

The images of the different CDFs show a clear correction of the bias in the datasets of the RCM against the observational values. The corrected values show the same distribution throughout the year as the observational values that were used as ground truth. The corrected datasets described above were provided by Nans Addor.

As it was already done before in section 3.2, the temperature series was corrected again for the bias in altitude.

However the data was not yet ready to use. Some of the climate scenarios consisted of years with 360 days, where every month has 30 days. This was corrected by adding a 31st day where necessary. The value of this day was a random value out of the same month, but never the value of the 30th. This was done to prevent the same event to occur two days in row. Especially if the 30th happens to be an extreme event, it is unlikely to have the same extreme event two days in a row. In February the 30th and 29th, or only the

30th day was deleted, depending on whether the year was a leap year or not.

After having corrected the climate scenarios they were used to create different scenarios for using them as input in the HBV simulations for the future. Most of the bias-corrected data is available from 1951 to 2099. Some of the RCM simulations start at 1961 and others only reach until the 31st of December in 2098. Therefore the periods for the scenarios were selected the following way: Three scenarios of a length of 30 years were produced: 1992-2021 as a reference period for the current climate, 2036-2065 as a mid term period and 2069-2098 as the long term period. These years were chosen to get scenarios representing medium term impacts in the middle of the century and long term impacts at the end of the century.

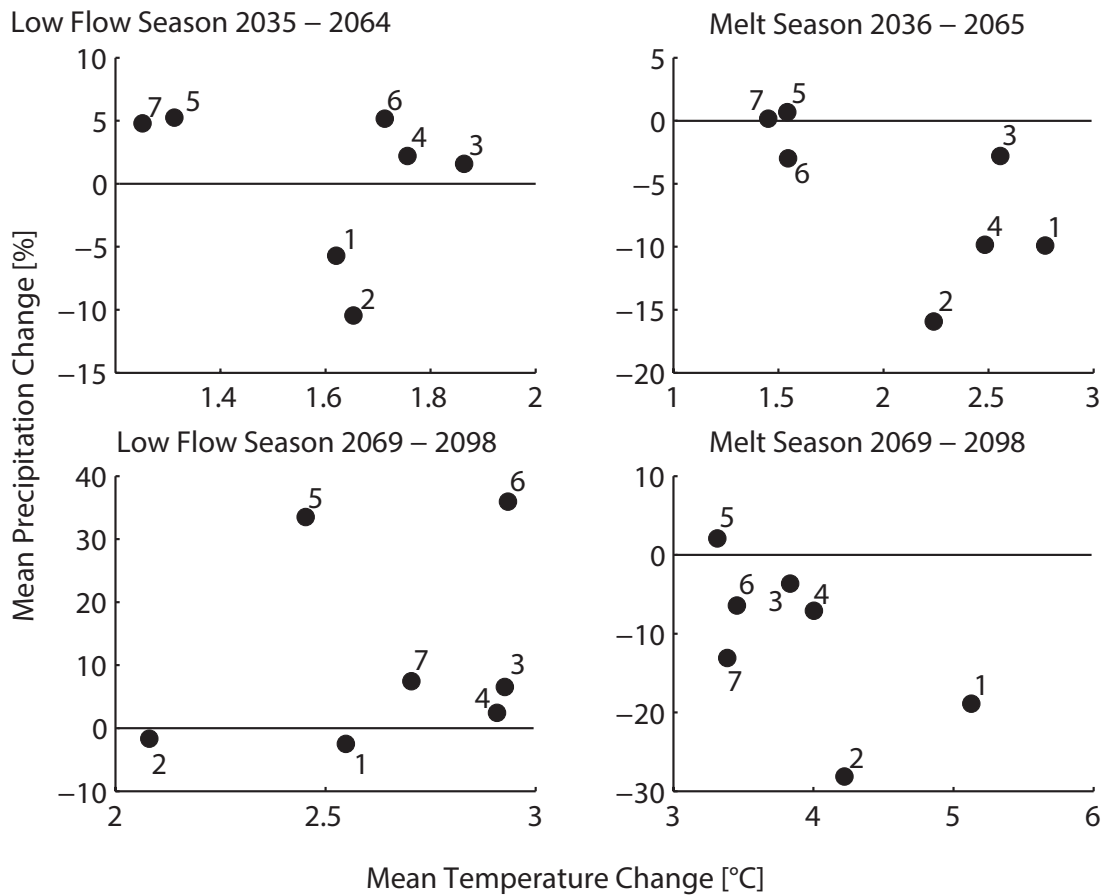


Figure 3.3.: Modelled climate changes in temperature and precipitation from the reference period (1992 - 2021) and the mid- and long-term scenarios, divided into low flow (January - April) and melt season (May - September). The numbers 1 - 7 correspond to the model combinations in Table 3.2.

The changes in the low and high flow seasons in the two scenarios in the mid-term and the long-term can be seen in Figure 3.3. All models predict rising temperatures for

3. Data

both periods of the year, whereas the changes later in the century are bigger. The spread of temperature rise in the low-flow season of the mid-term scenario is relatively narrow between 1.25 and 1.86 °C. In the melt season the spread is bigger (1.45 - 2.77). The development of the precipitation in the low flow season is rather uncertain. Five models predict a slight increase whereas two models with the ARPEGE-GCM predict a relatively large decrease (-10.47 - -5.72). In the melt season of the same period, five out of seven models foresee a decrease in precipitation (-15.93 - -2.56 mm). In the long-term period the spread of the temperature increase is again narrow (2.08 - 2.93 °C), but the difference to the baseline period (1992 - 2021) is bigger. Again in the melt season the spread is bigger compared to the low flow season, as well as the rise compared to the mid-term period (3.31 - 5.13 °C). The precipitation in the long-term period again rises in all GCMs except for the ARPEGE (-2.50 - -1.66). The model ECHAM5-r3 produces by far the highest values (33.52 and 35.94) the models HadCM3Q0 and BCM predict lower increases (2.45 - 7.50 mm). During the melt season the precipitation diminishes in all models but the ECHAM5-r3-KNMI-RACMO2 (2.08 mm) with a relatively large spread (-28.14 - -3.64 mm). The ARPEGE models constantly (the highest) precipitation decrease. Compared to Finger et al. (2012) the ranges are very similar and the relative changes of the models are often the same.

The spread of the data can also be seen in the long term mean annual values in Figure 3.4. However the inter-seasonal differences are not visible there. The rise in temperature that already occurred during the last decades is however visible. Further the temperature seems to be rising rather linear until 2099. The precipitation however shows no clear trend, there only inter seasonal trends could be found as was shown before. Further, a feature of climate models can be seen nicely here. The modelled datasets show magnitudes and frequencies similar to those of the observations but not at the same time. But since these models are only statistically correct over longer time-scales, a correct timing of single events is never given. Towards the end of the 21st century the variation of the climate scenarios gets a little bigger, there the model calculations start to differ more and more from each other.

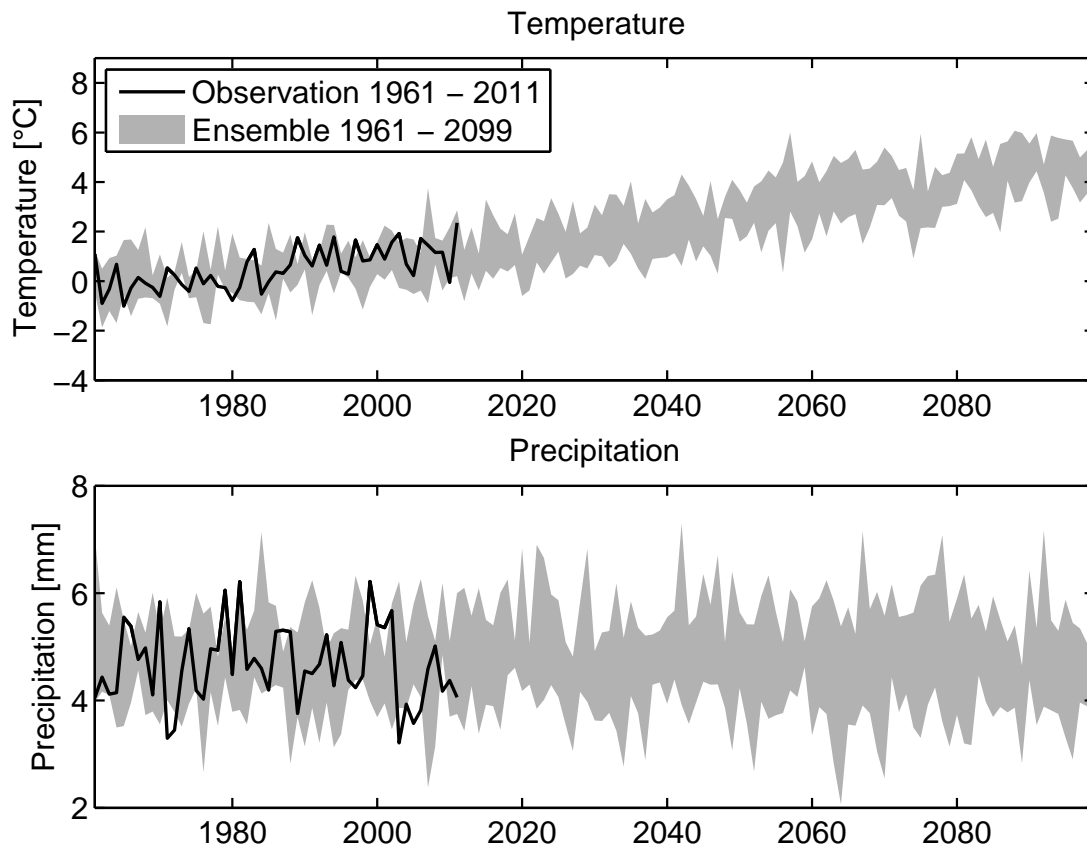


Figure 3.4.: Annual mean observed temperature and precipitation series from 1961 to 2011 and the simulated bias corrected GCM-RCM ensembles from 1961 to 2099.

4. Methods

4.1. Statistical Comparison of the Weather Datasets

To compare the three weather datasets some simple statistical indices were calculated using the Statistical Package for the Social Sciences (SPSS) (IBM Corp. Released, 2012). These are the minima, maxima, mean, median, standard deviation and the number of extremes above the 95% and below the 5%-quantile of all three datasets for the temperature data. (For the precipitation data the minimum is always 0 and therefore neglected.) Furthermore the maxima, the mean, the standard deviation and the extremes above the 95% quantile of all datasets was calculated. Additionally the mode was calculated. The mode is more robust to extremes, by just giving the most frequent value, whereas the mean is very sensitive to extremes which are typical for precipitation data. Whereas the median is more sensitive to the number of extremes Panofsky and Brier (1968). Furthermore some statistical tests were conducted to determine whether the differences between the three datasets were significant. These are the Kolmogorov-Smirnov-Test to determine whether the data is normally distributed. And afterwards the Friedman-Test to test whether the central tendencies of the weather datasets are significantly different or not.

4.2. The HBV Model

The HBV model was originally developed by Bergström (1976). The latest published version offers the possibility to include glacierised areas. It is described in Seibert and Vis (2012). For this thesis the HBV-model was updated with a glacier routine that dynamically adjusts the glaciers during the simulation once in a year. The benefit of including glacier mass balances in the HBV was shown before in Konz and Seibert (2010), however there the glacier areas did not change in extent over time.

The HBV model used in the study of the comparison of the weather datasets was a version published in February 2014. In this version it is possible to calibrate for snow cover. The calibration for glacier mass balances was not yet implemented when the studies for comparing the three weather datasets were done. (The glacier routine is explained in Section 4.5.1.) Since the modelled time period is rather short with four years of calibration and four years of validation, the glaciers are not expected to have a big influence anyway.

4.2.1. Model Structures

The HBV model comes with a number of possible structures, that take account of differing characteristics of a catchment. These include differing configurations of the upper soil zones, snow zones, various numbers of groundwater boxes and combinations of the above.

First some preliminary runs with data from the Gigerwald catchment where done. These runs showed no significant differences in their performances, therefore it was decided to stick to the standard version, which is shown in Figure 4.1. The standard version uses an overflow mechanism so, that there is additional runoff generated from the upper soil zone (*SUZ*) if the water hold capacity (*UZL*) is exceeded. Further the *SUZ* generates a steady runoff $Q1$ and also propagates its water partly into the lower soil zone (*SLZ*). From there it is partly evaporated or guided also into the runoff ($Q2$).

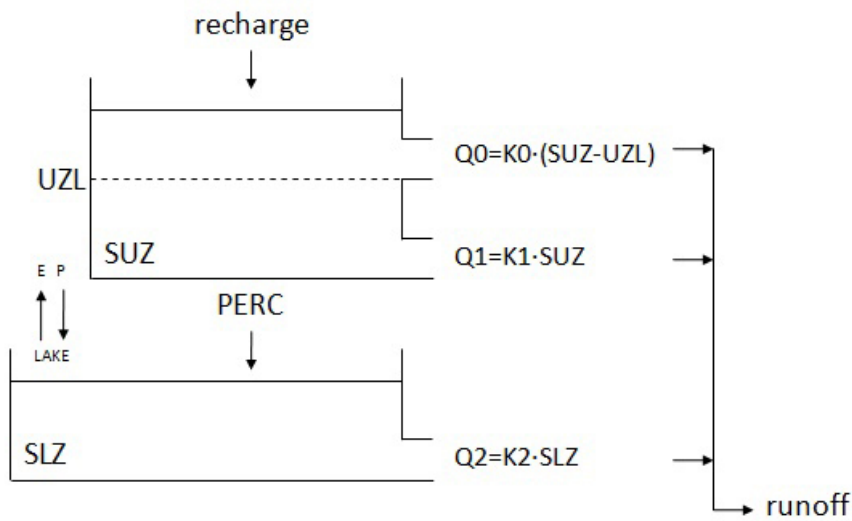


Figure 4.1.: Scheme of the HBV model soil-routine (Source: Seibert and Vis (2012))

Furthermore the model also accounts for the glacierised areas in the catchment. The determination of the glacierised area is described in Section 4.2.2. Using this feature, the different elevation-vegetation units can be characterized as glacier or non-glacierised area. These areas remain constant during the simulation in the version from February 2014, although runoff is also generated from these areas (Seibert and Vis, 2012).

4.2.2. Catchment Characterisation

To adapt the model settings of the HBV to the watershed of the Gigerwaldsee several operations had to be done with the geographic information system ArcGIS (ESRI, 2011). Since the catchment does not consist of only a naturally confined area, but also of the catchments of the neighbouring Weisstannental, the water intakes had to be localized as "pour points" (see table 2.1) to derive their catchments. In the end the natural catchment of the Gigerwaldsee as well as the eight catchments of the water intakes were merged into one single polygon in order to be modelled in HBV.

4. Methods

The HBV can be run with different altitude and vegetation zones. This makes it a semi-distributed model (Seibert and Vis, 2012). It would have been possible to generate multiple vegetation zones, but an increased model complexity does not necessarily lead to better simulation results (Finger et al., submitted). This was confirmed by the results of some preliminary test runs with three vegetation zones including forest and open soils or grass land. Therefore the catchment was split up into two zones, which simply consist of glacierized and non-glacierized areas, regardless of soil and vegetation type.

The DEM of the catchment was divided into 11 elevation zones, each covering 200 meters in altitude. Each of these elevation bands was split up further into three exposition groups: North, South and East/West combined. Each grid cell with a height and an elevation was then given a value of either one of the two zones. Thereby the relative amounts of glacierized and non-glacierized areas were determined for every elevation band and exposition.

For the comparison of the three weather datasets this model complexity was adequate to run the model. For the climate scenarios some more steps had to be done in order to characterize the glacier in more detail. Smaller elevation zones in steps of 10 m were determined. Again the amount of glacierized area relative to the entire catchment was determined. This time the operations were of counting the relative values were conducted using the commercial software package MATLAB (TheMathWorks Inc., 2013) since the amount of elevation zones had become too big to be easily handled using ArcGIS. Furthermore also the glacier water equivalent (WE) per elevation zone had to be known. This was done using the glacier thickness data described in Section 3.7. The glacier thickness was distributed on the elevation zones and then multiplied with a constant ice density of 900 kg/m^3 in order to obtain the WE for every 10 m elevation zone.

4.2.3. Performance Measures

The following efficiency measures were used in this thesis for assessing the performance of the HBV-simulations. These functions are all part of the used HBV-light model versions and were therefore regarded as given.

Nash-Sutcliffe Efficiency

The most commonly used performance measure in HBV is the Nash-Sutcliffe efficiency (see Formula 4.1). The formula by Nash and Sutcliffe (1970) compares the observed (Q_{obs}) discharge value with the simulated (Q_{sim}) at time steps $i - n$. The squared difference between the two is summed up and this sum is then further divided by the sum of the squared differences between the observed values and the average of the observed values. This is then subtracted from 1:

$$E_{NS} = 1 - \frac{\sum_{i=1}^n (Q_{i,obs} - Q_{i,sim})^2}{\sum_{i=1}^n (Q_{i,obs} - \overline{Q_{obs}})^2} \quad (4.1)$$

Thereby it is examined whether a simulation is better than a simulation by just looking at the mean of the observations. A perfect fit occurs at $E_{NS} = 1$. If it is below zero, the simulation is worse than the a simulation by simply taking the average discharge of the observations. Because of the squared differences this goodness of fit function gives more weight on high flow events. Since there the differences are generally bigger, the squaring of the differences puts more weight on those events than on low-flow events. Therefore also the Logarithmic Nash-Sutcliffe efficiency is used (see Formula 4.2). However this function has been used to determine model performance in a number of studies using the HBV model (Akhtar et al., 2009; Seibert and Uhlenbrook, 2000; Teutschbein and Seibert, 2012) and other models Finger et al. (2012, 2011).

Logarithmic Nash-Sutcliffe Efficiency

To introduce an estimate of model performance that gives more weight to the low flow season the logarithmic Nash-Sutcliffe efficiency is used. By using logarithmic discharge values the weight is more evenly distributed over all kinds of events.

$$E_{LogNS} = 1 - \frac{\sum_{i=1}^n (\ln(Q_{i,obs}) - \ln(Q_{i,sim}))^2}{\sum_{i=1}^n (\ln(Q_{i,obs}) - \overline{\ln(Q_{obs})})^2} \quad (4.2)$$

Volume Error

The volume error function looks at the modelled amounts of discharge. By dividing the sum of the absolute differences between the observed and simulated discharges by sum of the observed discharges the fraction should ideally be 0, which would result in an optimal volume error of 1.

$$E_{VolErr} = 1 - \frac{|\sum_{i=1}^n (Q_{i,obs} - Q_{i,sim})|}{\sum_{i=1}^n (Q_{i,obs})} \quad (4.3)$$

Snowcover RMSE

The Snowcover Root-Mean-Square Error (RMSE) in Formula 4.4 is a statistical measure to calculate the between the simulated snow cover (SC_{sim}) and the observed snowcover (SC_{obs}) of the entire catchment at time steps i to n . The snowcover is represented in fractions and ranges from 0 for no snowcover to 1 for an entirely snow covered catchment. By subtracting the root of the mean squared error from 1, the perfect match between observations and simulation would result in a RMSE of 1.

$$E_{SCRMSE} = 1 - \sqrt{\frac{1}{n} \sum_{i=1}^n (SC_{i,sim} - SC_{i,obs})^2} \quad (4.4)$$

4. Methods

Glacier Mass Balance Nash-Sutcliffe Efficiency

To be able to compare the performance of the generation of glacier mass balances over one hydrological year (October 1st - September 30th) the Glacier Mass Balance Nash Sutcliffe Efficiency (E_{MB-NS}) in Formula 4.5 has been introduced in the latest version of the HBV-light (June 3rd 2014):

$$E_{MB-NS} = 1 - \frac{\sum_{y=1}^m (MB_{y,obs} - MB_{y,sim})^2}{\sum_{y=1}^m (MB_{y,obs} - \overline{MB_{obs}})^2} \quad (4.5)$$

It compares the modelled glacier mass balance (MB) to external data, be it from a model or from measurements. The procedure is the same as in the calculation of the Nash-Sutcliffe Efficiency (NSE) for the discharge in Formula 4.1. The difference here is that the MBs are measured over a whole year (y), and therefore the no daily values are calculated.

The mass balance calculated in the model or used for the input file is not directly observable in nature. The MB of a point in time (y) consists of the relative area covered by glaciers (A_{rG}) at the start of the simulation (i.e. warm-up period) multiplied by the cumulative sum of WE-loss/gain over the whole simulation period, starting (always) with a value of zero at the day the warm up period of the simulation starts:

$$MB_y = \sum_{y=1}^m \delta W E_y * A_{rG} \quad (4.6)$$

Therefore the mass balances calculated according to Formula 4.6 are measured in mm relative to the initially glacierised area.

4.3. Comparison of Different Model Runs using Multivariable Calibration

Different datasets and multiple objective functions to calibrate hydrological models have been used in different studies in the past. The goal of the hydrologists was to limit the parameter sets to a certain part of the parameter space in instead of multiple equifinal sets of different places in the parameter space (Franks et al., 1998). Further a proper validation of the processes represented should also include an internal validation by comparing internal processes of models (Ambroise et al., 1995). Besides Finger et al. (2012) and Konz and Seibert (2010) multiple datasets were also used by many other authors. Since the 1990s different additional observational datasets were used in hydrological models. These were e.g. groundwater data (Kuczera and Mroczkowski, 1998; Seibert, 2000), saturated zones (Franks et al., 1998), salinity data (Kuczera and Mroczkowski, 1998), snowpack and soil water data (Ambroise et al., 1995). More recently for glacierised catchments also glacier mass balances at different time scales (Konz and Seibert, 2010;

4.3. Comparison of Different Model Runs using Multivariable Calibration

Schaefli and Huss, 2011) combined with snow cover data (Finger et al., 2012, 2011, submitted) where used.

Especially in mountainous watersheds where glaciers and snow are present the demand for such additional observational datasets is provides additional information to constrain the model parameters since the runoff is not only generated by rainfall but also by snow and glacier melt (Finger et al., submitted).

In the HBV model the model runs are evaluated in terms of the objective functions in Section 4.2.3. In the first part of this work four out of the five aforementioned objective functions where used. The Glacier MB NSE was not used in the comparison of the weather datasets, since the version of the HBV-light model used at that time did not yet support this feature. The four remaining objective functions cover several aspects of the discharge characteristics and also the snow covered area. The selection of these objective functions is assumed to represent the relative importance of the variables runoff and snow cover for the operation of the dammed lake. I assume that a well modelled fraction of the snow covered area is less important than a well represented discharge importance for the operators. The runoff, or rather the water running into the lake is assumed to be of highest importance. Accordingly the snow cover only accounts for one fourth of the objective functions.

For the evaluation of a possible benefit of the model performance the effects of several combinations of the objective functions to their own performance scores is explored. First a simulation using only objective functions evaluating the discharge performance are used. These are the NSE, LogNSE and the Volume Error each accounting for one third of the total. Then the discharge objective functions combined with the snow cover (SC) RMSE. In addition calibration to SC only was done too. The model was calibrated using a Monte Carlo (MC) simulation with 150'000 runs. From the whole amount of parameter sets, the Pareto optimal parameter sets where selected with the help of a Matlab-Script (Polityko, 2008). The function in the script checks for each parameter set if it performs better in at least one out of the four objective functions compared to every other parameter set. Only if this is fulfilled it is selected as a Pareto optimal set. They represent parameter combinations that reach scores in their objective functions such that the score of one function can not be improved without reducing the score of the others. This is done in a four dimensional space using all of the four objective functions during the period from 2006 - 2011.

From the Pareto Points in terms of the selected objective functions NSE, LogNSE, Volume Error and SC RMSE the values above a threshold of 0.8, for the functions NSE, LogNSE and SC RMSE and 0.95 for the generally very good scores in Volume Error respectively, where then selected. With this method a different number of sets is selected for every combination of objective functions.

4.4. Performance Assessment of the Weather Datasets

4.4.1. Model Calibration 1999 - 2002 and Validation 2003 - 2006

In order to calibrate the HBV model for each of the three datasets a MC simulation was applied to test a large amount of random parameter combinations (Seibert and Vis, 2012). In a first run the three datasets were tested with the default parameter values of the HBV, except for the values for the measurement stations for temperature and precipitation (*Telev* and *Pelev*). Then some scatter-plots, similar to those in Figures A.1, A.2 and A.3 in Appendix A.1.1 with the complete parameter space of 150'000 sets were created. From these it could be seen which parameters had their best performance (using the Nash-Sutcliffe efficiency in Formula 4.1) just at or close to their user-defined limits. Especially for the HYRAS dataset the range for the height of the precipitation measurements (*Pelev*) had to be lowered to around 1000 m to make it perform better. For the parameters *SCF*, *CFMAX* and *Pelev* the limits had to be expanded slightly in comparison to the recommended values in Seibert and Vis (2012). The MC simulation was run again with the new parameter settings until the scatter plots showed no more limitation of performance to possible parameter ranges (see Figures A.1, A.2 and A.3).

The optimal parameter sets could then be searched for depending using the the method in 4.5.2 and on the preferences of the author (Confesor and Whittaker, 2007). Depending on whether more focus was laid on the low flow, the peak flow or the overall volume one or another combination can be selected. Since for a dammed lake no simple decision for one efficiency measure can be made, the set of all four parameters was selected.

The above tests are designed to show whether the three tested datasets provide a useful source of information for the HBV model. However, from calibration only, it is not yet clear if the model would also perform well in a period different to the calibration period. Especially since at least the GRID dataset is intended to be used for the creation of future scenarios it is important to get an estimate of the model performance under conditions different to those during the calibration period. Therefore the models were tested using a split-sample test (Klemeš, 1986). Data for all three weather datasets and discharge data which cover the same period is only available for nine years and five months from 01-08-1997 until 31-12-2006. According to Seibert and Vis (2012) one year of warm up period is sufficient for the HBV model. To get a proper start at January 1st, the warm-up period was set to end at the 31-12-1998 and thus covers 17 months. The calibration period was set to four years from 01-01-1999 to 31-12-2002 and the validation period to 01-01-2003 to 31-12-2006. This split has the advantage to include the same two extreme events, the extremely dry year 2003 and the year 2005 with an extreme precipitation event in August (Bezzola et al., 2008), into the validation period as proposed in Koboltschnig et al. (2008), using the PREVAH model (Gurtz et al., 1999) with hourly discharge data. A drawback of this setting is the further reduced weight (i.e. 1/8) of the MODIS snowcover data compared to the discharge data due to its limited availability of only the years 2001 and 2002 during the calibration period.

These parameter combinations were then used in Batch Runs inside the HBV model to create multiple equifinal model simulations which were then evaluated using the NSE

and the LogNSE, since the other objective functions are not available in the results of batched runs.

Using the above process the three weather datasets GRID, HYRAS and IDW are evaluated and rated according to their performance in HBV model simulations over the same periods of calibration and validation.

4.5. Discharge Scenarios

4.5.1. HBV Simulations

The HBV model was used again in order to calculate future discharge in the Gigerwaldsee catchment. The model was calibrated again to measured discharge, snow cover and this time also glacier mass balances. The period chosen for calibration were the years from 2006 to 2011. This way not only the special years 2003 and 2005, but also the heavy precipitation events on melting snow in 1999 Aschwanden (2000) is included in the validation. The only drawback is, that MODIS snow cover data is only available from 2001 to 2008. Therefore only three years of calibration using snow cover can be evaluated. Which again reduces the final weight of the MODIS snowcover data from $1/4$ to $1/8$.

New HBV Glacier Routine

In the version of the HBV model that is used for the simulation of the climate scenarios a new routine that calculates the evolution of the extent and the water equivalent of glaciers over time was implemented. This part of the model was originally designed by Huss et al. (2010). The so called Δh -parametrization (see Formula 4.7 calculates the glacier surface elevation change in response to a change in mass balance. The parametrization of thickness change in the model of Huss et al. (2010) is done using DEM differences where data is available or, where no DEMs are available, by empirically derived parameters of known similar glaciers and the following formula:

$$\Delta h = (h_r + a)^\gamma + b * (h_r + a) + c \quad (4.7)$$

where h_r is a normalized elevation range and is calculated from $(h_{max} - h)/(h_{max} - h_{min})$. h_{max} and h_{min} are the maximum and the minimum glacier surface elevation. The parameters a , b , c and γ are empirically derived constants that change according to glacier size. Glaciers are classified as large ($>20 \text{ km}^2$), medium (between 5 and 20 km^2) and small ($<5 \text{ km}^2$) valley glaciers. The surface changes are calculated spatially distributed. At the end of the hydrological year the glacier extent is updated. The gained or lost ice volume is converted into a distributed thickness change under the assumption of immediate redistribution of surface accumulation due to ice flow. To give the aforementioned outputs the model needs a DEM and glacier outlines and the spatial distribution of surface mass balance calculations from differing models as well as estimates of the bedrock topography for ice thickness distributions and total ice volume.

4. Methods

The formula for the annual calculation of the change in glacier mass B_a in Huss et al. (2010) is as follows:

$$B_a = f_s * \rho_{ice} * \sum_{i=0}^{i=h_r} A_i * \Delta h_i \quad (4.8)$$

Since the HBV model is semi-distributed (Seibert and Vis, 2012) it can not take any DEM informations directly. Therefore the information about ice thickness and volume changes is calculated using the water equivalent as a parametrization of amounts of ice or changes in glacier thickness in Formula 4.7. The water equivalent has to be given to the model inside a file, with amounts of WE per elevation. Before any hydrological simulations are started, the model calculates a lookup table for possible glacier melt scenarios. Inside that table there are the resulting glacier areas for every elevation zone specified in the model resulting from glacier melt in 1%-steps of the total glacier volume. The volume is calculated by multiplying the area (specified in an input file) with the water equivalent. Then for each 1%-step at every elevation the normalized water equivalent change is computed according to Formula 4.7. However instead of the thickness change, the change in water equivalent is computed. The value for f_s in Formula 4.8 is then calculated based on that glacier volume change, i.e. change in water equivalent which corresponds to every percent of melt. The formula used in the HBV looks as follows:

$$\Delta WE_a = f_s * \sum_{i=0}^{i=h_r} A_i * \Delta h_i \quad (4.9)$$

ΔWE_a is known from the loss of glacier mass, i.e. glacier water equivalent of 1%, and δh_i is calculated from Formula 4.7 and A_i is known from an input file.

Then for each elevation the new water equivalent is computed according in the following way using f_s :

$$WE_1 = f_s * WE_0 + f_s + \Delta WE_i \quad (4.10)$$

where WE_1 is the updated water equivalent for the initial water equivalent WE_0 .

Then for each of the elevation zones (in 200 m steps) the new glacier area is computed. This is done by subtracting all areas from all elevations within a zone with a new water equivalent of <0 . This results in the aforementioned lookup table where the resulting glacier areas in the different elevation zones per percentage of melt are specified.

During the hydrological model simulation, using the degree-day method the glacier melt is calculated in mm. This melt is added to the water content of the glacier. The outflow of the melted water is then computed according to Stahl et al. (2008):

$$Q_{t,g} = KG(t,g) * S(t,g) \quad (4.11)$$

where $S(t,g)$ is the liquid water stored in the glacier water content of an elevation zone g at time t and $KG(t,g)$ is an outflow coefficient varying with time as a function of the

water equivalent in the glacier elevation zone g at time t :

$$KG(t, g) = KG_{min} + dKG * \exp[-AG * WE(t, g)] \quad (4.12)$$

where in Stahl et al. (2008) KG_{min} is a minimum value that represents conditions with only minimal outflow and $KG_{min} + dKG$ represents the outflow coefficient at maximum outflow, this two parameters are determined by calibration in the HBV model. AG is a calibration parameter as well, both in Stahl et al. (2008) and the HBV implementation and WE is the water equivalent of the glacier elevation zone g at time t .

Finally in each hydrological year and based on the percentage of melt in comparison to the original glacier volume, the corresponding glacier areas are selected from the lookup table and applied to the different elevation zones. In order to make sure that the glacier volume does not change due to resizing areas, the melted glacier water, which was not routed into runoff in the declining areas is being redistributed from the melted area to the non-melted area.

4.5.2. HBV Calibration for Climate Scenarios

For the determination of equifinal parameter sets the HBV was calibrated during the years 2006 - 2011. Compared to the calibration in Section 4.3 the procedure was changed slightly. The used weather dataset was the GRID dataset. The decision for the GRID dataset was made before finishing the comparison of the weather datasets. Since the QM of the climate data was therefore done using the GRID dataset and also due to time constraints it was decided to not switch to the HYRAS dataset. Furthermore the differences between the GRID and the HYRAS dataset were rather small anyway.

As explained in Section 4.5.1 the glacier routine for dynamically adapting glaciers of the HBV-light is used here for the first time. Therefore also glacier mass balances and more detailed glacier areas were needed. From the data described in Section 3.7, the relative amounts of glacierised area in the catchment were calculated. They were determined for small range elevation zones of only 10 m. Further the water equivalent in the same zones was derived from the glacier thicknesses described in Section 3.7 by multiplying with a constant density of 900 kg/m^3 . For calibration to glacier MB an input file with observed annual mass balances that were interpolated to unmeasured glaciers (Huss, 2012) was needed.

Finding the optimal parameter sets

As it is shown in Finger et al. (2011) and Finger et al. (submitted) the use of multiple datasets allowing to calibrate to multiple datasets leads to a higher model consistency and therefore creates discharge simulations that are right for the right reasons. The parameters were selected according to their performance in the five objective functions in Table 4.2. From another MC simulation with 150'000 runs with the parameter ranges in Table 4.1 every parameter set which contained any negative objective function score was removed. This way the big dataset was made smaller in order to get shorter computation times for the Pareto point calculation, which resulted in 7221 parameter sets. In contrast

4. Methods

to Section 4.3 the Pareto points were calculated from all parameters (except the ones containing negative values) directly. Then, the remaining 159 Pareto points (see Figure 4.2) were ranked as in Finger et al. (submitted). Each of the five objective functions should have been ranked over all parameter sets. The resulting ranks for every objective function of every parameter set were averaged and this was considered as the rank for the parameter set. However as was seen after applying those parameters, the results were rather bad when using all five objective functions, especially the modelled discharge in spring was strongly underestimated. After some tries, the best possible solution was found if the Glacier NSE was only used for the Pareto calculation but not for ranking the Pareto optimal parameter sets. So in the end it can be said that the discharge data has a weight of $27/40$, the MODIS snowcover data has $9/40$ and the glacier data $4/40$.

The 10 sets with the best ranks were selected and regarded as being equifinal (Beven, 2012) and are shown in Figure 4.2. The resulting objective function ranges of the final selection can be found in Table 4.2. By looking only at Pareto Points one does not necessarily get the points with the highest overall scores, but they are definitely a good compromise between all the objective functions and are more likely to be a local optimum in the parameter space. This can partly be verified by the widely scattered parameter values in nearly all parameters in Figure 4.3 and also shows nicely the equifinality of different parameter sets, they all have a comparable overall performance but use values from very different parts of the parameter space.

Compared to the studies of Finger et al. (2012, 2011, submitted) where only 10'000 MC simulations were done, the 150'000 runs done here seem quite a lot. However this way the probability increases for finding more better performing solutions to the equifinality problem (Beven, 2012) increases. However the parameter space is not really explored better. If we do the math, we take the 33rd root (for 33 parameter to calibrate) of 150'000 the number of resulting tries for every parameter is around 1.45 and for 10'000 it is 1.32. The number of runs may therefore be a bit high, but it does not make the results worse.

Those 10 sets of parameters were then used to drive the HBV-light model with the temperature and precipitation datasets from the seven climate scenarios. The results can be found in Section 5.2.3. Their performance was then evaluated during the calibration period from 2006 - 2011 and the preceding seven years from 1999 - 2005 as validation period. That way the special years 1999, 2003 and 2005 can be evaluated. Those results can be found in section 5.2.2.

Benefit of Calibration using Snowcover and Glacier Mass Balances

To assess the benefit of using multiple objective functions and input datasets several combinations of the former have been tested. The model was run with the same configuration and input data of temperature, precipitation, potential evaporation, discharge, fraction of snow covered area and glacier mass balances. The multi criteria evaluation was done based on the Pareto points for every combination. That way the effect of combining different objective functions can be seen more clearly. It was done for every combination of the three groups: Q (consisting of NSE, LogNSE and Volume Error), SC

Table 4.1.: Initial parameter ranges of the HBV-light model for the MC-simulation

Paramter	lower limit	upper limit
<i>KGmin</i>	0.01	0.2
<i>dKG</i>	0.01	0.5
<i>AG</i>	0	10
<i>PERC</i>	0	4
<i>UZL</i>	0	70
<i>K0</i>	0.1	0.5
<i>K1</i>	0.01	0.2
<i>K2</i>	0.00005	0.1
<i>MAXBAS</i>	1	6
<i>PCALT</i>	1	20
<i>TCALT</i>	0.1	1
<i>Pelev</i>	1000	2500
<i>Telev</i>	1000	2500
<i>TT</i>	-2	0.5
<i>CFMAX</i>	0.5	10
<i>SFCF</i>	0.5	0.9
<i>CFR</i>	0.05	0.05
<i>CWH</i>	0.1	0.1
<i>CFGlacier</i>	0.1(1 where no glacier)	5 (1 where no glacier)
<i>CFslope</i>	1	5
<i>FC</i>	100	550
<i>LP</i>	0.1	1
<i>BETA</i>	1	5

Table 4.2.: Ranges of the selected parameter sets.

Objective Function	Range of the 10 best Sets
NSE	0.69 - 0.87
LogNSE	0.76 - 0.86
Volume Error	0.87 - 1.00
Snowcover RMSE	0.79 - 0.81
Glacier Mass Balance NSE	0.23 - 0.97

4. Methods

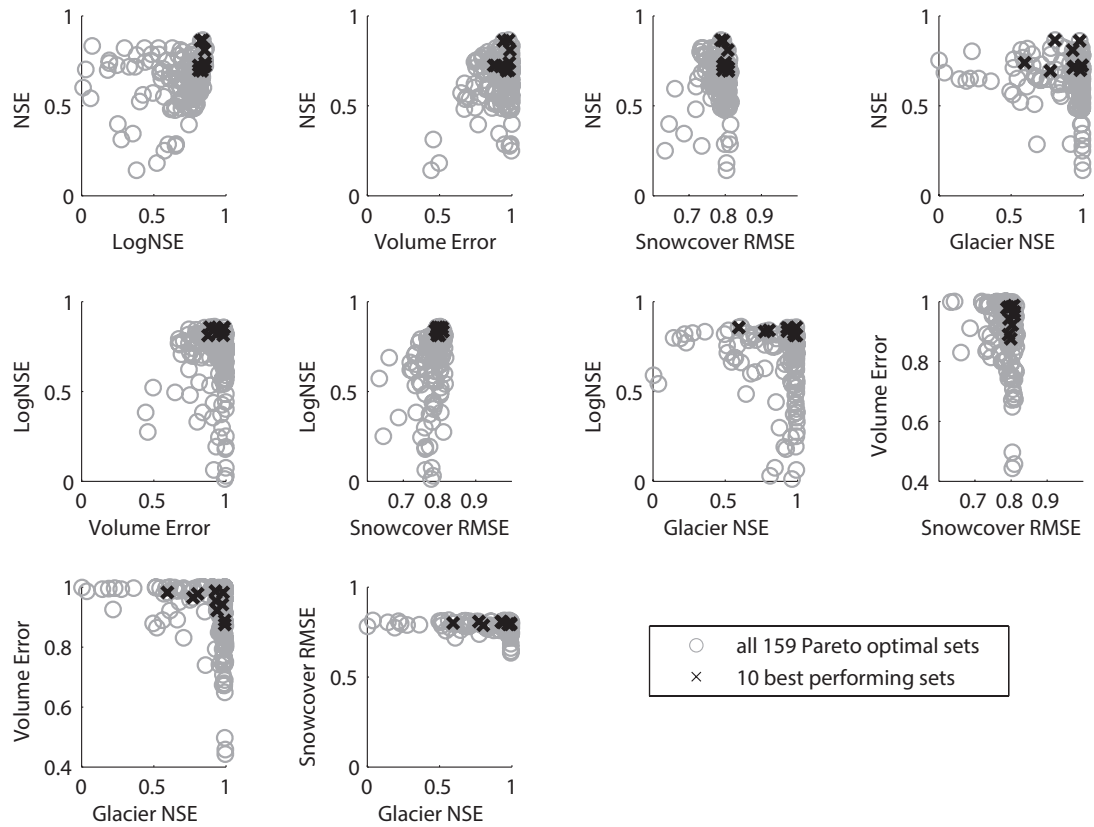


Figure 4.2.: The selection of the 10 equifinal parameter sets for the calculation of the climate scenarios out of the 159 Pareto points from 150'000 parameter sets (not displayed).

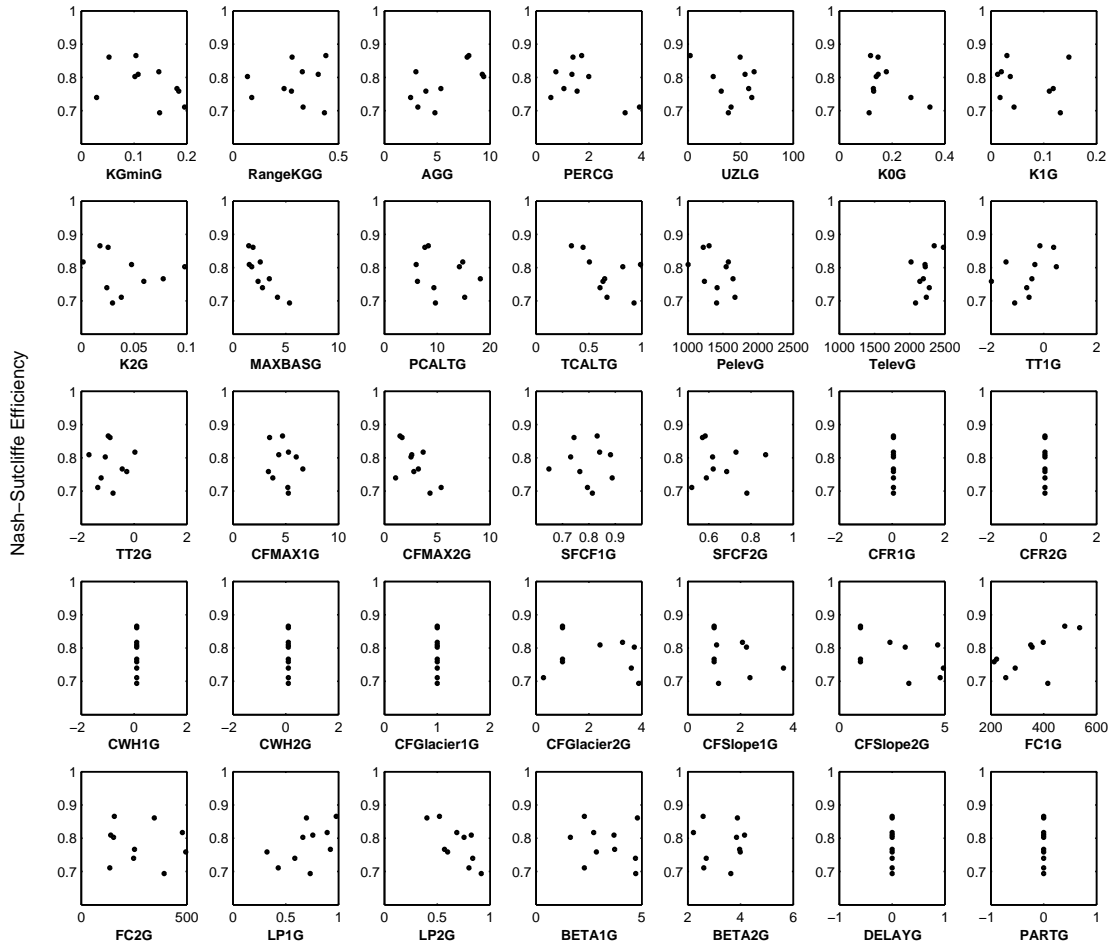


Figure 4.3.: The parameter values of the 10 equifinal parameter sets and their performance in reference to the NSE.

4. Methods

(consisting of the Snow Cover RMSE) and MB (consisting of the Glacier Mass Balance NSE). And, since the selection of the 10 best parameter sets was not done with the same objective functions as the Pareto selection was done the performance when using all five objective functions and when leaving out the MB is assessed. The results can be found in Section 5.2.1.

4.5.3. Analysis of Uncertainties

In a modelling chain as described in Section 4.5.1 many uncertainties are included. First there are the climate scenarios, where there are uncertainties from the GCM and the RCM and manifested in the many different outcomes of the seven combinations in Table 3.2. Second there are multiple equifinal parameter sets for the HBV runs. Third, and only for the Scenario 2035 - 2064, there are three different glacier extents, according to three different climate models. Therefore a two-way Analysis of Variance (ANOVA) for the periods from 1992 - 2021 and 2069 - 2098 and for the period from 2036 - 2065 a three-way ANOVA is conducted. The workflow was derived from the techniques described in von Storch and Zwiers (1999) and Bosshard et al. (2013) and inspired by the results in Finger et al. (2012). The goal was an analysis of the contributors to the global uncertainty, i.e. the relative contribution to the variance of the simulated discharge of the three "effects" as they are called in Bosshard et al. (2013). The three effects are the seven climate scenarios (C), three glacier scenarios (G) and the ten Parameter sets (P). According to the theory of ANOVA the sum of squares of the different independent variables (SSC , SSG , SSP) and the sum of squares of their interactions (SSI) sum up to the sum of squares of the total (SST). \circ stands for the average over the particular index, and i for each day in the time series:

$$SST_i = \sum_{c=1}^C \sum_{g=1}^G \sum_{p=1}^P (Q^{c,g,p} - Q^{\circ,\circ,\circ})^2 \quad (4.13)$$

$$SSC_i = G * P * \sum_{c=1}^C (Q^{c,\circ,\circ} - Q^{\circ,\circ,\circ})^2 \quad (4.14)$$

$$SSG_i = C * P * \sum_{g=1}^G (Q^{\circ,g,\circ} - Q^{\circ,\circ,\circ})^2 \quad (4.15)$$

$$SSP_i = C * G * \sum_{p=1}^P (Q^{\circ,\circ,p} - Q^{\circ,\circ,\circ})^2 \quad (4.16)$$

Since SST is the sum of all the above sum of squares, SSI can be simply calculated algebraically by:

$$SSI_i = SST_i - SSC_i - SSG_i - SSP_i \quad (4.17)$$

Then for the sums of the squares of each effect their fraction of the total variance (SST) for every day i is calculated as it is described in Bosshard et al. (2013):

$$\sigma_C^2 = \frac{1}{I} \sum_{i=1} \frac{SSC_i}{SST_i} \quad (4.18)$$

$$\sigma_G^2 = \frac{1}{I} \sum_{i=1} \frac{SSG_i}{SST_i} \quad (4.19)$$

$$\sigma_P^2 = \frac{1}{I} \sum_{i=1} \frac{SSP_i}{SST_i} \quad (4.20)$$

$$\sigma_{Interactions}^2 = \frac{1}{I} \sum_{i=1} \frac{SSI_i}{SST_i} \quad (4.21)$$

Using the relative variance fractions it is possible to look at every day of the simulation and determine the percentage of variance attributed to each of the three effects or the interactions of these. The introduced procedure is valid for the scenario 2036 - 2065. For the others the procedure is the same, only the terms belonging to the glacier scenarios are removed. That way the SST for the scenarios 1992 - 2021 and 1969 - 2098 consist of the SSC , SSP and their interactions.

5. Results

5.1. Comparison of Weather Datasets

The statistics of the central tendencies of the three weather datasets can be found in the Tables 5.1, 5.2 and 5.3. The result of the Kolmogorov-Smirnov Test with an asymptotic significance of 0 shows that, at a significance level of 5%, the null hypothesis can be rejected. Therefore none of the three datasets MeteoSwiss Grid (GRID), HYRAS Grid (HYRAS) and the interpolated station data (IDW) is normally distributed, neither for the temperature nor for the precipitation time series. Because of this, the matching test for checking whether such datasets are significantly differing in their central tendencies is the Friedman Test. The asymptotic significance is again 0 for the precipitation, which means that at a significance level of 5% the central tendencies of the precipitation datasets are significantly different over multiple time steps N . In contrast, the result of testing the altitude corrected temperature datasets is above the significance level of 5% and therefore the null hypothesis is accepted. Hence the temperature datasets are not significantly different in their central tendencies.

Table 5.1.: Results of the statistical comparison of the three datasets.

Weather Dataset	N^1	K.-S. Temp. ²	K.-S. Precip. ³	Friedman Temp. ⁴	Friedman Precip. ⁵
<i>all</i>					
MeteoSwiss GRID	10957	0.000	0.000		
HYRAS Grid	10957	0.000	0.000	0.105	0.000
MeteoSwiss IDW	10957	0.000	0.000		
<i>combinations</i>					
GRID & HYRAS				0.516	0.000
GRID & IDW				0.298	0.000
HYRAS & IDW				0.000	0.000

¹ N = the number of samples, covers the period of 1977 to 2006 in all datasets.

^{2,3} The asymptotic significance is 0.000. This means that with a significance level of 5% the null hypothesis of the Kolmogorov-Smirnov Test can be rejected. Hence the data is not normally distributed. This result is true for each of the datasets individually.

⁴ The asymptotic significance is 0.105, therefore, with a significance level of 5%, the null hypothesis of the Friedmann test is accepted. This means that the central tendencies of the three datasets do not differ significantly.

⁵ The asymptotic significance is 0.000. This means that with a significance level of 5% the null hypothesis of the Friedman Test can be rejected. Hence the central tendencies of the precipitation datasets are significantly differing from each other.

5.1. Comparison of Weather Datasets

The Friedman Test was also done for the combinations GRID & HYRAS, GRID & IDW and HYRAS & IDW. There the results were 0.52, 0.3 and 0 respectively. This shows that the GRID and the HYRAS temperatures have the most similar central tendencies of all combinations, and HYRAS and IDW share the least commonalities. For the precipitation all combinations showed an asymptotic significance of 0.

For the temperature datasets, which are all corrected for the altitude bias, the differences in other statistical measures are only marginal. The lowest temperatures are measured in the IDW dataset, which also has the biggest standard deviation with 7.53 °C. The IDW dataset also shows the biggest variation throughout the year. This is visible from the mean monthly temperature over the period in Figure 5.1(a). The IDW has the coldest average temperatures in winter and the warmest during summer (even if the differences are small to the HYRAS and GRID. However these differences are not significant as was already found by the Friedman test in Table 5.1.

The precipitation datasets show significant differences which is concluded by the result of the Friedman test, but is also clearly visible in the monthly averages in Figure 5.1(b). The IDW shows the lowest mean precipitation during all months, followed by HYRAS and the GRID dataset with the biggest amount (see Figure 5.4). The reason for these differences are partly evident and are discussed in section 6.1.

Table 5.2.: Comparison of the three temperature datasets.

Weather Dataset	Min [°C]	Max [°C]	Mean [°C]	Median [°C]	StDev [°C]	5th Perc. [°C]	95th Perc. [°C]
MeteoSwiss GRID	-25.9	19.1	0.7	0.8	6.8	-10.9	11.4
HYRAS Grid	-27.8	18.5	0.6	0.6	6.8	-11.2	11.3
MeteoSwiss IDW	-27.7	17.5	-0.2	0.3	7.5	-12.5	11.3

Table 5.3.: Comparison of the three precipitation datasets: IDW-Interpolated values from three MeteoSwiss-Stations in Chur, Elm and Bad Ragaz, MeteoSwiss-Grid and the HYRAS-Grid

Weather Dataset	Max [mm]	Mean [mm]	Median [mm]	Mode [mm] ¹	StDev [mm]	95th Perc. [mm]
MeteoSwiss GRID	129.3	4.8	0.3	0.100	9.4	751.0
HYRAS Grid	108.4	3.8	0.3	0.002	7.6	506.0
MeteoSwiss IDW	111.4	3.1	0.1	0.028	6.7	380.0

¹ The mode was calculated from all precipitation values above 0. If 0 is included in the calculation the mode is 0 for all datasets

5. Results

Table 5.4.: Comparison of the precipitation sums of the three datasets: IDW-Interpolated values from three MeteoSwiss-Stations in Chur, Elm and Bad Ragaz, MeteoSwiss-Grid and the HYRAS-Grid

Weather Dataset	All Time Sum [mm]	Winter Sum [mm] ¹	Spring Sum [mm] ²	Summer Sum [mm] ³	Fall Sum [mm] ⁴
MeteoSwiss GRID	52232	10989	12020	17363	11861
HYRAS Grid	41723	8766	9525	13913	9519
MeteoSwiss IDW	34059	6690	7710	11763	7896

¹ Winter Season from December to February

² Spring Season from March to May

³ Summer Season from June to August

⁴ Fall Season from September to November

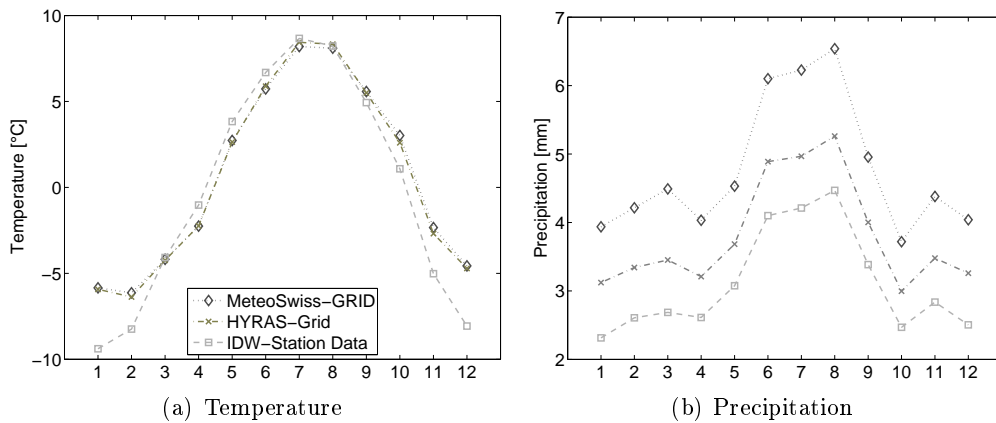


Figure 5.1.: Mean monthly temperature and precipitation of the three compared datasets over the period 1977 - 2006.

5.1.1. Results of Multivariable Calibration for the Weather Datasets

The differences between the combinations are very small if a Pareto selection is applied. So that in the end all combinations have about the same performance. Since the results showed such a stable behaviour if the Pareto selection was done and the thresholds applied (see Figure 5.2(a)), the same analysis was also run for the hundred best runs, in terms of every objective function combination 5.2(b).

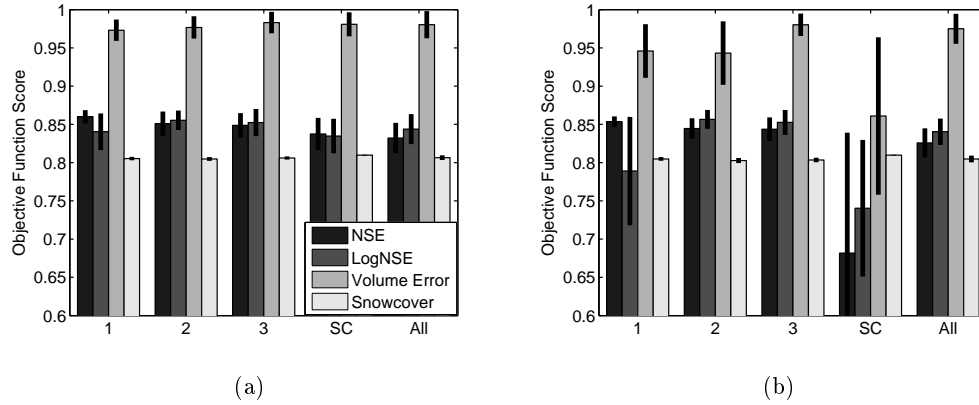


Figure 5.2.: a) After applying thresholds and the selection of the Pareto optimal parameter sets. Number of parameter combinations: 1-19, 2-23, 3-35, SC-5, All-23.

b) 100 best runs from the calibration. Before applying thresholds and selecting the Pareto parameter sets.

Mean objective function scores with different combinations of objective functions. 1 = NSE, 2 = NSE + LogNSE, 3 = NSE + LogNSE + Volume Error, SC = snowcover RMSE and All = all combined.

If not only the Pareto parameter sets are used but the 100 best parameter sets of 150'000 then the results are much more distinct. For the discharge measures the differences between three combinations are not as big as when snowcover is used alone. Also the standard deviation (black whiskers) become smaller in when using the Pareto parameter sets. Especially the score of the calibration to *SC* only drops remarkably. However it is visible in all combinations, that if an objective function is added to the procedure, its performance rises, whereas the performance of the others mostly drops slightly. Only the snow cover RMSE shows a very stable behaviour over all combinations. Its standard deviation is the smallest of all the objective functions, which is the case in both analyses.

5.1.2. Results of Weather Dataset Evaluation

From the 150'000 runs of the Monte Carlo simulation with each dataset the 100 best runs were taken. Of these 100 best runs the Pareto optimal solutions were selected. Then the four objective functions above 0.8, or 0.95 for the Volume Error, were selected. The ranges of the parameters after the selection are shown in Table 5.5.

5. Results

Table 5.5.: Ranges of the HBV model parameters after selecting the Pareto and applying the thresholds from the 150'000 runs of a Monte Carlo simulation in the calibration period 1999 - 2002

Parameter	GRID		HYRAS		IDW	
	min	max	min	max	min	max
<i>KGmin</i>	0.0	0.2	0.0	0.2	0.0	0.2
<i>RangeKG</i>	0.0	0.5	0.1	0.5	0.0	0.5
<i>AG</i>	0.5	9.8	0.4	8.5	0.5	10.0
<i>PERC</i>	0.7	3.8	0.8	4.0	1.0	3.5
<i>UZL</i>	0.6	63.7	1.0	66.7	9.9	68.0
<i>K0</i>	0.1	0.4	0.1	0.3	0.1	0.3
<i>K1</i>	0.0	0.2	0.0	0.2	0.0	0.2
<i>K2</i>	0.0	0.1	0.0	0.1	0.0	0.0
<i>MAXBAS</i>	1.0	2.4	1.0	2.4	1.0	2.4
<i>PCALT</i>	10.0	10.0	10.0	10.0	10.0	10.0
<i>TCALT</i>	0.6	0.6	0.6	0.6	0.6	0.6
<i>Pelev</i>	1357.3	1716.6	1017.3	1243.2	486.0	786.5
<i>Telev</i>	1833.9	2383.8	1779.2	2326.0	1756.9	2258.2
<i>TT₁</i>	-1.9	0.1	-1.9	0.5	-2.0	0.3
<i>CFMAX₁</i>	3.9	9.6	4.7	10.0	3.2	7.5
<i>SFCF₁</i>	0.7	0.9	0.6	0.9	0.7	0.9
<i>CFR₁</i>	0.1	0.1	0.1	0.1	0.1	0.1
<i>CWH₁</i>	0.1	0.1	0.1	0.1	0.1	0.1
<i>CFGlacier₁</i>	1.0	1.0	1.0	1.0	1.0	1.0
<i>CFSlope₁</i>	1.1	3.3	1.0	4.8	1.0	3.9
<i>FC₁</i>	100.3	537.8	103.7	508.0	110.3	539.0
<i>LP₁</i>	0.3	1.0	0.3	0.9	0.3	1.0
<i>BETA₁</i>	1.0	4.9	1.1	4.7	1.0	4.8
<i>TT₂</i>	-2.0	0.5	-1.8	0.4	-1.9	0.4
<i>CFMAX₂</i>	0.9	9.1	0.6	9.5	0.9	9.9
<i>SFCF₂</i>	0.5	0.8	0.5	0.9	0.5	0.9
<i>CFR₂</i>	0.1	0.1	0.1	0.1	0.1	0.1
<i>CWH₂</i>	0.1	0.1	0.1	0.1	0.1	0.1
<i>CFGlacier₂</i>	0.2	4.4	0.5	5.0	0.1	4.8
<i>CFSlope₂</i>	1.5	5.0	1.0	4.3	1.1	5.0
<i>FC₂</i>	111.6	522.0	116.3	521.0	113.2	535.4
<i>LP₂</i>	0.3	0.9	0.3	1.0	0.3	0.9
<i>BETA₂</i>	1.0	5.0	1.2	4.8	1.1	5.0

5.1. Comparison of Weather Datasets

The same number of parameter sets resulted for GRID and HYRAS with 23 parameter combinations for both and 28 for the IDW dataset. Those selected parameter sets were then used for evaluation of the model during calibration and validation period.

From the average NSE, LogNSE in Figures 5.3,5.4 and 5.5 it can be said, that all the models perform sufficiently well (unfortunately the HBV model supports no output of Volume Errors or Snowcover RMSE in the batched runs). The ranges of the parameter sets can be seen in Table 5.6. The amount of decline is in all models and both objective functions between 0.05 and 0.1. In terms of an overall performance the HYRAS dataset reaches the highest values and the GRID the lowest. However the differences are marginal and hardly significant. Further the errors and the general shape of the simulation is very similar in all three datasets, only the magnitudes or volumes of errors are differing slightly. Further, it comes clear that the performance of each model declines as expected in the validation period.

Table 5.6.: Ranges of the NSE and the LogNSE in the Calibration Period 1999 - 2002

Obj. Function	<i>Calibration</i>			<i>Validation</i>		
	min	max	mean	min	max	mean
	<i>GRID</i>					
NSE	0.80	0.86	0.83	0.72	0.82	0.77
LogNSE	0.80	0.87	0.84	0.73	0.82	0.79
	<i>HYRAS</i>					
NSE	0.82	0.86	0.86	0.73	0.86	0.80
LogNSE	0.81	0.89	0.87	0.64	0.84	0.77
	<i>IDW</i>					
NSE	0.80	0.79	0.83	0.66	0.79	0.73
LogNSE	0.80	0.89	0.86	0.73	0.85	0.78

As a first impression of the inspection of the hydrographs the timing of the discharge peaks as well as the general shapes of the hydrographs are represented pretty good by the parameter ensembles. However the amplitude of the peaks is often over- or underestimated. This is recognizable best in the Figures A.4, A.5 and A.6 covering every single day in the Appendix. Further the absolute errors (see Figures A.10, A.11 and A.12) in the calibration period are highest during the days 100 and 150 when using the GRID and the HYRAS datasets, in the IDW these errors occur less concentrated but are rather distributed evenly throughout the period between the days 150 and 300.

Moreover the three results show all a bad performance during the days 150 - 200 of the year in the validation period. These days correspond to May 30th and July 19th, so basically during June and July. Which can be seen as the second half of the high-flow season in spring and summer. At the same time, the discharge at the beginning of the high flow season around day 100 (April 10th) tends to be underestimated according to the error plots in Figures A.7 to A.12, which represent the differences between observation and simulation where the observed values are higher than the highest value or lower than the lowest value of the simulation at a certain day.

5. Results

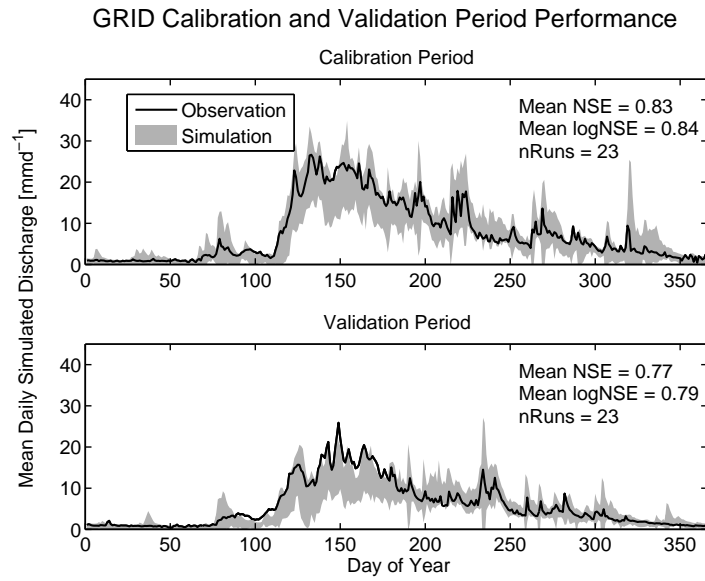


Figure 5.3.: Mean daily observed and the range of the simulated discharges of the GRID datasets.

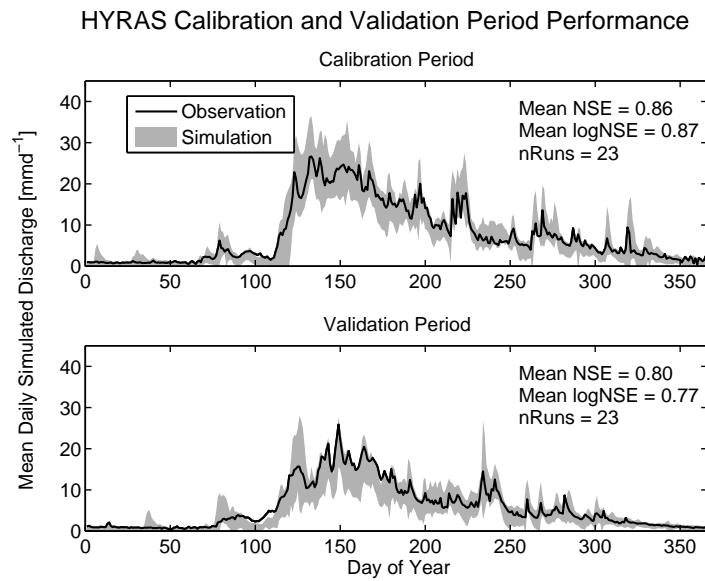


Figure 5.4.: Mean daily observed and the range of the simulated discharges of the HYRAS datasets.

5.1. Comparison of Weather Datasets

The borders of the grey areas in Figures 5.3, 5.4 and 5.5 represent the highest and lowest possible model outcomes for each day of the whole period of all Pareto optimal simulation results. Therefore the errors can not be directly be estimated from the Figures showing the average year. Concerning the errors during calibration all three datasets show a very similar behaviour during the days 200 (July 19th) to 300 (Oct 27th) and 350 (Dec 16th) to day 100 (Apr 10th). The GRID and HYRAS datasets both show a first small cluster of errors of underestimations between days 100 and 130 (May 10th), whereas this cluster is bigger for HYRAS. In return, the next, bigger cluster of underestimations is bigger with a higher amplitude in the GRID dataset and lasts around 20 days from around day 130 to day 150 (May 30th) in both. From this day on, their mean annual errors are very similar until day 300. Then during the days 300 to 350 (Dec 16th), HYRAS shows only one big overestimation of the simulation, whereas GRID shows several but smaller overestimations. The end of the year, especially during the validation period. The biggest errors when using the IDW dataset occur around 50 days later during the days between day 150 and 200. Its overestimations during the days 200 to 250 (Sept 7th) are slightly bigger than in the other two.

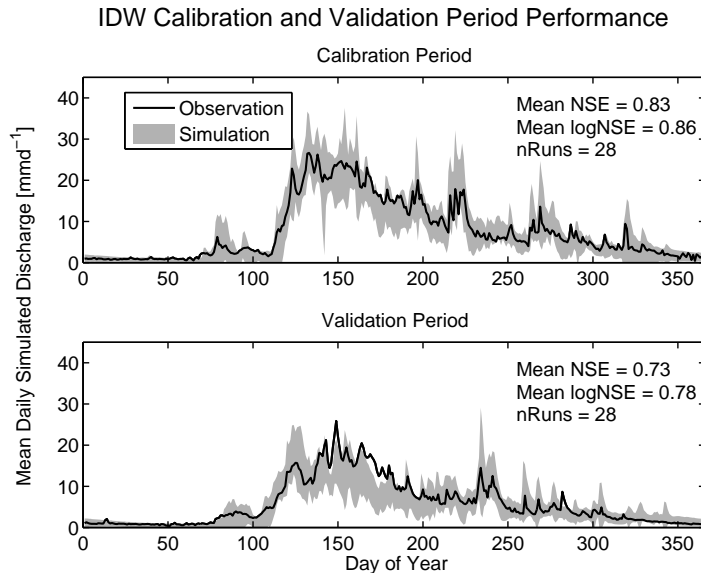


Figure 5.5.: Mean daily observed and the range of the simulated discharges of the IDW datasets.

Generally it can be said that the IDW dataset has the more distinct peaks, which often come rather as a single or short-duration event. Whereas this is the opposite in HYRAS and even more pronounced in the GRID-driven simulations (see Figures A.7, A.8 and A.9). This is very well visible in the errors during 2003, where IDW produces a smaller number of errors than the other two, but still has one event that shows a very large underestimation of measured discharge towards the end of the year. This peak is also present in the other two, but with a slightly smaller amplitude. The phenomena of higher amplitudes in IDW-driven simulations occurs during other events as well (e.g.

5. Results

in 2000, 2001 (overestimation), in 2002 (overestimation), in the validation period in the middle of 2004, 2005 towards the end of the year and also in 2006). In all three figures the extreme discharge event in August 2005 is visible as a very distinct peak. Further the dry summer in 2003 is in terms of errors represented pretty good compared to the years 2004 - 2006.

The plots of the relative errors in Figures A.13, A.14 and A.15 reveal a different side of the simulations. The relative errors are smallest for the periods with the biggest absolute errors mentioned before, which is basically the from day 100 until day 300. The period with the biggest relative errors are the winter days, where the absolute error is very small. Further, during the calibration period the shape and some distinct peaks show the same behaviour in all three datasets, only the amplitudes differ slightly. During the validation the mean relative errors of the GRID and HYRAS driven simulations show also a similar shape with with differing amplitudes. One exception occurs in the first 50 days of the year. There the GRID dataset produces a distinct negative peak, where the simulation was overestimated by a factor higher than two.

5.2. Discharge Scenarios

5.2.1. Multivariable Calibration

In Figure 5.6 the same effects are visible as in Section 5.1.1. Only now the Glacier NSE was added to the datasets. The presented method has the effect, that in the datasets of SC and MB only one parameter set is left, since the Pareto solution depending on only one objective function is only one set. If a calibration is done for discharge (Q), snowcover (SC) or glacier mass balances (MB) only, the score of the particular objective function(s) is highest compared to the combined runs. This means that adding another objective function is a trade-off between the performance of the model in respect to that function and the others. Several effects can be observed in Figure 5.6. The first is, that parameter sets that are not used for calibration are performing worse than if they are used too. This behaviour is strongest for the MB. Further the snowcover is never much higher than 0.8, be it when it is used alone for calibration or in combination with other functions. The LogNSE increases when snowcover is used for calibration, but decreases when a calibration to discharge only is done. The discharge produces worse results when the MB is added than if the SC is added. When both are used, the NSE gets worse than if only one of the two was used but the LogNSE improves compared to the performance with MB only.

The effect of the decision to leave out the mass balance when selecting the 10 best parameter sets is visible in Figure 5.7. The performance of the MB NSE is reduced pretty much, the Log NSE and the SC are as well slightly reduced. On the other hand the NSE increases as well as the Volume Error.

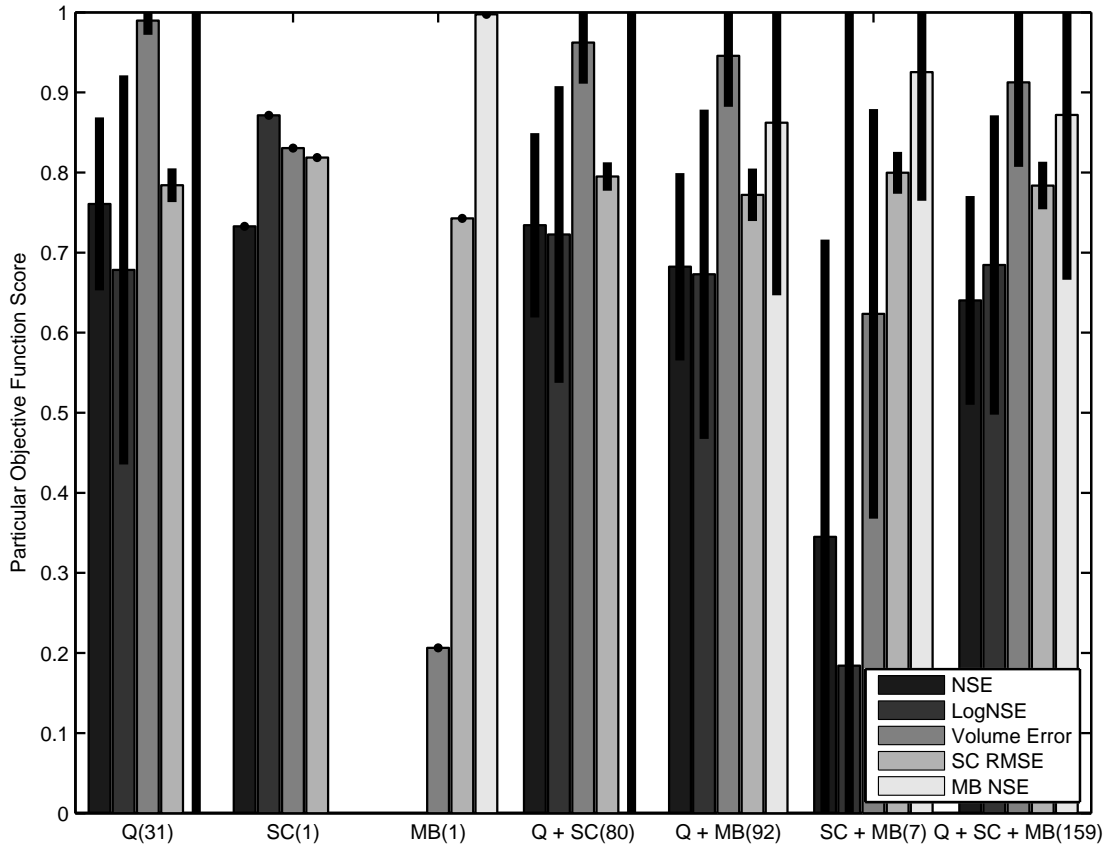


Figure 5.6.: Performance of the HBV-light by calibration to different combinations of objective functions. The bars represent the mean scores of the particular objective functions described in the legend. The thin black bars indicate the standard deviation from the mean. The values in brackets on the x-Axis represent the number of resulting parameter sets after the selection procedure described in 4.5.2.

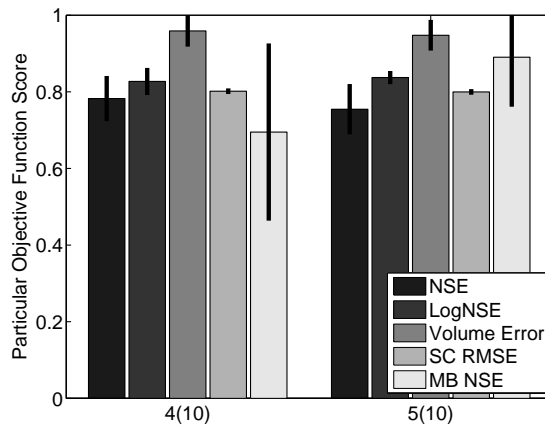


Figure 5.7.: The 10 best parameter sets. Left: without the MB NSE. Right: including MB NSE

5. Results

5.2.2. Model Performance during Calibration and Validation Period

The modelled discharge during the using the GRID weather dataset generally matches the observed discharges satisfactorily. The peak of the high flow event in August 2005 is rather good represented whereas other peaks are not simulated correctly. The model often has difficulties in simulating peak and low flows correctly. This is visible in 2003, a year with a very hot and dry summer, where peaks are often underestimated and low flow periods in late summer and fall overestimated. In Figure 5.8 the validation period from 2001 onwards shows a tendency for an underestimation of spring discharge which also occurs during the calibration period. This is also visible in Figure 5.9, where especially in the months from April to June the (mean) modelled discharge is rather too low. In return the mean modelled discharge in fall is to high.

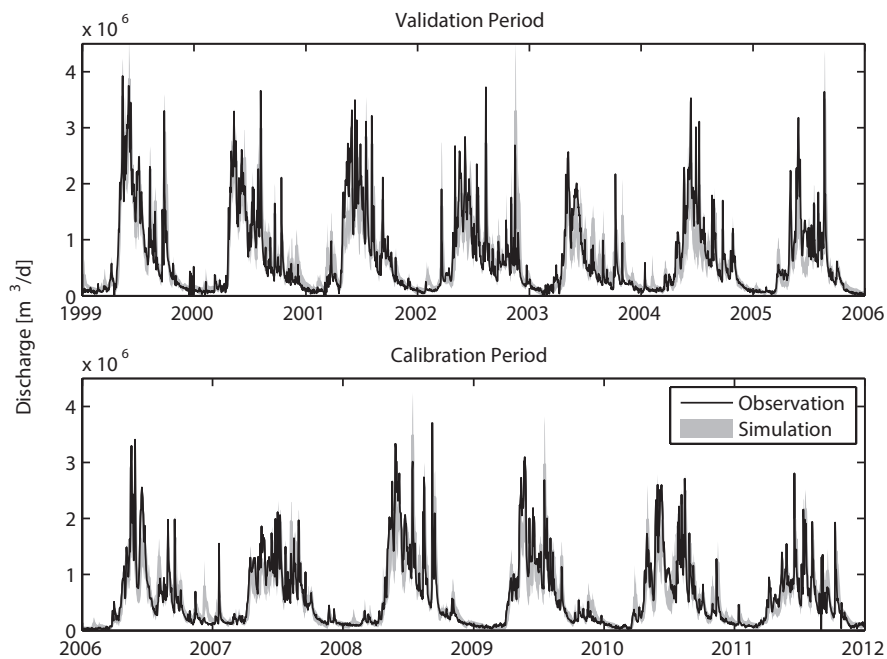


Figure 5.8.: Calibration (2006 - 2011) and validation period (1999 - 2005). The grey area depicts the whole bandwidth of the simulation from the daily minimum to its maximum.

The simulated and observed snowcover from MODIS imagery in Figure 5.10 shows that the general variability of the observed snowcover is higher in the observed data than in the simulation. The mean modelled snowcover is to high during the months January and May - September and November. The highest difference is in June where the overestimation of the fraction of the snow covered area is around 15%. During the other five months it fits the observations rather good. Furthermore the observed fraction of the snow covered area mostly lies inside the variability of the model uncertainty emerging from the 10 parameter sets.

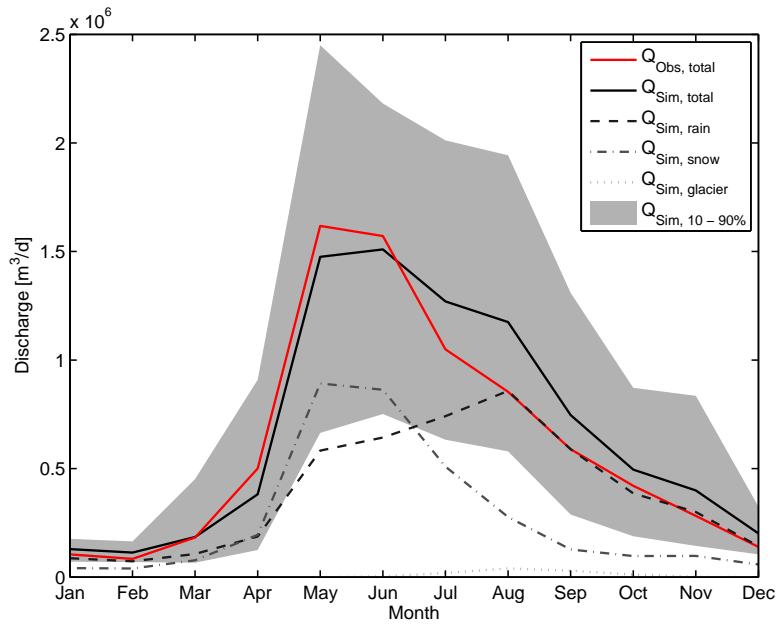


Figure 5.9.: The discharges accentuated to the different sources of water and the observed total discharge. The grey areas show the 10th and the 90th percentile of all the simulations of the total runoff.

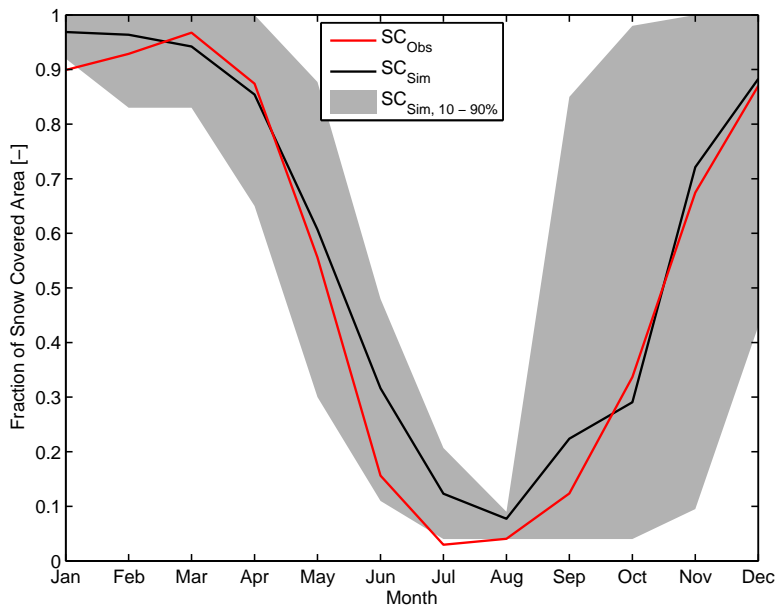


Figure 5.10.: The observed and simulated snowcover during the calibration and validation period (available only from 2001 - 2008). The grey areas depict the 10th and 90th percentile of all the simulations.

5. Results

5.2.3. Climate Change Effects on Discharge

In the top graph of Figure 5.11 the performance of the HBV with using climate scenarios as weather data during the reference period is shown. The most striking difference to the simulations using measured data is the bad representation of the discharge during May and June. During the rest of the year the modelled discharge is mainly higher than the observation, but except for May and June the simulations are rather good. In the future scenarios the mean monthly simulated discharge is more evenly distributed throughout the year, due to the comparably small peak in May. The discharge accounted to rain is biggest during summer and peaks in August. The snow melt discharge peaks in June. The discharge from glacier melt water is very small, with a peak in August in the order of $33'000 \text{ m}^3$ a day. In the future periods this distribution changes, mostly between the reference scenario and the mid-term scenario from 2036 - 2065. There the shape of the total discharge resembles more the current, observed discharge with peaks in May and June. The biggest difference occurs in the water from snow melt.

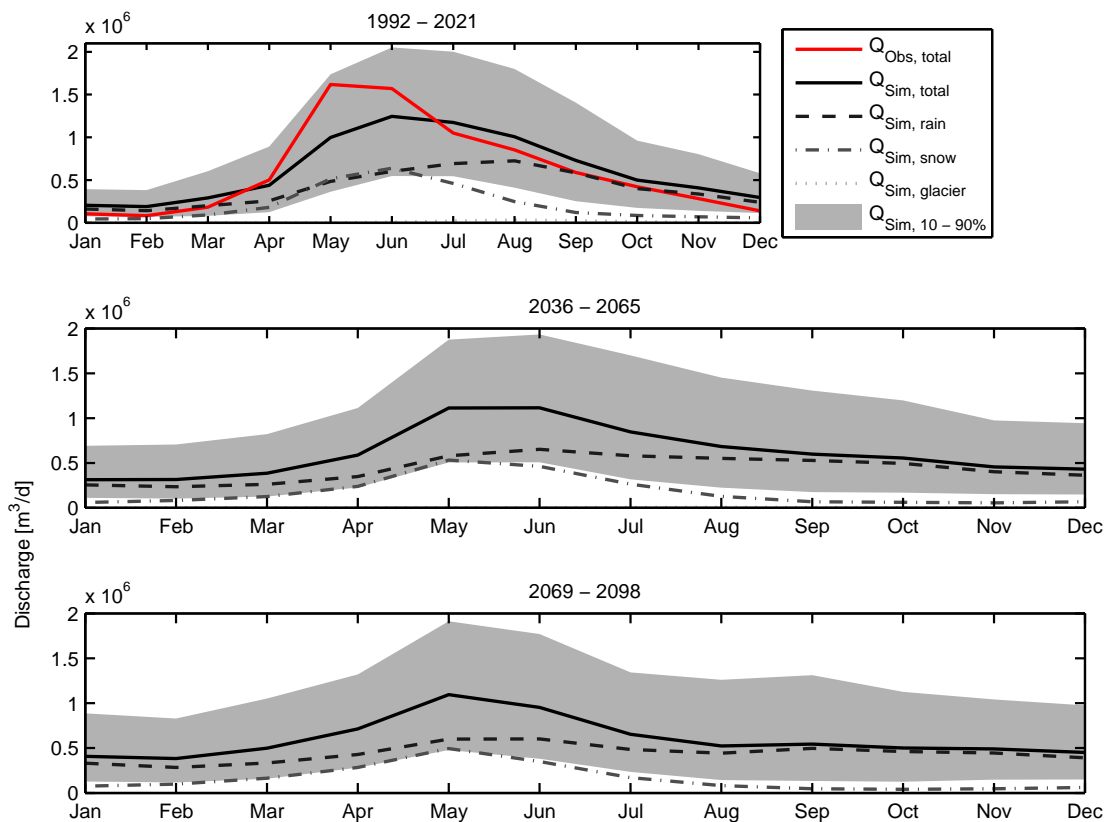


Figure 5.11.: The mean modelled discharge using climate scenarios in the three periods 1992 - 2021, 2036 - 2065 and 2069 - 2098 and its shares accounted to rain, snow melt and glacier melt water. Note the very thin dotted line at the bottom, representing the glacier melt water. The grey area shows the 10th and the 90th percentile of all the simulations of the total runoff.

There is much less water in fall, than in the reference period and the rain water peak occurs in May, which is a month earlier. Further there is more rain water in Winter. In the reference period during May and June the discharge from snow melt is bigger than the discharge from rain, but this changes already in the mid-term period. The trend of declining melt accentuated to snow melt continues in the long-term period (2069 - 2098). The snow melt water declines in the mid- and the long-term scenario with the biggest losses in June and July.

During the reference period the runoff from rain water peaks in August. Then until the mid-term the discharge increases in winter and decreases in summer and the peak shifts to June. In the long-term the trend continues, because the discharge from rain becomes less in June, the peak is then evenly distributed to May and June.

The glacier melt water declines more in the mid-term period, at the end of which the glaciers will have disappeared. Therefore there is no more glacier melt water in the long-term period.

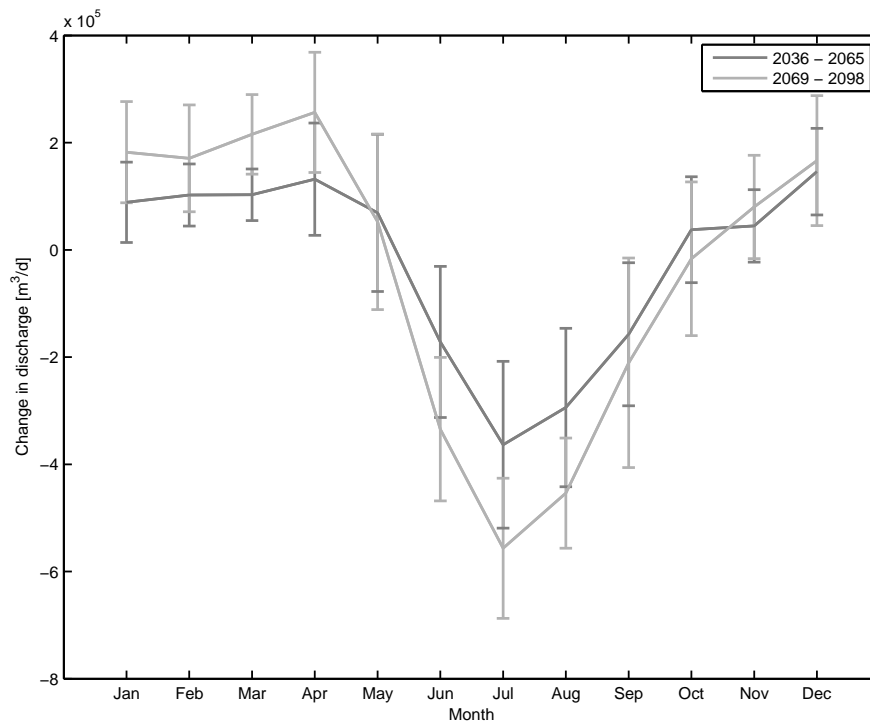


Figure 5.12.: The modelled change in discharge compared to the reference scenario 1992 - 2021. The vertical bars indicate the standard deviation of the change signal.

The total runoff shifts towards May, and less in June. In winter the modelled discharge increases in both scenarios. This results in a average year with smaller monthly discharge magnitudes and a more evenly distributed runoff throughout the year. However the representation of the observed discharge is rather bad and therefore the change is also looked at as a relative signal in Figure 5.12 compared to the reference scenario. They

5. Results

follow the same trends in the mid- and the long-term. The discharge is more concentrated in winter whereas it declines during summer. In October it increases in the mid-term period and then decreases again in the long-term. The changes are mostly significantly different from the mean(!) of the baseline period, however between the two scenarios the differences are never significant, since the standard deviations always overlap.

The sums of the discharges over one year in Table 5.7 show that the overall discharge follows a slightly decreasing trend. However the results are mostly not significant. The model predicts a decrease of $3.5(\pm 7.5)\%$ in the mid-term and a decrease of around $6(\pm 11.4)\%$ in the long-term of the overall discharge. At the same time the discharge ascribed to rain increases by about $7(\pm 15.3)$ or $8(\pm 17.8)\%$ respectively compared to the reference period. On the other hand the only significant results are the decline of runoff due to snow melt which is predicted to decrease by $20(\pm 19.1)$ and $28(\pm 20.5)\%$ respectively. And last, the glacier melt water will be reduced significantly by $85(\pm 16.0)\%$ in the mid-term and certainly disappear completely in the long-term scenario.

Table 5.7.: The changes of the discharge shares in the mid- and the long-term scenario compared to the reference scenario in Million m^3 s and percentages.

Discharge shares	Reference Period [M m^3] [%]	Mid-Term [M m^3] [%]	Long-Term [M m^3] [%]
Q_{tot}	234 100	226 96.5 (± 7.5)	220 94 (± 11.4)
Q_{rain}	150 100	160 107 (± 15.3)	162 108 (± 17.8)
Q_{snow}	81 100	65 80 (± 19.1)	58 72 (± 20.5)
$Q_{glacier}$	3 100	0.5 15 (± 16.0)	0 0 (± 0)

When comparing the observed weather data with the climate scenarios of the same period (see Figure 5.13) for finding causes for the difference in discharge and snowcover simulation using the scenarios and the observations it can be seen that the temperature simulation represents the monthly temperature variations quite well. Only in April, May and June the observed temperatures are above the scenarios, in April the difference the simulations are about 0.8°C above the measurements, in May the difference is a little smaller with about 0.6°C and in June the difference is biggest with 1.4°C . The simulated precipitation is quite different from the observed one. It is above the observed in January, March, April, June, September and November and below in February, May, August, October and December.

The simulated snow cover during the calibration period (see Figure 5.14) fails to represent the behaviour of the magnitude of the variations throughout the year. The decline of area covered with snow in spring occurs slower than in the observations. In the months June, July and August the difference is up to 20%. In return the representation is better from September to February. But still the variations over one year are more extreme in the observations, which means that the model simulates too little snow in winter and too much during summer. The onset of snow melt in March is earlier than in the observations, but is then happening slower.

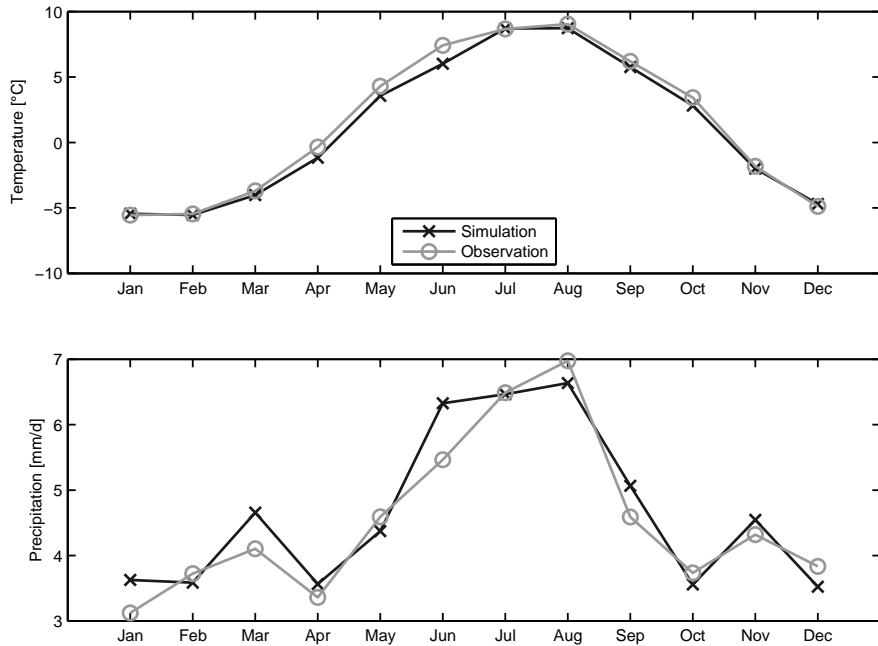


Figure 5.13.: Temperature and precipitation simulated by climate scenarios during the calibration and validation period (1999 - 2011).

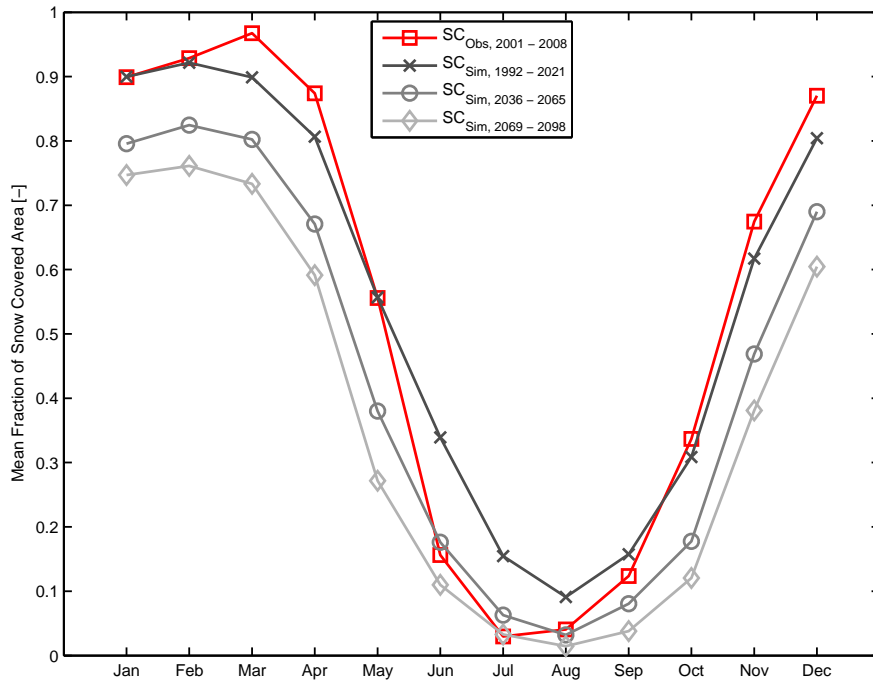


Figure 5.14.: The modelled fraction of the snow covered area during the baseline period from 1992 - 2021 and the scenarios from 2036 - 2065 and 2069 - 2098.

5.2.4. Analysis of Uncertainties

The ANOVA based uncertainty analysis reveals that the variance is mainly driven by the 7 different climate scenarios. From August to December their contribution is biggest (between 80 and 90%). From January to July it is below 80% but always bigger than 70%. The variance fraction of the parameter sets is around 10% and biggest during late spring and early summer. The contribution of the glacier scenarios is vanishingly small in the mid-term period, therefore that area is not visible in the Figure 5.15(a). The variance fraction accentuated to the interactions and errors is biggest in winter with around 15%. Between the two scenarios there is no big difference, even though there are no glaciers in the long term period. However the influence of the parameter sets becomes smaller in the long-term period during the whole year apart from June and July.

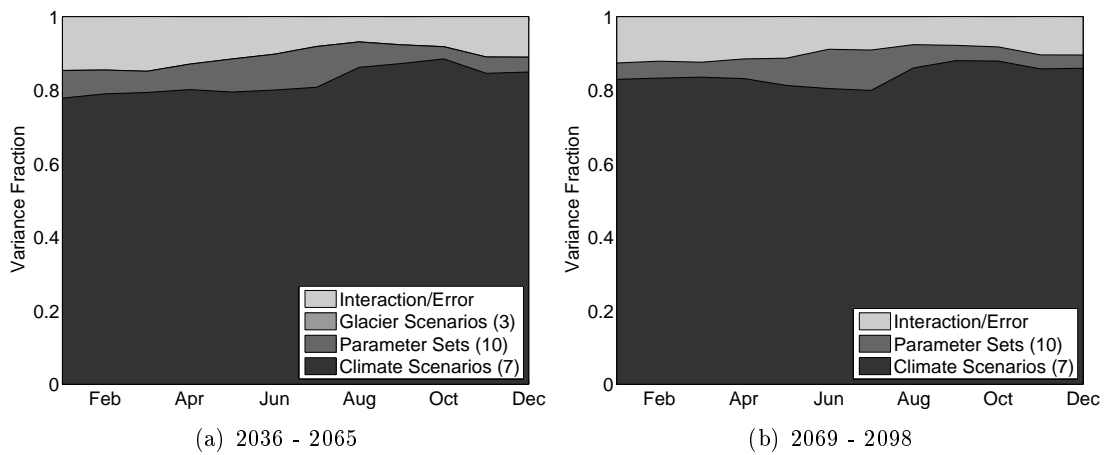


Figure 5.15.: Mean monthly relative contribution of the 7 climate scenarios and 10 parameter sets to the variance of the simulated discharge scenario for the two future periods

6. Discussion

6.1. Differences in Weather datasets

One goal of this thesis was a comparison of the three different weather datasets GRID, HYRAS and IDW at the catchment of the Gigerwaldsee in Switzerland. They are used for discharge simulations using the conceptual model HBV (Seibert and Vis, 2012). As can be seen in Sections 3.2, 3.3 and 3.1 the three datasets, to some extent, have the same base data, which are measurements of weather stations of the SwissMetNet network (Roulet et al., 2010).

6.1.1. Correction of Altitude Bias

The fact that the temperature dataset was corrected for the shift in altitude but the precipitation was not, may seem odd. The correction of the temperature data for the height can be done easily using the lapse rate applied in section 3.2 and 3.3. However precipitation is not believed to be as simply scalable for a height difference as temperature. Especially at horizontal distances below 40 km, as in the present study, the phenomena related to topography, such as the amplitude of rain shadow are very complex (Roe, 2005). Further simple correction would also alter the distribution of drizzle days, since most probably some multiplication factor would have been the simplest solution. Therefore it was decided that the precipitation datasets were not corrected further after the horizontal inverse distance weighting using the Euclidean Distances to the three surrounding stations. Since the difference in mean altitude between the stations (670 m) and the mean elevation of the catchment (2135 m) is not considered, the systematically lower values of the IDW compared to the other two are not surprising. This can be explained simply by the fact that precipitation is generally higher in greater altitudes due to orographic effects (Beniston, 2006; Jacobeit, 2007; Konrad I., 1996). In addition to that, gridded precipitation datasets show generally higher values when calculated using background or reference fields and anomalies than with simple interpolation of station measurements, this is because the latter rather underestimate the precipitation systematically since most stations are located in rather dry valley conditions (Isotta et al., 2013). The combination of the above explains the bias in the IDW dataset towards lower precipitation sums compared to HYRAS and GRID data.

The precipitation series of the two gridded datasets GRID and HYRAS are not corrected either. Since the grid spacing in both datasets is very large, there are believed to be bigger inconsistencies, since at daily time scales the spatial resolution is believed to be at the order as the grid spacing, which is 10-15 km (Isotta et al., 2013). Therefore

6. Discussion

such errors are believed to be much bigger than a possible shift due to a slight altitude inaccuracy of 50 m.

The temperature of the of GRID and HYRAS were corrected in the same way, because they both depend on the same DEM (USGS GTOPO30). Both data series in the end consist of single values per day which are averages over the entire the catchment. The average catchment height derived from the GTOPO30 when using the same grid cells as the temperature and precipitation data from GRID and HYRAS were derived from, is 2087 m. The average height, derived from the DHM25 is 2135 m. It is believed to be much more robust, compared to the GTOPO30 (RMSE of 97m globally¹), since its error in the Alpine area lies only in the order of 3-8 m². Therefore the temperature is overestimated by (0.288 °C). It should be noted that, due to the small number of raster cells covering the catchment, this procedure showed to be very sensitive to the method for selecting the cells for the average height calculation from GTOPO30. When selecting only cells that are entirely inside the catchment the average height was even bigger than 2135 m, which would have led to an increasing temperature after the correction. However, selecting the same number of cells as the weather data was derived from is believed to be the right solution.

The Kolmogorov-Smirnov and the Friedman tests in Table 5.1, where also done before the correction of the temperature dataset to altitude. There, the Friedmann-Test for the temperatures showed an asymptotic significance of 0, which means that at a significance level of 5% the central tendencies of the weather datasets were different. Therefore I conclude that after the correction the three temperature datasets were representative for the same elevation.

The main purpose of the comparison of the weather datasets in this thesis is to evaluate their performance in hydrological simulations. The HBV model is able to correct for systematic errors in weather datasets, therefore it is not of fundamental importance that the datasets match exactly the altitude of the catchment. It can always be accounted for by adjusting the parameters *Pelev* and *Telev* (Seibert and Vis, 2012). However the datasets have to represent the "true" weather pattern which regulates the discharge in its relative internal characteristics. This feature of the HBV however may lead to good results for the wrong reasons. As can be seen in Figure A.2 in the Appendix the altitude of HYRAS *Pelev* values is concentrated between 1000 and 1400 m although the possible range would have been up to 2500 m. Since the average height of the catchment is considerably higher (2135 m), it is therefore assumed, that HYRAS' precipitation values are systematically too low. On the other hand they seem to have the right relative internal characteristics of the weather patterns. Compared to that, the absolute values of GRID seem to be closer to the "true" magnitudes (see Figure A.1). However the relative characteristics seem to be differing, since the model results are constantly slightly worse compared to HYRAS. This indicates indeed better results for the HYRAS dataset for the wrong reasons, i.e. an unrealistic value for the virtual weather stations *Pelev* and *Telev*. Note that both precipitation datasets are biased towards a lower elevation, since

¹<http://www.eorc.jaxa.jp/JERS-1/en/GFMP/AM-3/docs/html/gtopo30.htm#dcwdem5>

²<http://www.swisstopo.admin.ch/internet/swisstopo/en/home/products/height/dhm25.html>

the values for *Pelev* in the scatter plots in Figures A.1 and A.2 are concentrated around 1500 and 1200 m respectively. For the IDW dataset the range for *Pelev* was set to 400 - 800 m (Figure A.3), because the precipitation values were not corrected for altitude. After some pretests the best model performances were found within that range, which would mean that the IDW values are representing the magnitudes rather good. Therefore it is assumed that HYRAS might have the biggest systematic errors, but the relative internal weather patterns are represented best.

Concerning the temperatures it can be said that they all show a distribution closely around the average catchment height. I therefore assume that the corrected temperatures match with the discharge measured at the Gigerwaldsee. Here it is always assumed that the discharge measurements are correct. Of course there are also uncertainties in the discharge measurements, in particular in this case as the discharge data was computed from lake level observations provided by the "Kraftwerke Sarganserland AG".

6.1.2. Assessment of Differences in GRID, HYRAS and IDW

Differences in Temperature

The values of the temperature are very similar in all three datasets. Before the correction due to the altitude see Sections 3.1 and 6.1.1 the temperatures of IDW and the other two were differing a lot. After the correction the central tendencies showed very similar values (see Table 5.1). The values of IDW showed the lowest mean temperature afterwards (see Table 5.2). The reason for that can be seen in the long-term monthly averages in Figure 5.1(a): IDW shows the lowest mean temperatures during the winter months, with a difference of about (4 °C). In contrast during summer it rises above the other two. This could to be an artefact from its origin. Since it originally stems from three locations at an average height of 670 m, the data still shows the same fluctuation pattern now at 2135 m as they did at the lower level. Further GRID always has the highest temperatures in the minima, maxima, means, median and the percentiles. HYRAS is always in between the two (except for the minimum) and the IDW has the lowest temperatures in these measures. However for the calibration of the HBV the general shape is important (see Section 6.1.1). There HYRAS and GRID show a very similar behaviour in the monthly means, with HYRAS showing slightly higher fluctuations.

Differences in Precipitation

The first difference in the two datasets is that the background fields in GRID rely on averages from the years 1971-1990 (Isotta et al., 2013) and those from HYRAS (Rauthe et al., 2013) on averages from 1961-1990. The differences between the HYRAS and GRID precipitation datasets are rather surprising. The reason for the difference of about 1 mm in daily averages per month over the period 1977 - 2006 (see Figure 5.1(b)) can only be guessed by assessing the differences in the calculation and used data. Both GRID (see (Isotta et al., 2013)) and HYRAS (see (Steiner, 2009)) are calculated using background fields and adding the anomalies of the observed day to that value. Both use

6. Discussion

linear regression for the calculation of the background field at cells without measurement stations and an inverse distance weighting method for the anomalies at a certain day. One difference lies in a detail of the calculation of the background fields. In both methods some stations are selected in the neighbourhood of each grid cell for the calculation of the background fields. In HYRAS these depend on only on a search radius (i.e. 20 km) (Rauthe et al., 2013; Steiner, 2009), whereas in GRID an minimum number of stations was defined. The background field was then calculated using the PRISM method by Schwarb (2000). Thereby the representative stations are selected according to their similarity in topographical properties, such as elevation and exposition. Then their relative weight in the linear regression is increased when they show similar properties (Isotta et al., 2013; Schwarb, 2000). This can lead to a different selection of stations for the interpolation of the background value at a certain grid cell. It is therefore possible, that stations that are located further away get higher weights, and such just being e.g. at the opposite side of a mountain ridge, but having a different exposition get much lower weights (Schwarb, 2000). As stated in Rauthe et al. (2013) an increased number of stations (or a denser measurement grid) can lead to locally differing values. The above procedures most probably lead to a differing number of stations for the same location. The varying selection could therefore be the explanation for the systematic differences in the precipitation estimates of GRID and HYRAS. The differing search radii for the interpolation of the anomalies could also contribute to the problem. Therefore one would have to know the considered stations for all grid cells and their respective values to be able to make a proper comparison. The shape of the long-term daily averages per month in Figure 5.1(b) is very similar in all three datasets. The biggest difference is visible in spring, where the increase in precipitation in the GRID is highest from January to March. In the other two the differences between the months is smaller during that period. I would generally say from visual inspection of the monthly averages, that GRID shows the highest fluctuations. The reason might be that GRID was designed specifically for mountainous areas, since there the precipitation fluctuations are bigger. Furthermore this might probably be the cause for the differing performance in the HBV simulations.

6.1.3. Calibration and Validation using GRID, HYRAS and IDW

The calibration and validation using the three datasets showed generally satisfying results. The general shape of the hydrographs is very similar, they mostly get the timing of the peaks right, only the amplitude is not always covered by the ensembles. In the IDW driven simulation this leads to the effect that the model produces a wrong distribution in the validation period, which is visible in Figure 5.5. There the average high flow season is shifted to earlier stages in the year. Interestingly this happens only during the validation period. In the other two (see Figures 5.3 and 5.3) this phenomena is visible as well to some extent, but not as pronounced as in the IDW. The origin in the single years is for the IDW and HYRAS in the two years 2005 and 2006, where the first discharge peak in the year is simulated rather good but the second (and a third in 2050) peak is mostly underestimated and therefore a source of large errors. The reasons for the different pronunciation of the average phenomena can only lie within the weather datasets, since the

rest of the model, including the snow covered area are the same. But the occurrence of the problem itself, regardless of its pronunciation can either be attributed to a lack of information within the datasets or to the model structure. However, generally it can be said, that the first two to four peaks during the validation periods cause the largest (absolute) errors.

Interestingly the absolute and the relative errors show a very contrasting image. While the absolute errors are bigger during high flows, the relative errors are highest during the low flow season (see Figures A.13, A.14 and A.15 in Appendix). This shows that at high runoff magnitudes a small percentage of deviation from the measurement causes a large absolute volume error. At the same time, small absolute deviations during the low flow season can easily be twice as much as the observation or even more. One has to bear this fact in mind, since it might often be present in hydrological simulations.

However the differences between the relative internal distribution of the three datasets are rather small, both in the datasets and in the discharge simulations: The magnitude of the differences between the different results seems to match, at least intuitively.

A source of uncertainty in these findings might be the fact that the long-term averages cover a longer timespan, whereas the model was run only in the years 1999 to 2006 (warm up starting at 01.08.1997), with a calibration period of only four years from 1999 to 2002. Furthermore, uncertainties in the measured data occur from measurement errors from small-scale weather variations, measurement device design and windy conditions (Beven, 2012). The used techniques in the creation of the weather data sets finally also add uncertainties that are then propagated into the modelling chain.

6.2. Multi-variable Calibration

The calibration of the two different model runs in this work was done quite differently. The second part was done with the updated version of the HBV model. In the meantime a decision was made to not use the threshold technique of the first part again in the second part. The definition of the thresholds is very subjective and produces a different number of parameter sets and the objective function scores might be different in other catchments, which might make it necessary to adapt the thresholds. Furthermore, if different thresholds for differing objective functions are chosen, a different weight is implicitly attributed to the different objective functions. This was not intended in this case. The intention in the first part was to chose the best performing parameter sets for every objective function. But this can also be achieved by creating a score calculated from all objective functions as it was done in the second part (see Section 4.5.2). However the performance of the two techniques is similar in the end. Moreover the decision for either thresholds or a number of best performing parameter sets is subjective in both cases, as well as the weight that is given to the datasets.

The calibration results of the first part in Figure 5.2(a) reveal an interesting property of the selection of Pareto optimal parameter sets and applying thresholds. The different calibrations, especially the one using snowcover only, reach much higher scores. This is because the thresholds where applied before the selection of Pareto points. So even

6. Discussion

though the snowcover was not used in the following calculation of the Pareto Points, it still reached a rather high score. This results finally in a very small number of well-performing parameter sets, e.g. the calibration to snow cover only has only 5 sets left out of 150'000.

The intention in the second part, finding the best possible parameter sets, was of course not changed. However the technique of using thresholds *and* Pareto points was discarded. The decision of sticking to the Pareto Points was made since this technique allows to take account for every objective function itself instead of merging all the functions into one (Beven, 2012). In my opinion, results from the Pareto selection favour results from various places in the parameter space. Because if there were two sets, both performing almost equally good over all measures, but one is always performs slightly better than the other, the Pareto technique would only select the better one, whereas when only working with thresholds or ranking techniques both could be selected. Furthermore the sets inside the selection are said to be "dominant" over those that were not selected (Beven, 2012). Therefore it is probably a better approach to find the really equifinal parameter sets instead of the almost equifinal sets. However the disadvantage is, that the overall performance of such a bunch of parameter sets could be worse overall, compared to the ranking method. Searching for Pareto points only would not be enough as can be seen in the rather bad simulations in Figure 5.6 even when all five functions were combined. Further depending on the number of earlier MC simulation results the number of resulting Pareto points would change too. Therefore and for finding really the best performing sets only, the ranking method of Finger et al. (submitted) was applied after the selection of the Pareto points as well.

But here also a very subjective method came into play. The decision to leave out the MB NSE in the selection of the 10 best sets out of the Pareto solutions can be justified with the better discharge simulation in spring during the calibration and validation period and the very small glaciers in the catchment. This can also be seen in Figure 5.7, where the NSE and the Volume Error show an improved performance when leaving the MB out. The discharge emerging from glacier melt is probably too small to be simulated adequately. This could also be seen in the big sensitivity for small changes in the parameter sets concerning the glacier mass balance in Figure 5.6.

To this end this method combines the advantages of both solutions: It should cover more distinct sets out of the parameter space and thereof only the top performing sets were selected.

Concerning the multi-variable calibration it can be said that the model robustness benefits from using more than one objective function Finger et al. (2011). It is clearly visible in Figure 5.2(b) and 5.6 that the results improve always for the added objective function, whereas the performance of the others gets slightly worse. As can be seen in Finger et al. (2011), the discharge measure is getting worse when using objective functions for discharge, snow cover and also glacier mass balances combined. Further in both studies the discharge simulations are rather bad, when only snow cover is used for calibration. The same effect was also found by Finger et al. (submitted); Parajka and Blöschl (2008) who also investigated the effect of MODIS snow cover images for

the calibration in the HBV model. But the new mean score mostly stays within the range of the standard deviation of the combination before a new function is added. Furthermore the internal consistency of the model is improved when multiple datasets are used, and therefore produces the correct results for the right reasons (Finger et al., 2011, submitted).

In this work the snowcover and the glacier MB receive a relatively small weight compared to the discharge which is calibrated with three objective functions. But I actually doubt that the performance of the snowcover would increase much in this model configuration, since the performance of the snowcover in the selection of the 10 best sets (see Figure 5.7) is pretty close to the performance of the very best snowcover RMSE when calibrating for snowcover only (see Figure 5.6). This could mean that there is something happening inside the model structure which does prevent the snowcover simulation from creating better results. Anyway, the results for the simulated snowcover are not satisfying, especially the overestimations of the simulation in June of more than 15% (see Figure 5.10). For this case an objective function applied only during the melt and accumulation season of snow (leaving out the winter months, when it should be easier to model the snowcover correctly) could have resulted in different parameter sets and also better representation of snowcover. An alternative to the presented solution could therefore be the "Correctly Predicted Snowcover Area" index used Finger et al. (submitted) from April 1st to August 1st. It is therefore thinkable that the use of other metrics (they also used a RMSE for the glacier MB calibration, instead of the NSE) and other weights in the multi-variable calibration could have changed the selection of the parameter sets and result in slightly different scenarios (see Section 6.3.2).

To sum up, using an additional objective function might diminish the performance of the other functions very slightly and increases its own performance at least a little bit, but using multiple objective functions increases the overall consistency of the model as was also shown by Finger et al. (2012, 2011) and Finger et al. (submitted). In the end always some subjectivity is introduced into the modelling process, which also allows to account for unique properties of the observed catchment. As long as the models do not represent the real world processes more adequate the selection of parameters using a multi-variable calibration is always a trade-off between ideals such as internal consistency and model performance.

6.3. Climate Scenarios

The creation of future scenarios asks for decisions to be made that can have an influence on the whole modelling chain. Starting from the selection of discharge data, going over observed weather, catchment characterisation, selection of climate scenarios, post-processing methods of those, model calibration method, parameter ranges, parameter selections and even analysis methods, every single step has its influence on the result and also brings uncertainties into the result. By using multiple climate scenarios for precipitation, temperature and even glacier extents it was tried to cover the uncertainty of the modelling chain to some extent. By using multiple parameter sets it was tried to

6. Discussion

take account of the equifinality problem (Beven, 2006) and as stated in (Finger et al., 2012) multiple parameter sets perform similarly in the evaluation period but differently in future periods and therefore cover more possible outcomes.

6.3.1. Performance of the HBV when using Climate Scenarios during Calibration Period

As was shown in the Results section, the performance of the HBV running with climate scenarios is quite bad in the spring months, especially in May and June. Since there is too little discharge in May and June, the reason could be too little snow melt in spring, emerging from too low temperatures. Snow cover is very sensitive to temperature changes, therefore an increase of e.g. 1°C could decrease the duration of the snow cover in Alpine areas by several weeks (IPCC, 2008). The simulated temperatures from the climate scenarios are in fact too low in May and June (see Figure 5.13). So this could indeed cause the too little snow melt in May and June in Figure 5.14. But on the other hand the precipitation does support this assumption. In June the simulated precipitation is higher than the observed one and in May it is slightly lower. This therefore should rather lead to more discharge, especially in June. These findings lead to the conclusion that the error emerges rather from the model structure and not from the input data. This is also supported by the fact that the discharge patterns of observed and simulated discharge are the same during the calibration and validation period using measured weather data. In both periods the discharge is simulated to low in spring and to high in fall. To my mind this is linked to the simulation of the snowcover simulation in the catchment. The observed snowcover in Figure 5.14 undergoes more extreme changes throughout the year, and declines much faster, particularly in spring, which of course leads to lower discharge from snowcover. The reason for the slow decline of snowcover could on the one hand nevertheless emerge from the too low temperatures, but also simply from insufficiencies in the model structure. This might have had a different outcome if the snowcover would have received more weight in during the calibration. However, the model never achieved a higher snowcover RMSE than 0.82, even when only calibrating for snowcover (see Figure 5.6). The HBV model uses the degree-day method for computing snow melt (Seibert and Vis, 2012), which only uses temperature and totally neglects any radiation interactions. Another reason might be the rather special catchment which actually consists of one natural catchment, which is the Calfeisental but also of several parts of the Weisstannental, where water is guided into the Gigerwaldsee with subsurface conduits. The source of the errors is however unknown, but to my mind it is a result of a combination of at least some of the above possibilities. Another possibility is thinkable: Since spring is the most important period for hydropower production (Finger et al., submitted), some artefacts from the management of the dam could have disrupted the discharge signal.

6.3.2. Changes in Runoff due to Climate Change

The results of the two future periods in Figure 5.11 are most probably affected with the same problem of producing too little discharge in spring, as during the calibration and validation period. Therefore the change was assessed using relative changes in the same way as in Finger et al. (2011) (see Figure 5.12). That way the impact of the changes can be visualized and the changes due to changing climate is assessed. As can be seen in Figure 3.3 the climate models produce quite different predictions for the future periods, even contradictory for precipitation. This can partly explain the large standard deviations in the change signal. But all models agree on rising temperatures, therefore warming temperatures can be seen as very certain for the future. In the mid-term the increases of the seven models in the low flow season (January - April) are around 1.5 °C and in the melt season (May - September) around 2 °C. In the long-term scenario the temperature increases around 2.5 °C during the low flow season and around 4 °C during the melt season. In the low flow season in the mid-term period five out of seven models predict increasing precipitation of around 5% and also five out of seven predict decreasing precipitation of around 10% during the melt season. In the long-term period these trends continue and manifest in bigger differences compared to the baseline period. The precipitation in the low flow season increases further, at least in 5 out of seven models and decreases in the melt season in 6 out of 7 models.

The rising temperatures result in less accumulation of snow during winter, which can be seen in Figure 5.14. This loss of potential melt water in spring during the low flow season might, in regard of discharge, be balanced out by the increasing precipitation. Figures 5.11 and 5.12 demonstrate that the overall discharge in the low flow season increases in both the mid- and the long-term season. Further the discharge distribution over the year is being shifted towards the winter and spring months. In summer the discharge is projected to become smaller. This can be accentuated to the smaller amount of remaining snow in summer, which in turn is a consequence of smaller amount of precipitation falling as snow in winter and increasing melt in spring due to higher temperatures. The discharge increases again towards the end of the year in November and December, probably again due to less precipitation falling as snow and melt events due to higher temperatures. October seems to be a month of transition where the discharge rises slightly in the mid-term, but then decreases in the long-term compared to the reference period due to a smaller snowcover in October compared to the mid-term period. In the two future scenarios the trend goes into the direction of more evenly distributed discharge throughout the year. However this is not certain due to the model failures in May during the calibration and validation period. Further the changes from the mid- to the long-term period are not significant, since the standard deviations are just too big or the changes too small. However the trend is clearly visible. Furthermore the snowcover in summer is overestimated in the calibration and validation period (see Figure 5.10). If this is propagated into the scenarios, then the summer discharge is overestimated and therefore the projected decline in summer discharge might in fact be bigger.

The glacier discharge was neglected so far in the above discussion. Glaciers would most probably produce more discharge in summer and early fall and play a crucial role when

6. Discussion

the snow cover is at its minimum (Finger et al., 2012). To my mind the present glaciers in this catchment are already too small and are believed to have disappeared by around 2050 according to the model by Huss et al. (2010). The small size of the glaciers might be a cause for the rather small and insignificant difference between the mid- and the long-term scenario compared to Finger et al. (2012), where the discharge from glacier melt water will be subject to much bigger changes than in the Calfeisental. In catchments where glacierisation is insignificant the runoff will already in the short term react to precipitation changes. In such with more glacierisation the short-term trends will rather go towards increased runoff due to increased glacier melt (Braun et al., 2000). However as glaciers shrink the annual hydrographs will go more towards the direction of those in the Gigerwaldsee catchment, with a strongly decreasing runoff in future summers (Huss et al., 2008).

However the trend in annual sums of discharges in Table 5.7 points in the same direction. The overall discharge within the average year of the scenario periods shows a slightly decreasing, but insignificant trend. The change in discharge from snow melt water is also modelled to decrease but this result is significant in both periods, because of its magnitude of more than one fourth in the long-term scenario compared to the reference period. For the rain water the opposite is the case, the overall discharge from rain water will increase, mainly due to increased precipitation in winter, however this is again insignificant.

Compared to the study in the Vispa valley of Finger et al. (2012) with the physically based TOPographic Kinematic APproximation and Integration (TOPKAPI) model, which even allowed integration of hydropower operational rules, the results of this thesis are created with a much simpler model setup. However the results are very similar. The seasonal distribution of future runoff shows the same trends. Both works predict an earlier melt season and a reduced runoff in summer, due to the advanced snow melt in spring. Nowadays the biggest flood events occur during summer (Bader, 2000), this might however change to earlier times of the year, not say in winter (Zierl and Bugmann, 2005). This change in the hydrological cycles might force the hydropower companies to change their management practices (Finger et al., 2012) to take account of the reduced runoff in late summer and fall and most probably also due to increased water need further downstream during the drier summer months.

6.3.3. Uncertainties

Such a modelling chain holds uncertainties in all the steps mentioned in Section 6.3. The ANOVA covers the uncertainty introduced by the selection of the seven climate scenarios, the ten parameter sets and in the mid-term period also the three glacier extents. In Figures 5.15(a) and 5.15(b) the overwhelmingly big contribution of the climate scenarios is visible. This is comprehensible when looking at Figure 3.3. The spread of the projections of future weather is rather big. The temperature differences between the models range up to 2 °C in the two scenarios and for precipitation not even all models agree whether it would increase or decrease.

Compared to that the contribution of the parameter sets is very small. If this result is

compared to the result of the same procedure in Finger et al. (2012) some differences occur. However the latter also shares the big contribution of the climate scenarios in winter and spring with the present result. Further the glaciers play a big role in months when they are melting from (June - September). However in the watershed of the Gigerwaldsee the glaciers are too small to even have a visible impact on the uncertainty. The parameter sets have their maxima in summer in both works, which could be explained with the biggest amounts of discharge in summer and therefore the biggest impact on absolute discharge if some parameter changes. Furthermore in summer all hydrological processes contribute to the runoff and therefore the parameters have their biggest influence during that time. A cause of the smaller impact of the parameters in this work could be that the fully distributed and physically based TOPKAPI model (Todini and Ciarapica, 2001) has more parameters to calibrate and therefore produces bigger uncertainties than the HBV model.

Besides the evaluated uncertainties above there can be others to influence the final result. Other climate scenarios than the A1B scenario were not looked at. Therefore different scenarios might have produced very differing results. Another source of uncertainty is the applied correction of $-0.288\text{ }^{\circ}\text{C}$ for all the temperature datasets. Which at least influences the absolute values of the results, but should not have altered the relative changes, since also the temperature for calibration and validation were corrected.

Further there are some things that were totally neglected by the modelling chain. These are for example changes in the land cover, which could emerge from climate changes. According to the IPCC (2008) the Alpine flora will change rather due to a decrease in snow cover than due to temperature rise directly. However an upward shift of the tree lines due to warming temperatures (Gehrig-Fasel et al., 2007) could increase the forest area in the catchment. If in winter more snow is stored in the tree canopies it is more exposed to the atmosphere and therefore water is lost by sublimation (Hedstrom and Pomeroy (1998); Lundberg and Halldin (2001) in: Zierl and Bugmann (2005)) which could alter the runoff regime (Zierl and Bugmann, 2005).

Errors and inaccuracies also occur in the input data, i.e. the precipitation, temperature and discharge measurements will also have produced artefacts in the final calculations.

Finally also the model structure has most probably also had its influence. It was not assessed whether it would have been better split up the catchment into the natural Catchment and the parts in the Weisstannental.

7. Conclusion

7.1. Comparison of weather datasets

Possible reasons for the different model simulation performances was identified in the datasets for the two weather variables temperature and precipitation. The effect of systematic differences between the datasets can be corrected by the HBV model, but relative differences inside the datasets are most likely to be a large contributor to differing results. The temperature dataset could be the main reason for the differences between the IDW dataset and GRID or HYRAS. There the temperature fluctuations and therefore the relative changes throughout the year are higher in the long-term mean than in the other two. In the precipitation dataset on the other hand the fluctuations seem biggest in the GRID dataset, whereas, apart from systematic differences, HYRAS and IDW show a similar shape of the monthly averages. This might be the largest contributor in the differences between the GRID and the HYRAS dataset.

The combination of precipitation and temperature as they are represented by the HYRAS dataset seem to lead to the best discharge simulations combined with the present HBV model configuration. Therefore the **Research Question 1** can be answered saying that the HYRAS dataset gives the best simulation results in the Alpine catchment of the Gigerwaldsee. Even though the differences between HYRAS and GRID are not that big they persist throughout different model settings and runs. However the rather small differences might not be reproducible in any other Alpine catchment or model setting. It might be that for other sites the GRID or even the IDW could produce higher objective function scores. For the CHR this means that the HYRAS dataset is a valid source for weather data even within the alpine area. It should therefore be possible to conduct hydrological simulations (with the HBV model) in the entire catchment of the Rhine river with the same dataset.

7.2. Climate Scenarios

In the second part of this work a modelling chain was presented that was partly inspired by the work of Finger et al. (2012). The used model was the HBV-light model with a newly implemented dynamic glacier routine, which allows glaciers to shrink during the simulation. Using discharge data that was derived from lake level changes of the Gigerwaldsee, temperature and precipitation data from a gridded dataset from MeteoSwiss, the use of a MC calibration and the subsequent Pareto solution determination and thereof selection of the best parameter sets, ten equifinal parameter sets were found to drive the scenario calculations. With the use of the A1B emission scenario and seven

resultant GCM-RCM combinations from the ENSEMBLES project the HBV-light model was driven to simulate a reference period and two future discharge scenarios. For the mid-term scenario, from 2036 - 2065, three glacier scenarios were calculated with the model presented in Huss et al. (2010). The baseline period was driven with interpolated glacier extents from measurement of surrounding glaciers with the methodology of Huss (2012). The long-term period was driven without any glacier data, since the glaciers in the catchment will have disappeared by then according to the model calculations of Huss et al. (2010).

With the results the research questions 2 - 5 raised in Section 1.5 can be answered:

Research Question 2:

An improvement of the model performance with regard to the total discharge could not be made. But the internal model consistency including discharge, snowcover and glacier mass balance simulation was improved. As was already stated in Finger et al. (2012) the result is a trade off between discharge, and the internal model consistency of the snow cover simulation and the glacier mass balances. This means that with regard to discharge better solutions would have been possible, but with the present configuration the maximum possible model consistency was found. Probably the results would have been different if discharge, snowcover and mass balance data would have had the same weight during the calibration.

Research Question 3:

The annual distribution of waters flowing into the Gigerwaldsee will change quite much during this century. Generally it can be said that the discharge increases during spring due to warmer temperatures, which cause increased snow melt. This is amplified by more precipitation falling as rain and a general increase of precipitation during the low flow season. The discharge from snow melt is the main contributor to the increased discharge in spring. During summer the discharge from snow melt is projected to decrease due to the increased melt in spring and therefore reduced snow in summer. Moreover the reduced precipitation in summer causes the discharge due to rain to decrease as well. These two in the end cause the reduced total runoff in summer. The role of the glaciers can be neglected due to their small size. In fall the discharge from snow melt is minimal, whereas towards the winter months the precipitation starts to increase again, causing more discharge from rain water.

Research Question 4:

Today, with reference to the reference period, the total discharge into the Gigerwaldsee from the Calfeisental and the Weisstannental combined is roughly 234 Million(M)m³ per year. The total discharge will, according to the mostly insignificant model predictions, decrease by 3.5(± 7.5)% in the mid-term, resulting in 226 Mm³ per year, and in the long-term by 6(± 11.4)% to around 220 Mm³ per year. These percentages also hold for

7. Conclusion

the decline in potential energy stored in the lake, compared to the 311 M kwh per year from 2000 to 2009, which mean roughly a potential energy per year of 300 and 292 M kWh.

For the discharge ascribed to rain the model predicts an increase of around $7(\pm 15.3)\%$ in the mid-term to 160 Mm^3 and an increase of around $8(\pm 17.8)\%$ in the long-term to around 162 Mm^3 per year.

The melt water from snow routed into the Gigerwaldsee of roughly 81 Mm^3 per year is projected to decrease by about $20(\pm 19.1)\%$ in the mid-term to around 65 Mm^3 and by about $28(\pm 20.5)\%$ in the long-term to 58 Mm^3 per year.

Finally the amount of glacier melt water of around 3 Mm^3 per year is projected to diminish by $85(\pm 16.0)\%$ to 0.5 Mm^3 per year in the mid-term. In the long-term scenario the glaciers are modelled to have disappeared completely.

Research Question 5:

In the ANOVA in Section 5.2.4 the contribution of the seven climate scenarios and ten parameter sets and the three glacier scenarios to the total variance of the global mean of all 70, or 210 model runs respectively was shown. In the mid-term period the biggest fraction of the variance is made up by the climate scenarios by roughly 82% on average throughout the year. The parameter sets make up less than 7% on average throughout the year and the glacier scenarios only about 0.00004%. The rest of about 11% is made up by interactions of the three.

In the long-term scenario without glaciers the proportions are about the same, since the glaciers have a very small contribution to the variance. The rough numbers are: 84% of the variance is made up by the climate scenarios, 6% by the parameter sets and around 10% by interactions and errors.

Final Remarks

To sum up the whole work it can be said that there are visible trends that can give a rough idea about the discharge distribution throughout the 21st century. But the development of hydrological models still has to go further to better represent the real-world processes as well as the development of the different climate models, which still produce a lot of uncertainties. Further also the techniques of parameter selection in hydrological models need to be refined in order to explore the parameter space more efficiently and select appropriate parameter sets. All in all a lot of uncertainties are contained in such a modelling chain, and many sophisticated decisions need to be made, which demand a lot of knowledge and understanding of the underlying processes.

Bibliography

- Akhtar, M., Ahmad, N. and Booij, M. J. (2009), 'Use of regional climate model simulations as input for hydrological models for the Hindukush-Karakorum-l-Himalaya region.', *Hydrology and Earth System Sciences* **13**(7), 1075–1089.
URL: <http://www.hydrol-earth-syst-sci.net/13/1075/2009/>
- Allen, R. G., Pereira, L. S., Raes, D. and Smith, M. (1998), 'Crop evapotranspiration - Guidelines for computing crop water requirements', *FAO Irrigation and drainage paper 56* pp. 1–15.
- Ambroise, B., Perrin, J. L. and Reutenauer, D. (1995), 'Multicriterion Validation of a Semidistributed Conceptual Model of the Water Cycle in the Fecht Catchment (Vosges Massif, France)', *Water Resources Research* **31**(6), 1467–1481.
URL: <http://doi.wiley.com/10.1029/94WR03293>
- Aschwanden, H. (2000), 'Hochwasser 1999 Analyse der Messdaten und statistische Einordnung', *Landeshydrologie und -geologie Bern* (28), 116.
- Aschwanden, H. and Weingartner, R. (1985), 'Die Abflussregimes der Schweiz', *Publikation Gewässerkunde* **65**, 237.
- Bader, S. (2000), *Water - From Climate Factor to Primeval Force*, in *Climate Risks - The Challenge for Alpine Regions*, Hochschulverlag AG an der ETH Zürich, Zürich.
- Beniston, M. (2006), Mountain Weather and Climate: A General Overview and a Focus on Climatic Change in the Alps, in A. Lami and A. Boggero, eds, 'Hydrobiologia', Vol. 562, Springer, pp. 562:3–16.
URL: <http://link.springer.com/10.1007/s10750-005-1802-0>
- Beniston, M. (2009), 'Trends in joint quantiles of temperature and precipitation in Europe since 1901 and projected for 2100', *Geophysical Research Letters* **36**(7), 6.
URL: <http://doi.wiley.com/10.1029/2008GL037119>
- Bergström, S. (1976), Development and application of a conceptual runoff model for Scandinavian catchments, Technical report, SMHI, Norrkömlping, Sweden.
- Beven, K. (2006), 'A manifesto for the equifinality thesis', *Journal of Hydrology* **320**(1-2), 18–36.
URL: <http://linkinghub.elsevier.com/retrieve/pii/S002216940500332X>
- Beven, K. (2012), *Rainfall-Runoff Modelling: The Primer*, 2 edn, John Wiley & Sons, Inc.

Bibliography

- Bezzola, G. R., Hegg, C., Koschni, A. and Frank, F. (2008), ‘Hochwasser 2005 in der Schweiz’, *Federal Department for Environment, Traffic, Energy and Communication UVEK* p. 24.
URL: www.umwelt-schweiz.ch/div-7529-d
- Boé, J. and Terray, L. (2007), ‘Statistical and dynamical downscaling of the Seine basin climate for hydro-meteorological studies’, *International Journal of . . .* **1655**(August), 1643–1655.
URL: <http://onlinelibrary.wiley.com/doi/10.1002/joc.1602/full>
- Bosshard, T., Carambia, M., Goergen, K., Kotlarski, S., Krahe, P., Zappa, M. and Schär, C. (2013), ‘Quantifying uncertainty sources in an ensemble of hydrological climate-impact projections’, *Water Resources Research* **49**(3), 1523–1536.
URL: <http://doi.wiley.com/10.1029/2011WR011533>
- Braun, L. N., Weber, M. and Schulz, M. (2000), ‘Consequences of climate change for runoff from Alpine regions’, *Annals of Glaciology* **31**(1), 19–25.
URL: <http://openurl.ingenta.com/content/xref?genre=article&issn=0260-3055&volume=31&issue=1&spage=19>
- Christensen, J. H., Boberg, F., Christensen, O. B. and Lucas-Picher, P. (2008), ‘On the need for bias correction of regional climate change projections of temperature and precipitation’, *Geophysical Research Letters* **35**(20), L20709.
URL: <http://doi.wiley.com/10.1029/2008GL035694>
- Confesor, R. and Whittaker, G. (2007), ‘Automatic Calibration of Hydrologic Models With Multi-Objective Evolutionary Algorithm and Pareto Optimization1’, *JAWRA Journal of the American Water Resources Association* **43**(4), 981–989.
URL: <http://onlinelibrary.wiley.com/doi/10.1111/j.1752-1688.2007.00080.x/full>
- Daly, C. (2006), ‘Guidelines for assessing the suitability of spatial climate data sets’, *International Journal of Climatology* **26**(6), 707–721.
URL: <http://doi.wiley.com/10.1002/joc.1322>
- Daly, C., Neilson, R. and Phillips, D. (1994), ‘A statistical-topographic model for mapping climatological precipitation over mountainous terrain’, *Journal of applied Meteorology* **33**, 140–158.
URL: [http://journals.ametsoc.org/doi/abs/10.1175/1520-0450\(1994\)033%3C0140:ASTMFM%3E2.0.CO;2](http://journals.ametsoc.org/doi/abs/10.1175/1520-0450(1994)033%3C0140:ASTMFM%3E2.0.CO;2)
- Déqué, M., Rowell, D., Lüthi, D. and Giorgi, F. (2007), ‘An intercomparison of regional climate simulations for Europe: assessing uncertainties in model projections’, *Climatic Change* **81**, 53–70.
URL: <http://link.springer.com/article/10.1007/s10584-006-9228-x>
- Déqué, M., Somot, S. and Sanchez-Gomez, E. (2012), ‘The spread amongst ENSEMBLES regional scenarios: regional climate models, driving general circulation models and

- interannual variability', *Climate Dynamics* .
URL: <http://link.springer.com/article/10.1007/s00382-011-1053-x>
- Dodson, R. and Marks, D. (1997), 'Daily air temperature interpolated at high spatial resolution over a large mountainous region', *Climate Research* **8**(Myers 1994), 1–20.
URL: [ftp://199.133.140.121/publications/1997/Marks-Daily air temperature interpolated at high spatial.pdf](ftp://199.133.140.121/publications/1997/Marks-Daily%20air%20temperature%20interpolated%20at%20high%20spatial.pdf)
- ESRI (2011), 'ArcGIS Desktop: Release 10'.
- Finger, D. (2014), Assessing the hydro power potential of two prospective sites in north eastern Iceland using hydrological modeling, Technical report, Icelandic Meteorological Office, Reykjavík.
- Finger, D., Heinrich, G., Gobiet, A. and Bauder, A. (2012), 'Projections of future water resources and their uncertainty in a glacierized catchment in the Swiss Alps and the subsequent effects on hydropower production during the 21st century', *Water Resources Research* **48**(2).
URL: <http://doi.wiley.com/10.1029/2011WR010733>
- Finger, D., Pellicciotti, F., Konz, M., Rimkus, S. and Burlando, P. (2011), 'The value of glacier mass balance, satellite snow cover images, and hourly discharge for improving the performance of a physically based distributed hydrological model', *Water Resources Research* **47**(7), 1–14.
URL: <http://doi.wiley.com/10.1029/2010WR009824>
- Finger, D., Vis, M., Huss, M. and Seibert, J. (submitted), 'The value of data availability versus model complexity for estimating snow, glacier and rain contribution to runoff in mountain streams', *Water Resources Research* p. 42.
- Fischer, M. and Huss, M. (in prep.), 'Surface elevation changes of all Swiss glaciers over the last 25 years', *The Cryosphere* .
- Fischer, M., Huss, M., Barboux, C. and Hoelzle, M. (submitted), 'The new swiss glacier inventory sgi2010: Relevance of using high-resolution source data in areas dominated by very small glaciers', *Arctic, Antarctic and Alpine Research* .
- Franks, S. W., Gineste, P., Beven, K. J. and Merot, P. (1998), 'On constraining the predictions of a distributed model: The incorporation of fuzzy estimates of saturated areas into the calibration process', *Water Resources Research* **34**(4), 787–797.
URL: <http://onlinelibrary.wiley.com/doi/10.1029/97WR03041/full>
<http://doi.wiley.com/10.1029/97WR03041>
- Frei, C. (2014), 'Interpolation of temperature in a mountainous region using non-linear profiles and non-Euclidean distances', *International Journal of Climatology* **34**(5), 1585–1605.
URL: <http://doi.wiley.com/10.1002/joc.3786>

Bibliography

- Frei, C. and Schär, C. (1998), ‘A precipitation climatology of the Alps from high-resolution rain-gauge observations’, *International Journal of Climatology* **900**, 873–900.
URL: ftp://iacftp.ethz.ch/pub_read/luethi/master_thesis/Frei_Schaer_1998.pdf
- Gehrig-Fasel, J., Guisan, A. and Zimmermann, N. E. (2007), ‘Tree line shifts in the Swiss Alps: Climate change or land abandonment?’, *Journal of Vegetation Science* **18**(4), 571–582.
URL: <http://onlinelibrary.wiley.com/doi/10.1111/j.1654-1103.2007.tb02571.x/abstract> <http://doi.wiley.com/10.1111/j.1654-1103.2007.tb02571.x>
- Gudmundsson, L., Bremnes, J. B., Haugen, J. E. and Engen-Skaugen, T. (2012), ‘Technical Note: Downscaling RCM precipitation to the station scale using statistical transformations – a comparison of methods’, *Hydrology and Earth System Sciences* **16**(9), 3383–3390.
URL: <http://www.hydrol-earth-syst-sci.net/16/3383/2012/>
- Gurtz, J., Baltensweiler, A. and Lang, H. (1999), ‘Spatially distributed hydrotope-based modelling of evapotranspiration and runoff in mountainous basins’, *Hydrological Processes* **13**(17), 2751–2768.
URL: <http://doi.wiley.com/10.1002/%28SICI%291099-1085%2819991215%2913%3A17%3C2751%3A%3AAID-HYP897%3E3.0.CO%3B2-O>
- Hall, D. K., Riggs, G. a., Salomonson, V. V., DiGirolamo, N. E. and Bayr, K. J. (2002), ‘MODIS snow-cover products’, *Remote Sensing of Environment* **83**(1-2), 181–194.
URL: <http://linkinghub.elsevier.com/retrieve/pii/S0034425702000950>
- Hall, D., Riggs, G. and Salomonson, V. (1995), ‘Development of methods for mapping global snow cover using moderate resolution imaging spectroradiometer data’, *Remote sensing of Environment* **1**, 127–140.
URL: <http://www.sciencedirect.com/science/article/pii/003442579500137P>
- Hartmann, D., Tank, A. K., Rusticucci, M., Alexander, L., Brönnimann, S., Charabi, Y., Dentener, F., Dlugokencky, E., Easterling, D., Kaplan, A., Soden, B., Thorne, P., Wild, M. and Zhai, P. (2013), Observations: Atmosphere and Surface, in T. Stocker, D. Qin, G.-K. Plattner, M. Tignor, S. Allen, J. Boschung, A. Nauels, Y. Xia, V. Bex and P. Midgley, eds, ‘Climate Change 2013: The Physical Science Basis. Contribution of Working Group I to the Fifth Assessment Report of the Intergovernmental Panel on Climate Change’, Cambridge University Press, United Kingdom and New York, NY, USA, chapter 2, pp. 159–254.
URL: <http://www.climatechange2013.org/>
- Hedstrom, N. R. and Pomeroy, J. W. (1998), ‘Measurements and modelling of snow interception in the boreal forest’, *Hydrological Processes* **12**(10-11), 1611–1625.

URL: [http://doi.wiley.com/10.1002/\(SICI\)1099-1085\(199808/09\)12:10/11<1611::AID-HYP684>3.0.CO;2-4](http://doi.wiley.com/10.1002/(SICI)1099-1085(199808/09)12:10/11<1611::AID-HYP684>3.0.CO;2-4)

Hock, R., Jansson, P. and Braun, L. (2005), Modelling the response of mountain glacier discharge to climate warming., in U. Huber, M. Reasoner and H. Bugmann, eds, 'Global change and mountain regions: A state of Knowledge Overview. Advances in Global Time Series', Springer, Dordrecht, pp. 243–252.

URL: http://link.springer.com/chapter/10.1007%2F1-4020-3508-X_25

Huss, M. (2012), 'Extrapolating glacier mass balance to the mountain-range scale: the European Alps 1900–2100', *The Cryosphere* **6**(4), 713–727.

URL: <http://www.the-cryosphere.net/6/713/2012/>

Huss, M. and Farinotti, D. (2012), 'Distributed ice thickness and volume of all glaciers around the globe', *Journal of Geophysical Research* **117**(F4), 10.

URL: <http://doi.wiley.com/10.1029/2012JF002523>

Huss, M., Farinotti, D., Bauder, A. and Funk, M. (2008), 'Modelling runoff from highly glacierized alpine drainage basins in a changing climate', *Hydrological Processes* **22**(19), 3888–3902.

URL: <http://onlinelibrary.wiley.com/doi/10.1002/hyp.7055/abstract>
<http://doi.wiley.com/10.1002/hyp.7055>

Huss, M., Juvet, G., Farinotti, D. and Bauder, A. (2010), 'Future high-mountain hydrology: a new parameterization of glacier retreat', *Hydrology and Earth System Sciences* **14**(5), 815–829.

URL: <http://www.hydrol-earth-syst-sci.net/14/815/2010/>

IBM Corp. Released (2012), 'IBM SPSS Statistics for Windows'.

Ines, A. V. and Hansen, J. W. (2006), 'Bias correction of daily GCM rainfall for crop simulation studies', *Agricultural and Forest Meteorology* **138**(1-4), 44–53.

URL: <http://linkinghub.elsevier.com/retrieve/pii/S0168192306000979>

IPCC, . (2013), Summary for Policymakers., in T. Stocker, D. Qin, G.-K. Plattner, M. Tignor, S. Allen, J. Boschung, A. Nauels, Y. Xia, V. Bex and P. Midgley, eds, 'Climate Change 2013: The Physical Science Basis. Contribution of Working Group I to the Fifth Assessment Report of the Intergovernmental Panel on Climate Change', climate ch edn, Cambridge University Press, United Kingdom and New York, NY, USA.

IPCC (2008), Climate change and water. Technical Paper VI, Technical report, IPCC Secretariat, Geneva.

URL: <http://www.cabdirect.org/abstracts/20083307083.html>

Isotta, F. a., Frei, C., Weigluni, V., Perćec Tadić, M., Lassègues, P., Rudolf, B., Pavan, V., Cacciamani, C., Antolini, G., Ratto, S. M., Munari, M., Micheletti, S., Bonati,

Bibliography

- V., Lussana, C., Ronchi, C., Panettieri, E., Marigo, G. and Vertačnik, G. (2013), 'The climate of daily precipitation in the Alps: development and analysis of a high-resolution grid dataset from pan-Alpine rain-gauge data', *International Journal of Climatology* **1675**(August 2013), 1657–1675.
URL: <http://doi.wiley.com/10.1002/joc.3794>
- Jacob, D., Bärring, L., Christensen, O. B. s., Christensen, J. H., Castro, M., Déqué, M., Giorgi, F., Hagemann, S., Hirschi, M., Jones, R., Kjellström, E., Lenderink, G., Rockel, B., Sánchez, E., Schär, C., Seneviratne, S. I., Somot, S., Ulden, A. and Hurk, B. (2007), 'An inter-comparison of regional climate models for Europe: model performance in present-day climate', *Climatic Change* **81**(S1), 31–52.
URL: <http://link.springer.com/10.1007/s10584-006-9213-4>
- Jacobeit, J. (2007), Klimageographie, in H. Gebhard, R. Glaser, U. Radtke and P. Reuber, eds, 'Geographie - Physische Geographie und Humangeographie', Elsevier Spektrum Akademischer Verlag, chapter 8, pp. 188–259.
- Jaeger, E. B., Anders, I., Lüthi, D., Rockel, B., Schär, C. and Seneviratne, S. I. (2008), 'Analysis of ERA40-driven CLM simulations for Europe', *Meteorologische Zeitschrift* **17**(4), 349–367.
URL: <http://openurl.ingenta.com/content/xref?genre=article&issn=0941-2948&volume=17&issue=4&spage=349>
- Klein Tank, A. M. G., Wijngaard, J. B., Können, G. P., Böhm, R., Demarée, G., Gocheva, A., Mileta, M., Pashiardis, S., Hejkrlik, L., Kern-Hansen, C., Heino, R., Bessemoulin, P., Müller-Westermeier, G., Tzanakou, M., Szalai, S., Pálsdóttir, T., Fitzgerald, D., Rubin, S., Capaldo, M., Maugeri, M., Leitass, A., Bukantis, A., Aberfeld, R., van Engelen, a. F. V., Forland, E., Miletus, M., Coelho, F., Mares, C., Razuvaev, V., Nieplova, E., Cegnar, T., Antonio López, J., Dahlström, B., Moberg, A., Kirchhofer, W., Ceylan, A., Pachaliuk, O., Alexander, L. V. and Petrovic, P. (2002), 'Daily dataset of 20th-century surface air temperature and precipitation series for the European Climate Assessment', *International Journal of Climatology* **22**(12), 1441–1453.
URL: <http://doi.wiley.com/10.1002/joc.773>
- Klemeš, V. (1986), 'Operational testing of hydrological simulation models', *Hydrological Sciences Journal* **31**(1), 13–24.
URL: <http://www.tandfonline.com/doi/abs/10.1080/02626668609491024>
- Koboltschnig, G. R., Sch, W., Zappa, M., Kroisleitner, C. and Holzmann, H. (2008), 'Runoff modelling of the glacierized Alpine Upper Salzach basin (Austria): multi-criteria result validation', **3964**(August), 3950–3964.
- Konrad I., C. E. (1996), 'Relationships between Precipitation Event Types and Topography in the Southern Blue Ridge Mountains of the Southeastern USA', *International Journal of Climatology* **16**(1), 49–62.

- URL:** <http://doi.wiley.com/10.1002/%28SICI%291097-0088%28199601%2916%3A1%3C49%3A%3AAID-JOC993%3E3.0.CO%3B2-D>
- Konz, M. and Seibert, J. (2010), 'On the value of glacier mass balances for hydrological model calibration', *Journal of Hydrology* **385**(1-4), 238–246.
URL: <http://linkinghub.elsevier.com/retrieve/pii/S0022169410000958>
- Kotlarski, S., Block, A., Böhm, U., Jacob, D., Keuler, K., Knoche, R., Rechid, D. and Walter, A. (2005), 'Regional climate model simulations as input for hydrological applications: evaluation of uncertainties', *Advances in Geosciences* **5**, 119–125.
URL: <http://www.adv-geosci.net/5/119/2005/>
- Kuczera, G. and Mroczkowski, M. (1998), 'Assessment of hydrologic parameter uncertainty and the worth of multiresponse data', *Water Resources Research* **34**(6), 1481–1489.
URL: <http://doi.wiley.com/10.1029/98WR00496>
- Latenser, M. and Schneebeli, M. (2003), 'Long-term snow climate trends of the Swiss Alps (1931-99)', *International Journal of Climatology* **23**(7), 733–750.
URL: <http://doi.wiley.com/10.1002/joc.912>
- Lehner, B., Czisch, G. and Vassolo, S. (2005), 'The impact of global change on the hydropower potential of Europe: a model-based analysis', *Energy Policy* **33**(7), 839–855.
URL: <http://linkinghub.elsevier.com/retrieve/pii/S0301421503003112>
- Leibundgut, C., Weingartner, R. and Aschwanden, H. (1984), 'Abflussregimeforschung und ihre praktische Bedeutung', *Geographica Helvetica : schweizerische Zeitschrift für Geographie* **39**, 149–153.
URL: <http://dx.doi.org/10.5169/seals-60025>
- Lu, G. Y. and Wong, D. W. (2008), 'An adaptive inverse-distance weighting spatial interpolation technique', *Computers & Geosciences* **34**(9), 1044–1055.
URL: <http://linkinghub.elsevier.com/retrieve/pii/S0098300408000721>
- Lundberg, A. and Halldin, S. (2001), 'Snow interception evaporation: Review of measurement techniques, processes, and models', *Theoretical and Applied Climatology* **70**, 117–133.
- Martin, E. and Etchevers, P. (2005), 'Impact of climatic changes on snow cover and snow hydrology in the French Alps', *Global change and mountain regions* pp. 235–242.
URL: http://link.springer.com/content/pdf/10.1007/1-4020-3508-X_24.pdf
- McGuinness, J. and Bordne, E. (1972), *A comparison of lysimeter-derived potential evapotranspiration with computed values*, number 1452.
- Mountain Agenda (1998), *Mountains of the World: Water Towers for the 21 st Century Case studies from Asia*, Technical report, Paul Haupt AG, Bern.

Bibliography

- Müller, F., Caffish, T. and Müller, G. (1976), *Firn und Eis der Schweizer Alpen: Gletscherinventar*, Geographisches Institut, ETH Zürich, Zurich, Switzerland.
- Nash, J. and Sutcliffe, J. (1970), 'River flow forecasting through conceptual models, part 1-a discussion of principles', *Journal of Hydrology* **10**, 282–290.
- Norrant, C. and Douguédroit, A. (2006), 'Monthly and daily precipitation trends in the Mediterranean (1950–2000)', *Theoretical and Applied Climatology* **83**, 89–106.
URL: <http://link.springer.com/article/10.1007/s00704-005-0163-y>
- Oudin, L., Hervieu, F., Michel, C., Perrin, C., Andréassian, V., Anctil, F. and Loumagne, C. (2005), 'Which potential evapotranspiration input for a lumped rainfall-runoff model?', *Journal of Hydrology* **303**(1-4), 290–306.
URL: <http://linkinghub.elsevier.com/retrieve/pii/S0022169404004056>
- Panofsky, H. and Brier, G. (1968), *Some Applications of Statistics to Meteorology*, The Pennsylvania State University Press, Philadelphia.
- Parajka, J. and Blöschl, G. (2008), 'The value of MODIS snow cover data in validating and calibrating conceptual hydrologic models', *Journal of Hydrology* **358**(3-4), 240–258.
URL: <http://linkinghub.elsevier.com/retrieve/pii/S0022169408002862>
- Pardé, M. (1933), *Fleuves et rivières*, Librairie Armand Colin, Paris.
- Penman, A. H. L. (1948), 'Natural Evaporation from Open Water, Bare Soil and Grass', *Proceedings of the Royal Society of London. Series A, Mathematical and Physical Sciences* **193**(1032), 120–145.
- Polityko, E. (2008), 'Calculation of Pareto points'.
URL: <http://www.mathworks.ch/matlabcentral/fileexchange/22507-calculation-of-pareto-points#comments>
- Prein, A. F., Gobiet, A. and Truhetz, H. (2011), 'Analysis of uncertainty in large scale climate change projections over Europe', *Meteorologische Zeitschrift* **20**(4), 383–395.
URL: <http://openurl.ingenta.com/content/xref?genre=article&issn=0941-2948&volume=20&issue=4&spage=383>
- Prudhomme, C., Reynard, N. and Crooks, S. (2002), 'Downscaling of global climate models for flood frequency analysis: where are we now?', *Hydrological Processes* **16**(6), 1137–1150.
URL: <http://doi.wiley.com/10.1002/hyp.1054>
- R-Team (2005), 'R: A Language and Environment for Statistical Computing', *R foundation for Statistical Computing*.
URL: <http://www.r-project.org/>

- Rauthe, M., Steiner, H., Riediger, U., Mazurkiewicz, A. and Gratzki, A. (2013), ‘A Central European precipitation climatology – Part I: Generation and validation of a high-resolution gridded daily data set (HYRAS)’, *Meteorologische Zeitschrift* **22**(3), 235–256.
URL: <http://openurl.ingenta.com/content/xref?genre=article&issn=0941-2948&volume=22&issue=3&spage=235>
- Rhein, M., Rintoul, S., Aoki, S., Campos, E., Chambers, D., Feely, R., Gulev, S., Johnson, G., Josey, S., Kostianoy, A., Mauritzen, C., Roemmich, D., Talley, L. and Wang, F. (2013), Observations: Ocean, in T. Stocker, D. Qin, G.-K. Plattner, M. Tignor, S. Allen, J. Boschung, A. Nauels, Y. Xia, V. Bex and P. Midgley, eds, ‘Climate Change 2013: The Physical Science Basis. Contribution of Working Group I to the Fifth Assessment Report of the Intergovernmental Panel on Climate Change’, chapter 3, pp. 255–316.
- Roe, G. H. (2005), ‘Orographic Precipitation’, *Annual Review of Earth and Planetary Sciences* **33**(1), 645–671.
URL: <http://www.annualreviews.org/doi/abs/10.1146/annurev.earth.33.092203.122541>
- Roulet, Y., Landl, B., Félix, C. and Calpini, B. (2010), ‘Development and challenges in SwissMetNet, the new Swiss meteorological network’, *MeteoSwiss* pp. 1–6.
URL: www.meteoschweiz.ch
- Schaeffli, B. and Huss, M. (2011), ‘Integrating point glacier mass balance observations into hydrologic model identification’, *Hydrology and Earth System Sciences* **15**(4), 1227–1241.
URL: <http://www.hydrol-earth-syst-sci.net/15/1227/2011/>
- Schwarb, M. (2000), The Alpine precipitation climate: Evaluation of a high-resolution analysis scheme using comprehensive rain-gauge data, PhD thesis, Swiss Federal Institute of Technology Zurich.
- Seibert, J. (2000), ‘Multi-criteria calibration of a conceptual runoff model using a genetic algorithm’, *Hydrology and Earth System Sciences* **4**(2), 215–224.
URL: <http://www.hydrol-earth-syst-sci.net/4/215/2000/hess-4-215-2000.pdf>
- Seibert, J. and Uhlenbrook, S. (2000), ‘Multiscale calibration and validation of a conceptual rainfall-runoff model’, *Physics and Chemistry of . . .* **25**(1), 59–64.
URL: <http://www.sciencedirect.com/science/article/pii/S1464190999001215>
- Seibert, J. and Vis, M. J. P. (2012), ‘Teaching hydrological modeling with a user-friendly catchment-runoff-model software package’, *Hydrology and Earth System Sciences* **16**(9), 3315–3325.
URL: <http://www.hydrol-earth-syst-sci.net/16/3315/2012/>

Bibliography

- Sharma, M., Coulibaly, P. and Dibike, Y. (2010), 'Assessing the need for downscaling RCM data for hydrologic impact study', *Journal of Hydrologic Engineering* pp. 534–539.
URL: [http://ascelibrary.org/doi/abs/10.1061/\(ASCE\)HE.1943-5584.0000349](http://ascelibrary.org/doi/abs/10.1061/(ASCE)HE.1943-5584.0000349)
- Shepard, D. (1984), 'Computer mapping: The SYMAP interpolation algorithm', *Spatial Statistics and Models* **40**, 133–145.
URL: http://link.springer.com/chapter/10.1007/978-94-017-3048-8_7
- Stahl, K., Moore, R. D., Shea, J. M., Hutchinson, D. and Cannon, a. J. (2008), 'Coupled modelling of glacier and streamflow response to future climate scenarios', *Water Resources Research* **44**(2), n/a–n/a.
URL: <http://doi.wiley.com/10.1029/2007WR005956>
- Steiner, H. (2009), 'Zwischenbericht zum Projekt HYRAS - Erstellung hydrologisch relevanter Raster- und Gitterpunktsdatensätze für das Bundesgebiet und internationalen Flussgebietsanteile von Rhein, Donau und Elbe auf der Basis qualitätsbewerteter meteorologischer Beobachtung', *Referat KU 41 Hydrometeorologische Beratungsleistungen* p. 106.
- Suklitsch, M., Gobiet, A., Truhetz, H., Awan, N. K., Göttel, H. and Jacob, D. (2010), 'Error characteristics of high resolution regional climate models over the Alpine area', *Climate Dynamics* **37**(1-2), 377–390.
URL: <http://link.springer.com/10.1007/s00382-010-0848-5>
- Sun, F., Roderick, M. L., Lim, W. H. and Farquhar, G. D. (2011), 'Hydroclimatic projections for the Murray-Darling Basin based on an ensemble derived from Intergovernmental Panel on Climate Change AR4 climate models', *Water Resources Research* **47**(12), 1–14.
URL: <http://doi.wiley.com/10.1029/2010WR009829>
- Terink, W., Hurkmans, R. T. W. L., Torfs, P. J. J. F. and Uijlenhoet, R. (2009), 'Bias correction of temperature and precipitation data for regional climate model application to the Rhine basin', *Hydrology and Earth System Sciences Discussions* **6**(4), 5377–5413.
URL: <http://www.hydrol-earth-syst-sci-discuss.net/6/5377/2009/>
- Teutschbein, C. and Seibert, J. (2010a), 'Regional Climate Models for Hydrological Impact Studies at the Catchment Scale: A Review of Recent Modeling Strategies', *Geography Compass* **4**(7), 834–860.
URL: <http://doi.wiley.com/10.1111/j.1749-8198.2010.00357.x>
- Teutschbein, C. and Seibert, J. (2010b), 'Regional climate models for hydrological impact studies at the catchment scale: a review of recent modeling strategies', *Geography Compass* **4**(7), 834–860.
URL: <http://onlinelibrary.wiley.com/doi/10.1111/j.1749-8198.2010.00357.x/full>

Teutschbein, C. and Seibert, J. (2012), ‘Bias correction of regional climate model simulations for hydrological climate-change impact studies: Review and evaluation of different methods’, *Journal of Hydrology* **456-457**, 12–29.

URL: <http://linkinghub.elsevier.com/retrieve/pii/S0022169412004556>

Teutschbein, C. and Seibert, J. (2013), ‘Is bias correction of regional climate model (RCM) simulations possible for non-stationary conditions?’, *Hydrology and Earth System Sciences* **17**(12), 5061–5077.

URL: <http://www.hydrol-earth-syst-sci.net/17/5061/2013/>

TheMathWorks Inc. (2013), ‘MATLAB’.

Todini, E. and Ciarapica, L. (2001), The TOPKAPI model, *in* V. Singh and D. Frevert, eds, ‘Mathematical Models of Large Watershed Hydrology’, Water Resources Publications, Littleton, Colorado, chapter 12, p. 914.

URL: <http://www.cabdirect.org/abstracts/20033121368.html;jsessionid=A90E92A112020041887E7E0A9AED>

Uppala, S. M., KåDñillberg, P. W., Simmons, a. J., Andrae, U., Bechtold, V. D. C., Fiorino, M., Gibson, J. K., Haseler, J., Hernandez, a., Kelly, G. a., Li, X., Onogi, K., Saarinen, S., Sokka, N., Allan, R. P., Andersson, E., Arpe, K., Balmaseda, M. a., Beljaars, a. C. M., Berg, L. V. D., Bidlot, J., Bormann, N., Caires, S., Chevallier, F., Dethof, a., Dragosavac, M., Fisher, M., Fuentes, M., Hagemann, S., Hólm, E., Hoskins, B. J., Isaksen, L., Janssen, P. a. E. M., Jenne, R., Mcnally, a. P., Mahfouf, J.-F., Morcrette, J.-J., Rayner, N. a., Saunders, R. W., Simon, P., Sterl, a., Trenberth, K. E., Untch, a., Vasiljevic, D., Viterbo, P. and Woollen, J. (2005), ‘The ERA-40 re-analysis’, *Quarterly Journal of the Royal Meteorological Society* **131**(612), 2961–3012.

URL: <http://doi.wiley.com/10.1256/qj.04.176>

van der Linden, P. and Mitchell, J. F. B. (2009), Climate change and its impacts: Summary of research and results from the ENSEMBLES project, Technical report, Met Office Hadley Center, FitzRoy Road, Exeter EX1 3PB.

Vaughan, D., Comiso, J., Allison, I., Carrasco, J., Kaser, G., Kwok, R., Mote, P., Murray, T., Paul, F., Ren, J., Rignot, E., Solomina, O., Steffen, K. and Zhang, T. (2013), Observations: Cryosphere, *in* T. Stocker, D. Qin, G.-K. Plattner, M. Tignor, S. Allen, J. Boschung, A. Nauels, Y. Xia, V. Bex and P. Midgley, eds, ‘Climate Change 2013: The Physical Science Basis. Contribution of Working Group I to the Fifth Assessment Report of the Intergovernmental Panel on Climate Change’, Cambridge University Press, United Kingdom and New York, NY, USA, chapter 4, pp. 317–382.

URL: <http://www.climatechange2013.org/>

Vidale, P. L., Lüthi, D., Wegmann, R. and Schär, C. (2007), ‘European summer climate variability in a heterogeneous multi-model ensemble’, *Climatic Change* **81**(S1), 209–232.

URL: <http://link.springer.com/10.1007/s10584-006-9218-z>

Bibliography

von Storch, H. and Zwiers, F. W. (1999), *Statistical analysis in climate research*, Cambridge University Press.

URL: <http://www.amazon.de/Statistical-Analysis-Climate-Research-Storch/dp/0521012309>

Wood, a. W., Leung, L. R., Sridhar, V. and Lettenmaier, D. P. (2004), 'Hydrologic Implications of Dynamical and Statistical Approaches to Downscaling Climate Model Outputs', *Climatic Change* **62**(1-3), 189–216.

URL: <http://link.springer.com/10.1023/B:CLIM.0000013685.99609.9e>

World Commission on Dams (2000), Dams and development - a new framework for decision-making. The Report of the World Comission on Dams, Technical Report November, Earthscan, London, UK.

Zierl, B. and Bugmann, H. (2005), 'Global change impacts on hydrological processes in Alpine catchments', *Water Resources Research* **41**(2), 1–13.

URL: <http://doi.wiley.com/10.1029/2004WR003447>

Acronyms

- ANOVA** Analysis of Variance. 38, 54, 66
- AR5** Assessment Report 5. 1
- ASTER** Advanced Space-borne Thermal Emission and Reflection Radiometer. 16
- CDF** cumulative distribution function. 19, 20
- CHR** Commission for the Hydrology of the Rhine Basin. 4, 68
- DEM** digital elevation model. 12, 13, 16, 26, 31, 32
- DWD** German Weather Service (*German*: Deutscher Wetterdienst). 4
- GCM** global circulation model. 5, 16, 17, 18, 19, 21, 22, 38, 68
- GERM** Glacier Evolution Runoff Model. 16
- HBV** Hydrologiska Byråns Vattenavdelning. 4, 5, 10, 14, 16, 19, 21, 24, 25, 26, 28, 29, 30, 31, 32, 33, 34, 38, 43, 45, 50, 57, 58, 59, 61, 62, 64, 66, 68, 85, 93
- IPCC** Intergovernmental Panel on Climate Change. 1
- MB** mass balance. 28, 29, 33, 34, 48, 62, 63
- MC** Monte Carlo. 29, 33, 34, 62, 68
- MODIS** Moderate Resolution Imaging Spectrometer. 4, 15, 16
- NDSI** Normalized Difference Snow Index. 15, 16
- NSE** Nash-Sutcliffe Efficiency. 28, 29, 30, 33, 34, 43, 45, 48, 62, 63
- QM** Quantile Mapping. 19, 20, 33
- RCM** regional climate model. 16, 17, 18, 19, 20, 21, 22, 38, 68
- RG1** Randolph Glacier Inventory. 16
- RMSE** Root-Mean-Square Error. 27, 29, 43, 63, 64

Terms and abbreviations

SC snow cover. 29, 34, 48

SGL Swiss Glacier Inventory. 16

SPSS Statistical Package for the Social Sciences. 24

SRTM Shuttle Radar Topography Mission. 16

TOPKAPI TOPographic Kinematic APproximation and Integration. 66

WE water equivalent. 26, 28, 32

A. Appendix

A.1. Figures of the Calibration and Validation Period of the 3 Datasets

A.1.1. Dotty Plots

Dotty Plots of the used parameter combinations for the calibration of the HBV model using the the three datasets. Parameters with vertical lines are either kept constant (CFR, CWH) or not used in the used model structure (DELAY, PART).

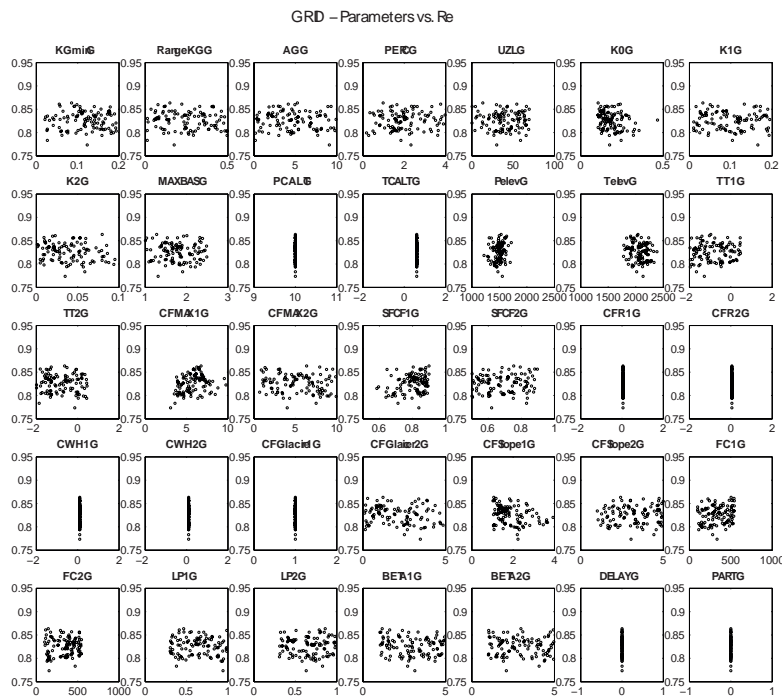


Figure A.1.: Dotty Plots of the used parameter combinations using the IDW dataset.

A. Appendix

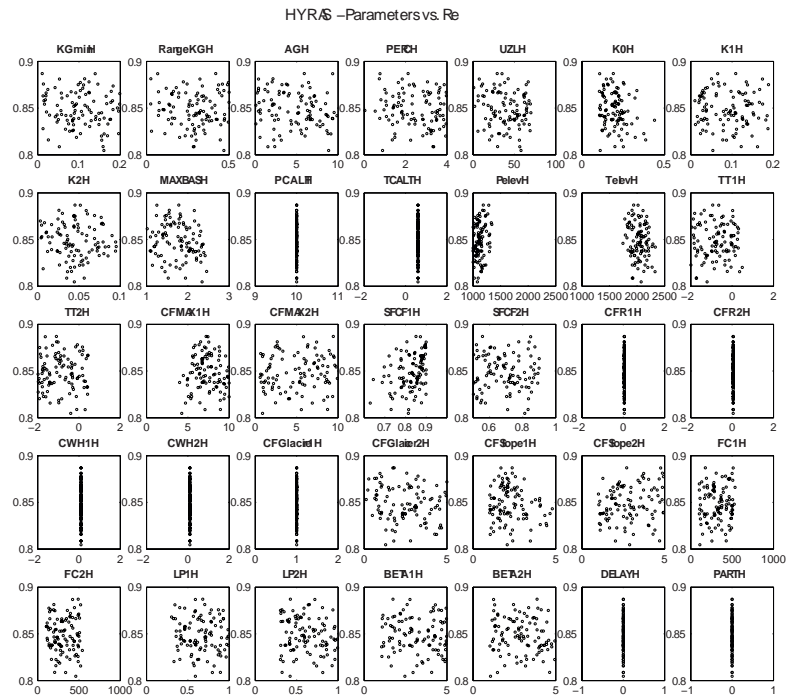


Figure A.2.: Dotty Plots of the used parameter combinations using the IDW dataset.

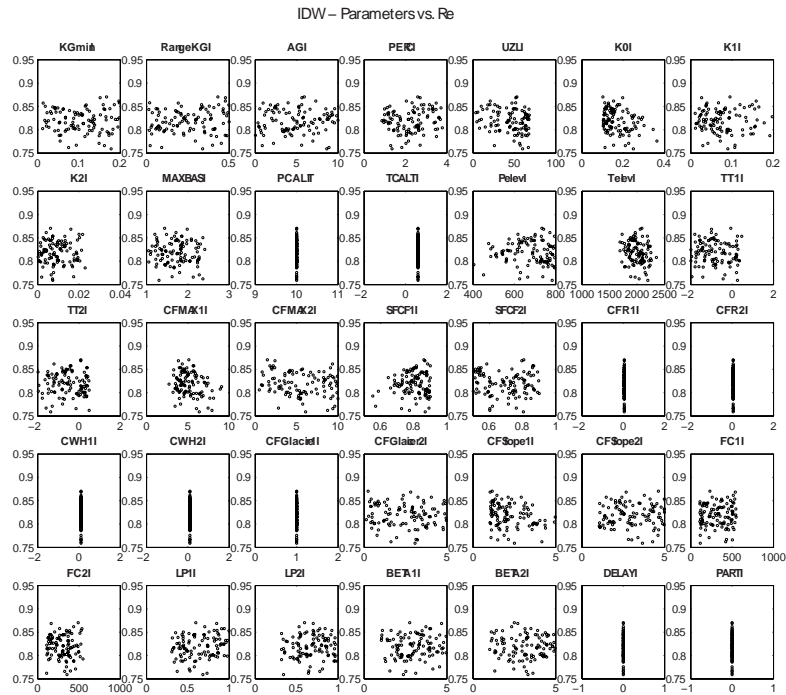


Figure A.3.: Dotty Plots of the used parameter combinations using the IDW dataset.

A.1.2. Discharge Plots

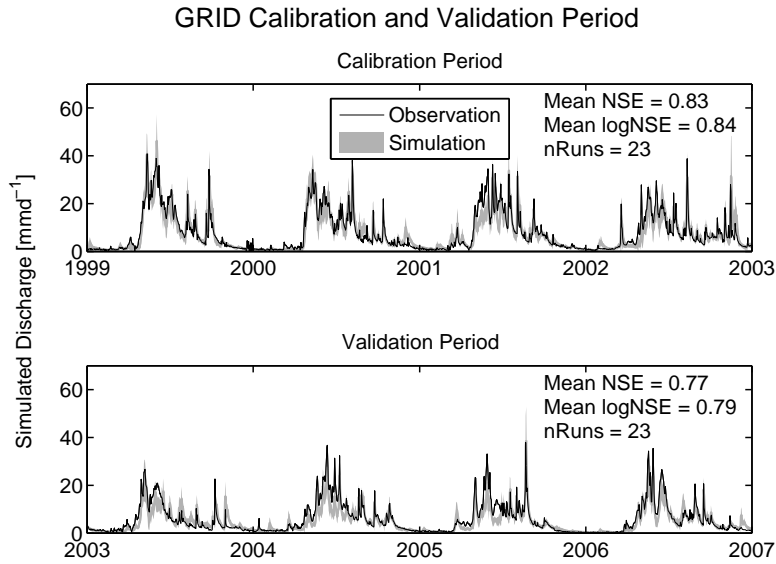


Figure A.4.: Daily discharge of calibration and validation period using the GRID dataset.

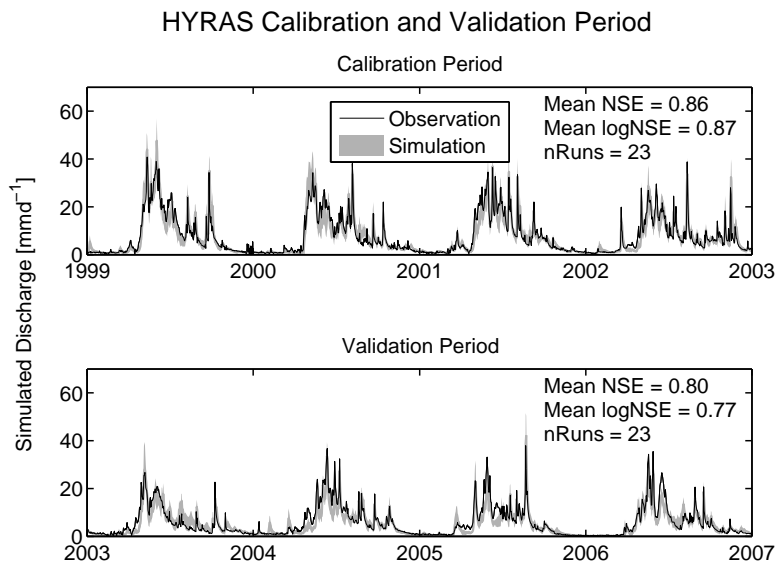


Figure A.5.: Daily discharge of calibration and validation period using the HYRAS dataset.

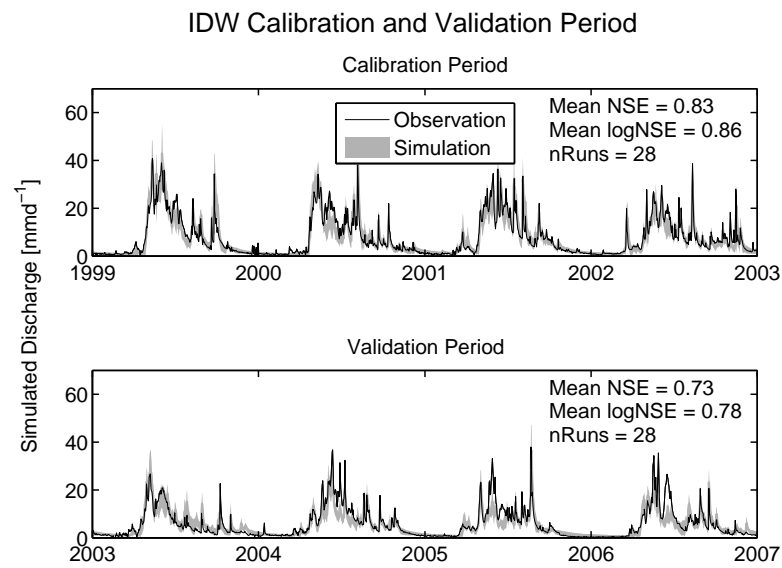


Figure A.6.: Daily discharge of calibration and validation period using the IDW dataset.

A.1.3. Errors

Absolute Errors

Note that the errors represent the differences between observation and simulation where the observed values are higher than the highest value in the simulation or lower than the lowest of the simulation at a certain day.

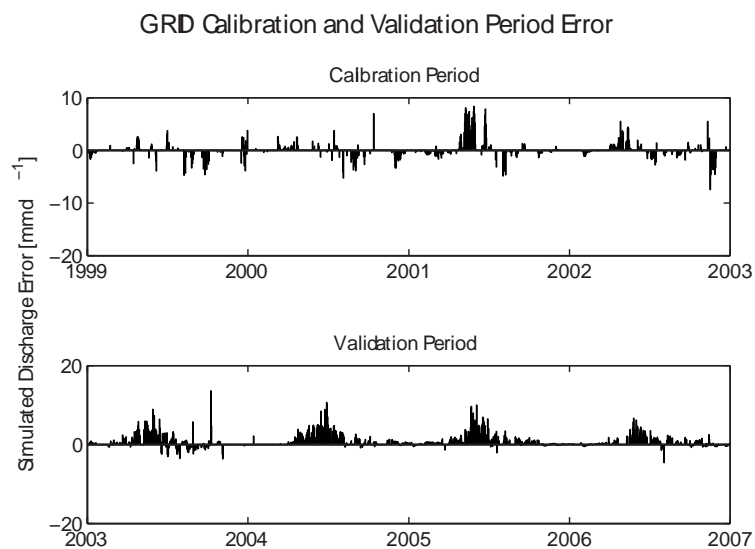


Figure A.7.: Daily discharge errors of calibration and validation period using the GRID dataset.

A.1. Figures of the Calibration and Validation Period of the 3 Datasets

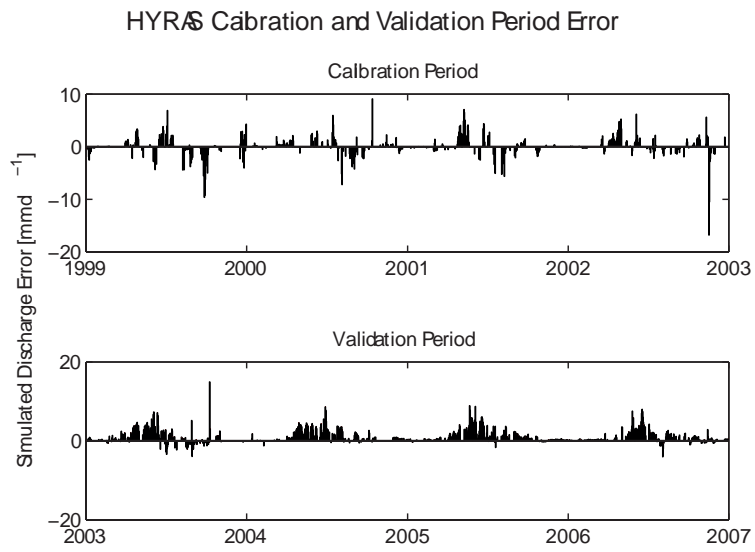


Figure A.8.: Daily discharge errors of calibration and validation period using the HYRAS dataset.

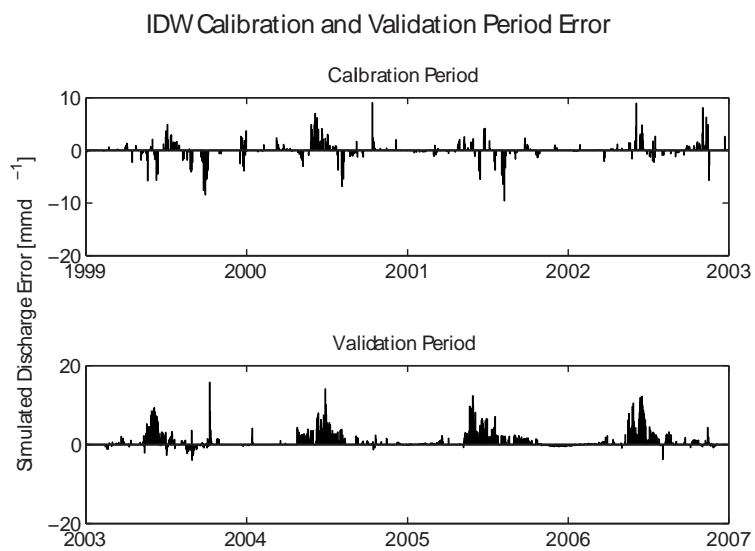


Figure A.9.: Daily discharge errors of calibration and validation period using the IDW dataset.

A. Appendix

Average Errors

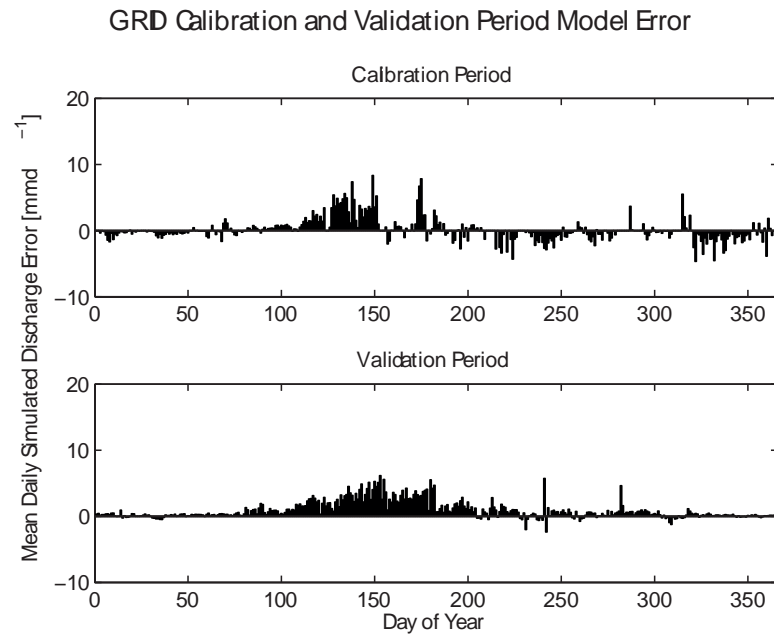


Figure A.10.: Average daily discharge errors of calibration and validation period using the GRID dataset.

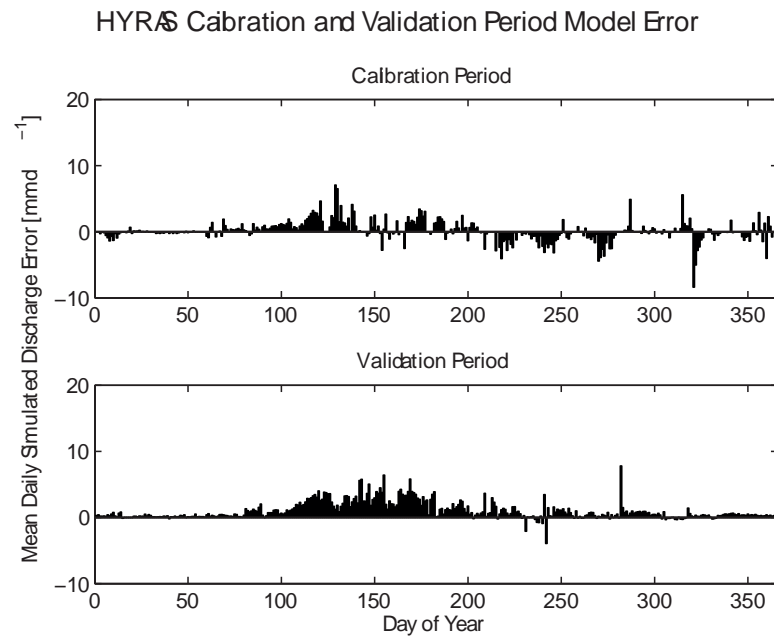


Figure A.11.: Average daily discharge errors of calibration and validation period using the HYRAS dataset.

A.1. Figures of the Calibration and Validation Period of the 3 Datasets

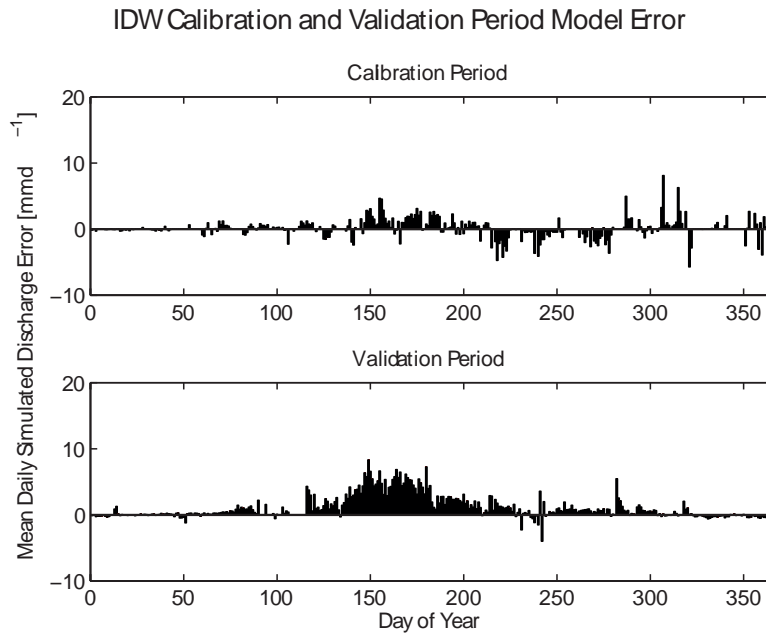


Figure A.12.: Average daily discharge errors of calibration and validation period using the IDW dataset.

Relative Average Errors

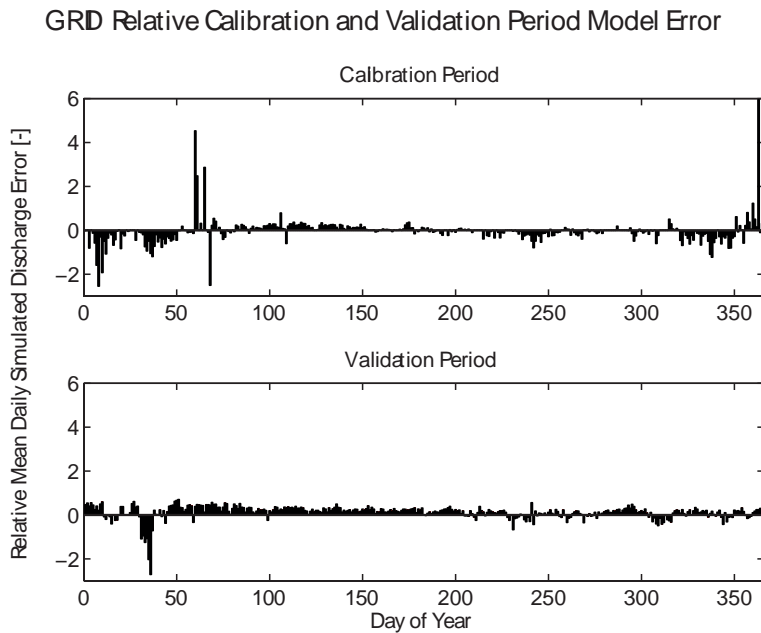


Figure A.13.: Relative Errors of the Calibration and Validation Period of the mean daily discharge values using the GRID dataset.

A. Appendix

HYRAS Relative Calibration and Validation Period Model Error

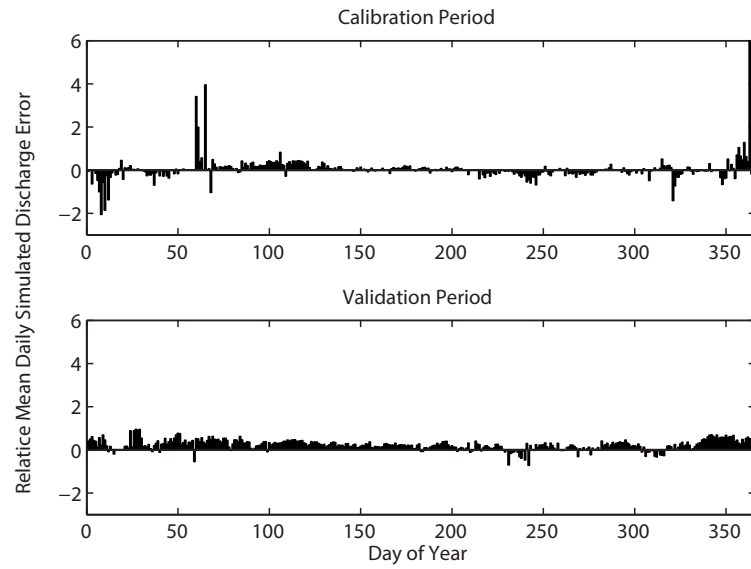


Figure A.14.: Relative Errors of the Calibration and Validation Period of the mean daily discharge values using the HYRAS dataset.

IDW Relative Calibration and Validation Period Model Error

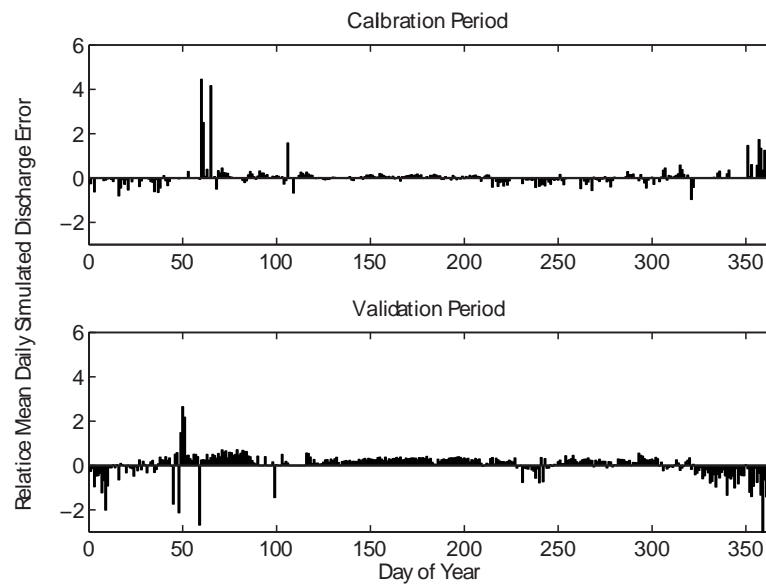


Figure A.15.: Relative Errors of the Calibration and Validation Period of the mean daily discharge values using the IDW dataset.

Acknowledgements

I want to thank my supervisor Dr. David Finger for the support, the fruitful discussions in countless meetings, Skype-sessions and E-mails throughout the past year even though he lived and worked in Iceland during most of the time when I wrote this thesis.

Further I want to thank Jan Seibert for the inputs and the time he took in several meetings and the quick responses in E-mails, which is definitely not a matter of course.

I also want to thank Marc Vis for the time-consuming work on the HBV-light model and the time he took for technical support, answering questions and an open mind for inputs.

Particularly I want to thank Dr. Matthias Huss for providing several glacier datasets and for many inputs in E-mails as well as Nans Addor for providing the quantile mapped climate scenarios and inputs by E-Mail and a meeting during a short stay in Switzerland.

Then I would also like to thank the Kraftwerke Sarganserland AG, which made this whole work possible by providing the discharge data.

Then I also want to thank Ling Wang for providing me inputs on the Pareto technique.

A big thanks goes to Corin Meier who accompanied me on the adventurous trip to the Gigerwaldsee for getting an impression of the lake and taking some nice pictures.

A special thanks goes to all my fellow students in- and outside the G10 at the University of Zurich for the good times, distractions, open ears, help and support we could give each other.

Last but not least I also want to thank my family who always supported me throughout my whole studies.

Personal Declaration

I hereby declare that the submitted thesis is the result of my own, independent work.
All external sources are explicitly acknowledged in the thesis.

Simon Etter